

This is a repository copy of *Cyanotriazoles are selective topoisomerase II poisons that rapidly cure trypanosome infections*.

White Rose Research Online URL for this paper:

<https://eprints.whiterose.ac.uk/id/eprint/204462/>

Version: Accepted Version

Article:

Rao, Srinivasa P S, Gould, Matthew K, Noeske, Jonas et al. (39 more authors) (2023) Cyanotriazoles are selective topoisomerase II poisons that rapidly cure trypanosome infections. *Science* (New York, N.Y.). pp. 1349-1356. ISSN: 0036-8075

<https://doi.org/10.1126/science.adh0614>

Reuse

Items deposited in White Rose Research Online are protected by copyright, with all rights reserved unless indicated otherwise. They may be downloaded and/or printed for private study, or other acts as permitted by national copyright laws. The publisher or other rights holders may allow further reproduction and re-use of the full text version. This is indicated by the licence information on the White Rose Research Online record for the item.

Takedown

If you consider content in White Rose Research Online to be in breach of UK law, please notify us by emailing eprints@whiterose.ac.uk including the URL of the record and the reason for the withdrawal request.

Cyanotriazoles, A New Class of Topoisomerase II Poison, Rapidly Cure Trypanosome Infections

Authors

Srinivasa P. S. Rao^{1,4*}, Matthew K. Gould², Jonas Noeske³, Manuel Saldivia¹, Rajiv S. Juman¹, Pearly S. Ng⁴, Olivier René¹, Yen-Liang Chen¹, Marcel Kaiser^{5,6}, Ryan Ritchie², Amanda F. Francisco⁷, Nila Johnson¹, Debjani Patra¹, Harry Cheung¹, Colin Deniston⁸, Andreas D. Schenk⁹, Wilian A. Cortopassi³, Remo S. Schmidt^{5,6}, Natalie Wiedemar^{5,6}, Bryanna Thomas¹, Rima Palkar¹, Nahdiyah A. Ghafar⁴, Vanessa Manoharan⁴, Catherine Luu³, Jonathan E. Gable¹, Wan K. Fei⁴, Elmarie Myburgh¹⁰, Jeremy C. Mottram¹⁰, Whitney Barnes⁸, John Walker⁸, Charles Wartchow³, Natasha Aziz¹, Colin Osborne¹, Juergen Wagner^{4,9}, Christopher Sarko¹, John M. Kelly⁷, Ujjini H. Manjunatha^{1, 4}, Pascal Mäser^{5,6}, Jan Jiricek^{1, 4}, Suresh B. Lakshminarayana^{1, 4}, Michael P. Barrett^{2*}, Thierry T. Diagana^{1,4*}

Affiliations:

¹Novartis Institute for Tropical Diseases, Emeryville, CA, USA

²University of Glasgow, Glasgow, UK

³Novartis Institutes for BioMedical Research, Emeryville, CA, USA

⁴Novartis Institute for Tropical Diseases, Singapore

⁵Swiss Tropical and Public Health Institute, Allschwil, Switzerland

⁶University of Basel, Basel, Switzerland

⁷London School of Hygiene and Tropical Medicine, London, UK

⁸Novartis Institutes for BioMedical Research, San Diego, CA, USA

⁹ Novartis Institutes for BioMedical Research, Basel, Switzerland

¹⁰University of York, York, UK

5 **Abstract:**

Millions living in Latin America and sub-Saharan Africa are at risk of trypanosomatid infections, causing Chagas disease and human African trypanosomiasis (HAT), respectively. Improved HAT treatments are available, but Chagas disease therapies rely on two nitroheterocycles, which suffer from lengthy drug regimens and safety concerns that cause frequent treatment discontinuation. Phenotypic screening against trypanosomes identified a class of cyanotriazoles (CT) with potent trypanocidal activity both in vitro and in murine models of Chagas disease and HAT. CT compounds act through selective, irreversible inhibition of trypanosomal topoisomerase II by stabilizing double stranded DNA:enzyme cleavage complex confirmed by cryogenic electron microscopy structure. This work paves the way to transformative therapeutics for the treatment of Chagas disease.

10

15

One Sentence Summary: Cyanotriazoles are fast-acting trypanosomatid-specific topoisomerase II inhibitors.

Main Text:

More than a billion people living in tropical and sub-tropical regions worldwide are at risk of infection from kinetoplastid parasites such as *Trypanosoma cruzi* (etiological agent of Chagas disease) (1), *T. brucei* subspecies (human African trypanosomiasis – HAT, or sleeping sickness) (2), *Leishmania donovani* (visceral leishmaniasis – VL) (3), and other *Leishmania* species (cutaneous leishmaniasis – CL) (4). Current treatments are decades old and suffer from toxicity and limited efficacy. A fledgling drug-pipeline, powered by public-private partnerships, has addressed some unmet medical needs for HAT (5-7) and, to some level, VL (8-12). However, progress against Chagas disease has been scant (13, 14). The two standard Chagas disease therapies, benznidazole and nifurtimox, are poorly tolerated, and treatment regimens are lengthy and often discontinued due to adverse effects, which leaves patients vulnerable to life-threatening cardiac and gastrointestinal complications associated with chronic *T. cruzi* infection (1). More effective, safer, and shorter duration therapeutics for Chagas disease are urgently needed.

Assay miniaturization and automation have enabled large chemical library screens against causative agents of neglected tropical diseases. Over the past two decades, such phenotypic screening approaches have yielded notable advances against malaria (15), tuberculosis (16), leishmaniasis and the African trypanosomiasis (8-12, 17). This approach has enabled new chemical entities to enter clinical trials and the discovery of new mechanisms of action and novel drug targets. Among the targets for new anti-leishmanials, advancing to human clinical trials, are the 20S proteasome (8, 10, 11), cdc2 related kinase 12 (CRK12) (12) and cleavage and

polyadenylation specificity factor 3 (CPSF3) (9); these may offer potential for use against human trypanosomiasis too. Here we report a cyanotriazole (CT) compound class, that showed robust anti-kinetoplastid activity *in vitro* and fast sterilizing activity in rodent models of both African and American trypanosomiasis. Mechanistic investigations revealed that CTs act through topoisomerase II inhibition that selectively induced rapid and irreversible damage to trypanosome DNA.

Cyanotriazoles (CT) are pan-kinetoplastid inhibitors with rapid sterilizing activity

Identification of CT. A whole-cell based growth inhibition screen of the Novartis compound library against bloodstream form *T. brucei brucei*, identified CT0 as a potent growth inhibitor also active against *T. b. gambiense* and *T. b. rhodesiense*, pathogens that cause HAT (Table 1). CT0 belongs to the cyanotriazole compound class which also proved to be potent growth inhibitors of a panel of kinetoplastid parasites, including *T. cruzi* and *L. donovani* (Table 1, fig. S1, A & B). Importantly, CTs were non-cytotoxic (Table 1, fig. S1, C & D) nor active against a range of non-trypanosomatid microbial pathogens (table S1). Preliminary structure-activity relationship (SAR), which involved chemical modifications to CT0 to evaluate potential for optimization of potency and physicochemical properties of this series was carried out. Analogs of CT0 demonstrated that this class of compounds was amenable for optimization and retained cellular potency against multiple kinetoplastid parasites, indirectly suggesting that CTs may have a conserved mechanism of action (MOA) across all kinetoplastids (fig. S1, A & B).

Despite its exquisite potency, CT0 displayed limited solubility and unfavorable physico-chemical properties, resulting in poor oral bioavailability and no measurable brain exposure, which is necessary for curing stage II HAT (Table 1). To obtain a suitable lead molecule for evaluation in rodent disease models, medicinal chemistry efforts optimized properties of the CT scaffold for oral dosing and brain penetration. Removing the hydrogen-bond donor of the aminomethylfuran core of CT0 through cyclization led to a novel aza-isoindoline scaffold. Further diminishing the cyanophenyl substituent's polarity, resulted in molecule CT1 with improved solubility, oral bioavailability, and moderate free brain exposure (Table 1). Finally, replacement of the aza-isoindoline core with an isoindoline moiety and restoring polarity by introducing a 5-fluoro-2-(trifluoromethyl)pyridine substituent on the left-hand side of the molecule, lead to molecule CT3. This nitrogen shift strategy allowed CT3 to preserve solubility while displaying excellent oral bioavailability and free brain exposure (Table 1), yielding pharmacokinetic properties suitable for profiling in vivo in various animal models of human trypanosomatid diseases (table S2).

In vitro and in vivo potency of CTs. Rapid onset of action and a short dosing regimen are desirable properties for anti-infective therapies. These properties typically require drugs with fast-sterilizing activity that is time and concentration-dependent. Rate of kill and wash-off experiments revealed time and concentration-dependent sterilizing activity of CT3 that compared favorably to the standard-of-care drugs for Chagas disease and HAT, indicating a potential to act fast and offer shorter drug regimens than the current therapies (fig. S2, A-D).

In vitro to in vivo translatability of CT3 sterilizing activity was evaluated in murine models of trypanosomatid diseases. Chagas disease requires complete parasite clearance in vivo to prevent relapse from residual parasites, as seen with posaconazole in mouse models of infection (18) and during human clinical trials (19). Hence, we tested CT3 in a bioluminescent mouse model of chronic Chagas disease, with immunosuppression to confirm sterile cure (20). In this model, dosing at 30 mg.kg⁻¹ once daily for five days reduced parasitemia beyond the limit of detection. Parasites remained undetectable in all treated mice even after three rounds of immunosuppression, suggesting that complete/sterile cure had been achieved. Ex vivo imaging of selected organs and tissues confirmed the absence of detectable parasites (Fig. 1A). Pharmacokinetic analysis of treated mice showed the free blood concentration of CT3 was above the EC₅₀ for ~17 hours (fig. S3A). CT3 was also evaluated in the more stringent acute model of infection with higher parasite burden, in which benznidazole, the standard of care, fails to achieve cure with a dose of 100 mg.kg⁻¹ once daily for five days. However, CT3 showed complete sterile cure when dosed at 30 mg.kg⁻¹ once daily for five days (fig. S4A).

We also assessed CT3 in mouse models of HAT (17, 21), which also require parasite eradication to achieve complete cure. Treatment with 10 mg.kg⁻¹ CT3 once daily for four days cured the stage I (hemolympathic) infection (fig. S4B), whereas seven days treatment with 10 mg.kg⁻¹ once daily was required to cure the stage II (meningoencephalitis) infection (fig. S4C). Given the rapid in vitro sterilizing activity (6 hours) of CT3 treatment during wash-off assays (fig. S2D), we also evaluated the ability to achieve single-dose cure in both murine models described above. CT3

achieved relapse-free sterile cure after single dose oral administration of 40 mg.kg⁻¹ in stage I (fig. S4B) and 100 mg.kg⁻¹ in stage II HAT mouse models (Fig. 1B). Ex vivo analysis of brains post-treatment showed complete clearance of parasites. Pharmacokinetic analysis of mice treated with a single dose of 100 mg.kg⁻¹ CT3 showed that the free brain concentration was above EC₅₀ for over 24 hours (fig. S3B). Acoziborole, an oxaborole molecule, has completed phase II/III clinical development for HAT where its long half-life has enabled cure, even of stage 2 disease, with a single dose (6).

CT-treated parasites showed defects in nuclear DNA replication and exhibited an upregulated DNA damage response

Understanding the mechanism of action and identifying drug target(s) facilitates medicinal chemistry through structure-based optimization that helps design molecules with better potency and selectivity. A multi-pronged strategy, including phenotypic, metabolomic, genetic and biochemical approaches, was used to deconvolute the CTs' target.

Firstly, the effect of six hours of treatment with 5x EC₅₀ of CT1 and CT3 on cell cycle progression was examined in bloodstream form *T. b. brucei*. DNA staining using DAPI showed arrest in S-phase, denoted by an increased 2K1N population, compared to untreated control (fig. S5A), suggesting that CTs affected nuclear but not kinetoplast DNA replication. EdU (a thymidine analog that incorporates into newly synthesized DNA) staining was used to probe the impact of CT on DNA synthesis. Two hours treatment of *T. cruzi* with 50x EC₅₀ of CT3 prevented EdU incorporation into nuclear

DNA, confirming that CTs hinder nuclear but not kinetoplastid DNA replication (Fig. 2A).

We also performed untargeted metabolomics, which has helped assign drug mode of action in kinetoplastids (22, 23). After exposing *T. b. brucei* to CTs (CT1, CT3), over 600 metabolites were detected by mass spectrometry and profound increases in deoxynucleotide abundance were observed (fig. S6, dataS2), a profile similar to that of *Staphylococcus aureus* following exposure to fluoroquinolone inhibitors of DNA gyrase (24).

As DNA replication appeared to be affected, we next evaluated whether CTs cause DNA damage in trypanosomatids. Immunoblotting with antibodies against phosphorylated histone (γ H2A), a marker of double-strand DNA (dsDNA) breaks (25), revealed significant increases in γ H2A in *T. b. brucei* (fig. S5B). In situ fluorescence microscopy, also showed increased γ H2A in both *T. b. brucei* and *T. cruzi* exposed to CTs, while GNF6702, a known kinetoplastid proteasome inhibitor, did not induce increased γ H2A (Fig. 2B & C). Moreover, *T. b. brucei* mutants, lacking either of the dsDNA break repair enzymes BRCA2 or RAD51, were hypersensitive to CT compounds, suggesting that either they interfered with the cellular DNA strand-breakage repair machinery, or they caused DNA damage which is enhanced when the repair machinery is disrupted (table S3).

Drug resistance to CTs involved mutations in the topoisomerase II α gene of *T. b. brucei*

Drug resistant mutants were independently selected against two different CTs (CT1 and CT4) in *T. b. brucei* in vitro (table S4). Resistant clones were isolated using limiting dilution and each showed significant resistance to CT molecules while retaining sensitivity to other known trypanocides (Fig. 3A, fig. S7). Whole genome sequencing of mutants revealed multiple single nucleotide polymorphisms (SNPs) in each individual mutant, but three of the four mutant strains (CT1.1, CT1.2 and CT4.1) carried an F540L SNP in the topoisomerase II alpha (*topollα*) gene (data S2). All other SNPs were unique to individual parasite mutant lines. Sanger sequencing of the topo II region of the mutants confirmed a homozygous F540L mutation in resistant lines CT1.1, CT1.2 and CT4.1 (fig. S8A). Sanger sequencing of CT4.2 parasites revealed, in the N-terminal encoding region of *topollα*, multiple heterozygous mutations that code for the matching amino acids found in *topollβ* (fig. S8B). Independent CT resistant mutants were also generated against a third CT compound (CT5; table S4) and Sanger sequencing of the *topollα* gene region identified homozygous SNPs encoding L491F and S492N mutation in CT5.1 and G598S mutation in CT5.2 (fig. S8A).

T. b. brucei has two topoisomerase II enzymes, Topollα and Topollβ, and RNAi experiments have shown that only *topollα* is essential for *T. b. brucei* bloodstream form survival (26). Depletion of *topollα* by RNAi affects nuclear but not kinetoplast DNA replication, similar to our observations with CT-treated parasites. Sequence alignment of Topollα and Topollβ shows that the N-terminal region is highly conserved, while the C-terminal region after amino acid 1067 is more divergent (fig. S9). F540 is present in both Topoll isoforms, while L491, S492 and G598 in Topollα are respectively F491,

N492 and S598 in Topoll β . The SNPs identified in *topoll α* in the resistant lines CT5.1 and CT5.2 corresponded to amino acids found in wildtype Topoll β .

The biologically active form of Topoll α is a homodimer. All Topoll α mutations found in the drug resistant mutants clustered in the protein's Toprim domain (Fig. 3B), which is essential for DNA cleavage and religation activity (27, 28). Residue F540 is conserved in kinetoplastids, yeast, and humans (fig. S10) pointing into the hydrophobic core of the Toprim domain, while G598 is located at the topoisomerase dimer interface (Fig. 3B) (29, 30). Furthermore, comparison to structures of the full-length yeast Topoll reveal that residues equivalent to L491 and S492 lie proximal to residues in the ATPase transducer domain structures (29), while in the pre-open state structure of the full-length human topoisomerase II α (hTOP2A), the equivalent residues are proximal to the K-loop of the transducer domain (30). The K-loop is important in coupling DNA binding with ATP turnover and strand passage (29). The presence of Topoll α mutations in multiple *T. b. brucei* CT-resistant mutants points to Topoll α as a potential target, consistent with genetic, phenotypic and metabolomic observations.

We assessed the impact of reduced expression of *Topoll α* by doxycycline-inducible RNAi. Since *topoll α* is essential, partial rather than full knockdown was achieved with transient induction of RNAi by pulsing a range of doxycycline concentrations to allow gene expression to recover before the enzyme's absence led to cell death. The higher the dose of doxycycline in pulsed induction of RNAi, the less sensitive cells became to CTs (table S5). This is consistent with observations in mammalian cells exposed to Topoll poisons where reduced enzyme activity diminishes dsDNA break formation (31).

To further confirm Topoll α as the target for CTs, we introduced one of the drug resistant allele mutations into *T. b. brucei* using the CRISPR-Cas9 system (fig. S11A). The resulting CRISPR-edited parasites were selected for CT drug resistance at five times its EC₅₀ against wild-type (fig. S11B). Parasites transfected with the mutating DNA repair template, and induced to express the Cas9 protein, recovered within days, while the control transfection with no Cas9 expression did not grow under selective pressure. EC₅₀ values with a range of CT compounds confirmed that the CRISPR-edited parasites were highly resistant to CTs (Fig. 3C). Whole-genome sequencing of the CRISPR-edited parasites identified no mutations outside the intended *topoll* gene cluster. Sanger sequencing revealed that both *topoll* α and *topoll* β genes carried the F540L mutation (expected as the guide-RNA target sequence and homology flanks of the transfected repair template, are conserved in both genes). Interestingly, the Topoll α sequence also revealed other changes in the vicinity of F540L, including L491F and S492N that were observed in the Topoll α sequence of other CT-resistant mutants and also the wild-type sequence of the Topoll β (Fig. 3C). This indicated that in selecting CRISPR edited parasites for CT resistance, a domain swap may have introduced a section of the *topoll* β gene into the *topoll* α gene in addition to the F540L mutation.

CTs selectively inhibited DNA relaxation activity of trypanosome Topoll by stabilizing dsDNA:enzyme complex.

Topoll inhibitors are divided into two broad classes: catalytic inhibitors and Topoll poisons. The latter stabilize the covalent DNA:enzyme complex, leading to double-

strand DNA breaks (32). To characterize the inhibitory activity of the CTs, we expressed and purified *T. cruzi* Topoll (Tc Topoll) using a baculovirus expression system. Tc Topoll shares 82% identity with *T. b. brucei* over the first 1,181 amino acids (in contrast to the mammalian orthologue, which diverges substantially in this region) (fig.S10).

5 Residues F540, and G598 that were detected as mutations in the *T. b. brucei* drug resistant mutants, are conserved in all kinetoplastids, whilst TbTopoll α L491 and S492 residues are isoleucine (I491) and arginine (R492), respectively, in *T. cruzi* (fig. S10).

The effect of CTs on TcTopoll, was measured using a Topo2 cleavage assay which measures the stabilization of double-strand DNA breaks. Addition of CTs (CT1, CT3) to
10 TcTopoll promoted selective accumulation of linearized DNA indicative of CT stabilizing the topoisomerase double-strand DNA cleavage complex (Fig. 4A; fig S12; fig. S13). In contrast, a pharmacologically inactive closely related analog (CT2) did not result in linearized DNA accumulation by TcTopoll (Fig. 4A, Table S4). Importantly, CTs (CT1, CT3) did not affect human TOP2A cleavage activity (fig. S14). The effect of CT1 on the
15 binding kinetics of TcTopoll to DNA was determined using surface plasmon resonance (SPR). The equilibrium dissociation constant (K_D) of TcTopoll binding to immobilized 36 bp dsDNA decreased by ~1,000 fold from 1.33 μ M to 1 nM in the presence of CT1, suggesting a stabilization of the topoisomerase DNA cleavage complex as observed in the DNA cleavage assay. The dissociation rate constant (k_d) of the protein-DNA
20 complex decreased by more than 130-fold in the presence of CT1 compared to the DMSO control indicating that the increase in binding affinity for this complex is primarily driven by a slower dissociation rate constant (Fig. 4B).

Cryo-electron microscopy showed that CTs interact covalently with C477 and bind at the DNA cleavage site.

Mechanistically, CTs belong to the class of topoisomerase poisons characterized by their stabilizing effect on the topoisomerase cleavage complex. These include clinically used drugs for cancer (e.g. etoposide) and bacterial infections (e.g. fluoroquinolones) (33). To provide a structural rationale for the mode of action of the CTs, we solved the cryo-electron microscopy (cryo-EM) structure of the *T. cruzi* TopoII DNA-binding domain (amino acids 401-1178) bound to double stranded DNA and CT1 at ~ 2.9 Å resolution (fig. S15, S16). EM density for CT1 was observed at the DNA cleavage site extending to C477 (Fig. 4C; fig. S16A, D). The trifluoromethylphenyl portion of CT1 intercalated between the DNA base pairs at the cleavage site and occupied a space similar to etoposide bound to hTOP2A (PDB 5GWK; (34); Fig. 4D) and fluoroquinolones bound to bacterial gyrase (35) (fig. S16B). The cyanotriazole portion of CT1 is positioned near C477 allowing the formation of a covalent bond with the nucleophilic thiol of the cysteine, represented by continuous EM density between CT1 and C477 (fig. S16A, D). Cyanoazole heterocycles are known to form reversible covalent interactions with cysteines (36). C477, which is uniquely conserved in trypanosomatid TopoII provides the basis for CT compound selectivity (the equivalent residue is asparagine in human TOP2A). Mutations found in *T. b. brucei* strains selected for CT-resistance are highlighted in the cryo-EM structure of TcTopoII (Fig. 4E-I), and residues L491 and S492 which mutate in selected *T. b. brucei* CT resistant mutants were only about 9 Å from the reactive cysteine.

Topoisomerase II inhibitors as treatment of trypanosomatid diseases.

Our data demonstrated that cyanotriazole compounds (CTs) are potent growth inhibitors of multiple kinetoplastid parasites. The CTs acted through selective kinetoplastid topoisomerase II inhibition which enabled rapid and complete sterilizing activity in murine models of Chagas disease and HAT. Given their remarkable therapeutic efficacy, we are undertaking advanced preclinical profiling of further optimized CT analogs to identify clinical candidates with a suitable safety profile. CT3 was relatively safe in preliminary pre-clinical safety profiling (Table S7). Further, the identification of trypanosomal TopoII as the molecular target of CTs, offers the opportunity to discover alternative chemical classes through high-throughput screening and structure-based drug design. We anticipate that these findings will underpin the development of potent, safe, and shorter duration therapies that will transform the management of Chagas disease and other kinetoplastid parasitic infections.

References

1. J. A. Perez-Molina, I. Molina, Chagas disease. *Lancet* **391**, 82-94 (2018).
2. P. Buscher, G. Cecchi, V. Jamonneau, G. Priotto, Human African trypanosomiasis. *Lancet* **390**, 2397-2409 (2017).
3. S. Burza, S. L. Croft, M. Boelaert, Leishmaniasis. *Lancet* **392**, 951-970 (2018).
4. R. Reithinger *et al.*, Cutaneous leishmaniasis. *Lancet Infect Dis* **7**, 581-596 (2007).
5. E. A. Dickie *et al.*, New Drugs for Human African Trypanosomiasis: A Twenty First Century Success Story. *Trop Med Infect Dis* **5**, (2020).
6. V. K. Betu Kumeso *et al.*, Efficacy and safety of acoziborole in patients with human African trypanosomiasis caused by *Trypanosoma brucei gambiense*: a multicentre, open-label, single-arm, phase 2/3 trial. *Lancet Infect Dis*, (2022).
7. V. Mesu *et al.*, Oral fexinidazole for late-stage African *Trypanosoma brucei gambiense* trypanosomiasis: a pivotal multicentre, randomised, non-inferiority trial. *Lancet* **391**, 144-154 (2018).
8. S. Khare *et al.*, Proteasome inhibition for treatment of leishmaniasis, Chagas disease and sleeping sickness. *Nature* **537**, 229-233 (2016).
9. C. E. Mowbray *et al.*, DNDI-6148: A Novel Benzoxaborole Preclinical Candidate for the Treatment of Visceral Leishmaniasis. *J Med Chem* **64**, 16159-16176 (2021).

10. A. Nagle *et al.*, Discovery and Characterization of Clinical Candidate LXE408 as a Kinetoplastid-Selective Proteasome Inhibitor for the Treatment of Leishmaniasis. *J Med Chem* **63**, 10773-10781 (2020).
11. S. Wyllie *et al.*, Preclinical candidate for the treatment of visceral leishmaniasis that acts through proteasome inhibition. *Proc Natl Acad Sci U S A* **116**, 9318-9323 (2019).
12. S. Wyllie *et al.*, Cyclin-dependent kinase 12 is a drug target for visceral leishmaniasis. *Nature* **560**, 192-197 (2018).
13. S. P. S. Rao *et al.*, Drug Discovery for Kinetoplastid Diseases: Future Directions. *ACS Infect Dis* **5**, 152-157 (2019).
14. A. M. Padilla *et al.*, Discovery of an orally active benzoxaborole prodrug effective in the treatment of Chagas disease in non-human primates. *Nat Microbiol* **7**, 1536-1546 (2022).
15. M. f. M. Venture. (2022), vol. 2022.
16. S. T. Partnership. (Working Group on TB drugs, 2022), vol. 2022.
17. S. P. S. Rao *et al.*, Anti-Trypanosomal Proteasome Inhibitors Cure Hemolymphatic and Meningoencephalic Murine Infection Models of African Trypanosomiasis. *Trop Med Infect Dis* **5**, (2020).
18. A. F. Francisco *et al.*, Limited Ability of Posaconazole To Cure both Acute and Chronic *Trypanosoma cruzi* Infections Revealed by Highly Sensitive In Vivo Imaging. *Antimicrob Agents Chemother* **59**, 4653-4661 (2015).
19. I. Molina *et al.*, Randomized trial of posaconazole and benznidazole for chronic Chagas' disease. *N Engl J Med* **370**, 1899-1908 (2014).
20. M. D. Lewis *et al.*, Bioluminescence imaging of chronic *Trypanosoma cruzi* infections reveals tissue-specific parasite dynamics and heart disease in the absence of locally persistent infection. *Cell Microbiol* **16**, 1285-1300 (2014).
21. E. Myburgh *et al.*, In vivo imaging of trypanosome-brain interactions and development of a rapid screening test for drugs against CNS stage trypanosomiasis. *PLoS Negl Trop Dis* **7**, e2384 (2013).
22. P. C. Steketee *et al.*, Benzoxaborole treatment perturbs S-adenosyl-L-methionine metabolism in *Trypanosoma brucei*. *PLoS Negl Trop Dis* **12**, e0006450 (2018).
23. A. Trochine, D. J. Creek, P. Faral-Tello, M. P. Barrett, C. Robello, Benznidazole biotransformation and multiple targets in *Trypanosoma cruzi* revealed by metabolomics. *PLoS Negl Trop Dis* **8**, e2844 (2014).
24. K. Dorries, R. Schlueter, M. Lalk, Impact of antibiotics with various target sites on the metabolome of *Staphylococcus aureus*. *Antimicrob Agents Chemother* **58**, 7151-7163 (2014).
25. L. Glover, D. Horn, Trypanosomal histone gammaH2A and the DNA damage response. *Mol Biochem Parasitol* **183**, 78-83 (2012).
26. T. Kulikowicz, T. A. Shapiro, Distinct genes encode type II Topoisomerases for the nucleus and mitochondrion in the protozoan parasite *Trypanosoma brucei*. *J Biol Chem* **281**, 3048-3056 (2006).
27. L. Aravind, D. D. Leipe, E. V. Koonin, Toprim--a conserved catalytic domain in type IA and II topoisomerases, DnaG-type primases, OLD family nucleases and RecR proteins. *Nucleic Acids Res* **26**, 4205-4213 (1998).
28. B. H. Schmidt, A. B. Burgin, J. E. Deweese, N. Osheroff, J. M. Berger, A novel and unified two-metal mechanism for DNA cleavage by type II and IA topoisomerases. *Nature* **465**, 641-644 (2010).

29. B. H. Schmidt, N. Osheroff, J. M. Berger, Structure of a topoisomerase II-DNA-nucleotide complex reveals a new control mechanism for ATPase activity. *Nat Struct Mol Biol* **19**, 1147-1154 (2012).
30. A. Vanden Broeck *et al.*, Structural basis for allosteric regulation of Human Topoisomerase II α . *Nat Commun* **12**, 2962 (2021).
31. A. C. Porter, Depletion and mutation of topoisomerase II in animal cells. *Methods Mol Biol* **582**, 245-263 (2009).
32. K. R. Vann, A. A. Oviatt, N. Osheroff, Topoisomerase II Poisons: Converting Essential Enzymes into Molecular Scissors. *Biochemistry* **60**, 1630-1641 (2021).
33. J. L. Delgado, C. M. Hsieh, N. L. Chan, H. Hiasa, Topoisomerases as anticancer targets. *Biochem J* **475**, 373-398 (2018).
34. Y. R. Wang *et al.*, Producing irreversible topoisomerase II-mediated DNA breaks by site-specific Pt(II)-methionine coordination chemistry. *Nucleic Acids Res* **45**, 10861-10871 (2017).
35. D. A. Veselkov *et al.*, Structure of a quinolone-stabilized cleavage complex of topoisomerase IV from *Klebsiella pneumoniae* and comparison with a related *Streptococcus pneumoniae* complex. *Acta Crystallogr D Struct Biol* **72**, 488-496 (2016).
36. A. Keeley, P. Abranyi-Balogh, G. M. Keseru, Design and characterization of a heterocyclic electrophilic fragment library for the discovery of cysteine-targeted covalent inhibitors. *Medchemcomm* **10**, 263-267 (2019).
37. M. Saldivia *et al.*, Targeting the trypanosome kinetochore with CLK1 protein kinase inhibitors. *Nat Microbiol* **5**, 1207-1216 (2020).
38. A. T. Chao *et al.*, Development of a Cytopathic Effect-Based Phenotypic Screening Assay against *Cryptosporidium*. *ACS Infect Dis* **4**, 635-645 (2018).
39. B. R. Taft *et al.*, Discovery and Preclinical Pharmacology of INE963, a Potent and Fast-Acting Blood-Stage Antimalarial with a High Barrier to Resistance and Potential for Single-Dose Cures in Uncomplicated Malaria. *J Med Chem* **65**, 3798-3813 (2022).
40. D. J. Creek, A. Jankevics, K. E. Burgess, R. Breitling, M. P. Barrett, IDEOM: an Excel interface for analysis of LC-MS-based metabolomics data. *Bioinformatics* **28**, 1048-1049 (2012).
41. S. Khare *et al.*, Utilizing Chemical Genomics to Identify Cytochrome b as a Novel Drug Target for Chagas Disease. *PLoS Pathog* **11**, e1005058 (2015).
42. B. Raz, M. Iten, Y. Grether-Buhler, R. Kaminsky, R. Brun, The Alamar Blue assay to determine drug sensitivity of African trypanosomes (*T.b. rhodesiense* and *T.b. gambiense*) in vitro. *Acta Trop* **68**, 139-147 (1997).
43. R. McCulloch, J. D. Barry, A role for RAD51 and homologous recombination in *Trypanosoma brucei* antigenic variation. *Genes Dev* **13**, 2875-2888 (1999).
44. C. L. Hartley, R. McCulloch, *Trypanosoma brucei* BRCA2 acts in antigenic variation and has undergone a recent expansion in BRC repeat number that is important during homologous recombination. *Mol Microbiol* **68**, 1237-1251 (2008).
45. E. Rico, L. Jeacock, J. Kovarova, D. Horn, Inducible high-efficiency CRISPR-Cas9-targeted gene editing and precision base editing in African trypanosomes. *Sci Rep* **8**, 7960 (2018).
46. A. D. Schenk, S. Cavadini, N. H. Thoma, C. Genoud, Live Analysis and Reconstruction of Single-Particle Cryo-Electron Microscopy Data with CryoFLARE. *J Chem Inf Model* **60**, 2561-2569 (2020).

47. A. Kucukelbir, F. J. Sigworth, H. D. Tagare, Quantifying the local resolution of cryo-EM density maps. *Nat Methods* **11**, 63-65 (2014).
48. Y. Z. Tan *et al.*, Addressing preferred specimen orientation in single-particle cryo-EM through tilting. *Nat Methods* **14**, 793-796 (2017).
- 5 49. D. Liebschner *et al.*, Macromolecular structure determination using X-rays, neutrons and electrons: recent developments in Phenix. *Acta Crystallogr D Struct Biol* **75**, 861-877 (2019).
50. O. S. Smart, Womack, T. O., Sharff, A., Flensburg, C., Keller, P., Paciorek, W., Vornrhein, C., Bricogne, G. . (Global Phasing Ltd, 2011).

10 **Acknowledgments:** The authors would like to acknowledge Grace Baxley, Hannah Roughley, Lee Chang Bok, Ying-Bo Chen, Sarah Williams, Julia Roquigny for the technical assistance. Authors also thank David Beer, Francesca Blasco for insightful discussions. We are grateful to Professor Richard McCulloch (Glasgow) for providing *T. brucei* RAD51 and BRCA2 mutants and Professor David Horn (Dundee) for the *T. brucei* inducible cas9 cell line. The authors are

15 grateful to project management, alliance management and partnering, legal and finance team (Gu Feng, Thomas Krucker, Mark Hopkins, and Jean Claude Poilevey).

Funding: This research was supported by the Wellcome Trust (grant nos. 103024/Z/13Z, 104976/Z/14/Z and 108517/Z/15/Z, 219639/Z/19/Z). MPB, MG were also funded by an MRC Newton grant “Bridging epigenetics, metabolism and cell cycle in pathogenic

20 trypanosomatids” MR/S019650/1 and the Wellcome Trust Wellcome Centre for Integrative Parasitology (grant number 104111/Z/14/Z). **Author contributions:** Conceptualization: SPSR, MKG, UHM, JJ, MPB, TTD; Methodology: SPSR, MKG, JN, MS, RSJ, DB, PSN, MK, RR, AFF, HC, CD, ADS, WAC, CL, EM, CW, CO, JMK, UHM, JJ ; Investigation: DB, BT, PSN, JN, MS, RJ, PSN, RR, OR, YLC, AFF, NJ, DP, HC, CD, ADS, WAC, RSS,

25 NW, BT, RP, NG, VM, CL, CW, WKF, EM, WB; Formal analysis: SPSR, MKG, JN, MS, RSJ, PSN, OR, YLC, MK, RR, AFF, NJ, HC, CD, ADS, RSS, NW, CL, JEG, WKF, EM, WB, JW, CW, CO, JMK, UHM, JJ, SBL Visualization: WB, JW, JN, CD, ADS, WAS, MS;

Funding acquisition: SPSR, MPB, JCM, PM, TTD; Project administration: SPSR, MPB, NA, TTD; Supervision: SPSR, MPB, CO, CS, MK, PM, JW, JJ, JEG, JCM, EM, CW, Jwa, JMK, UHM, TTD; Writing – original draft: SPSR, MKG, JN, OR, MPB, TTD; Writing – review & editing: SPSR, JN, MS, RSJ, OR, YLC, SBL, EM, CS, EM, UHM, PM, MPB, TTD;

5 **Competing interests:** SPSR, JN, MS, RJ, OR, YLC, DB, HC, CD, ADS, WAC, BT, CL, JEG, WB, JW, CW, NA, CO, Jwa, CS, UHM, SBL, TTD are Novartis employees.

Cyanotriazoles compounds have been patented by Novartis with JJ, PSN, SPSR listed as authors (US Patent App. 17/253,737, 2022). All other authors declare that they have no competing interests. **Data and materials availability:** Data the support the findings of this
10 study are available from corresponding authors upon request. The cryo-EM map is available from the Electron Microscopy Data Bank with accession code EMD-29930. The atomic model has been deposited in the Protein Data Bank with the accession code PDB ID 8GCC. Metabolomics data has been deposited into metabolomics database with accession number MTBLS6845 and MTBLS7666.

15 **Supplementary Materials**

Materials and Methods

Figs. S1 to S16.

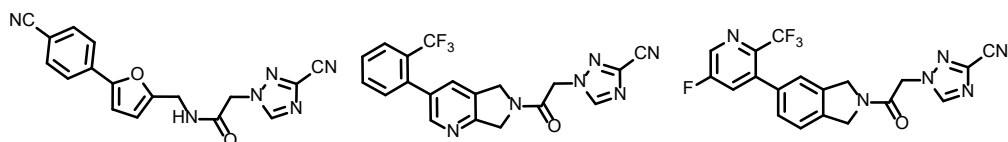
Tables S1 to S7

Data S1, S2

20 References (37-50)

Table 1. Cyanotriazoles inhibit growth of trypanosomatid parasites in vitro.

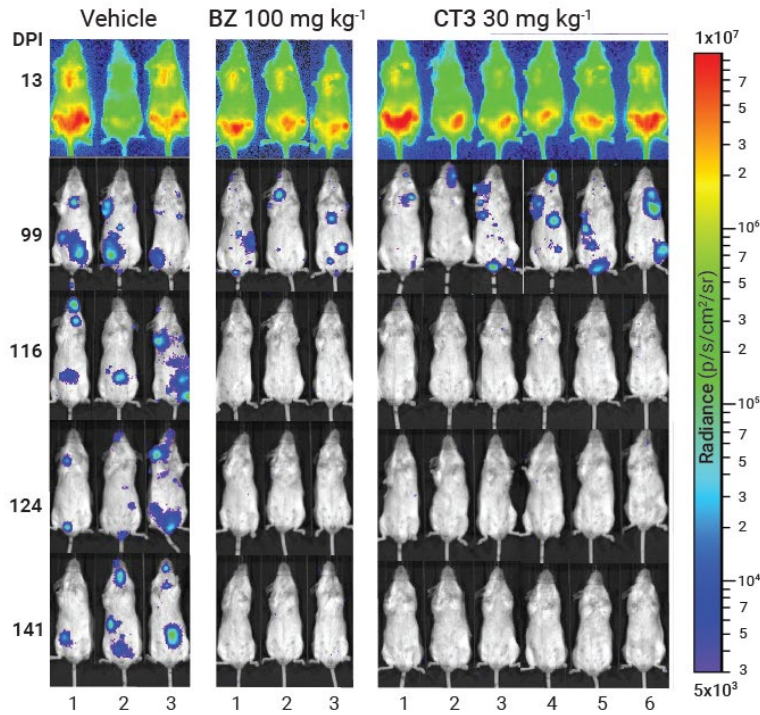
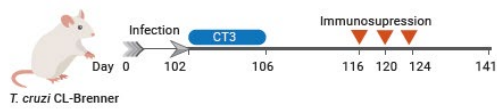
Chemical structure, anti-parasitic activity, cytotoxicity, physicochemical properties, and pharmacokinetics of CT compounds.



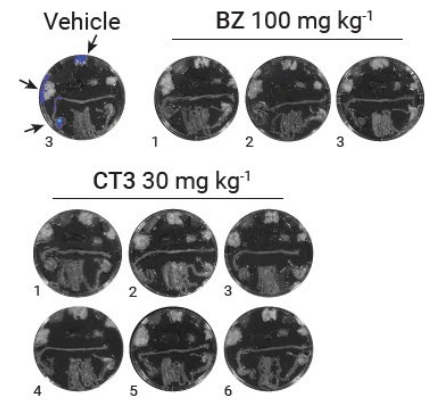
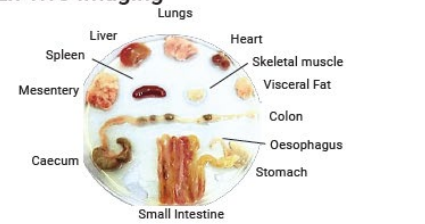
	CT0	CT1	CT3
In vitro anti-parasitic activity EC₅₀ (nM)			
<i>T. b. brucei</i>	66 ± 26	160 ± 35	180 ± 58
<i>T. b. gambiense</i>	94 ± 25	110 ± 11	31 ± 15
<i>T. b. rhodesiense</i>	16 ± 3	22 ± 5	57 ± 14
<i>T. cruzi</i>	69 ± 15	87 ± 27	78 ± 19
<i>L. donovani</i>	497 ± 70	1350 ± 1200	134 ± 52
Cytotoxicity CC₅₀ (nM)			
HepG2	14,600	24,000	>50,000
NIH 3T3	>20,000	>20,000	>20,000
Physicochemical properties			
Polar Surface Area	121	88	88
Hydrogen bond donors	1	0	0
Solubility (pH6.8, μM)	<2	230	34
Mouse in vivo pharmacokinetics			
Oral bioavailability (%)	5	80.8	100
Brain to Plasma ratio (K _p /K _{p_{uu}})	< 0.05 / < 0.05	0.7 / 0.5	0.7 / 1.4

HepG2: human hepatocellular carcinoma cells; NIH 3T3: fibroblast cells; Kp: brain to plasma ratio, total; Kp_{uu}: brain to plasma ratio, unbound (corrected by mouse plasma protein binding and rat brain tissue binding); EC₅₀ and CC₅₀ represent the half-maximum growth inhibition concentration against bloodstream form of *T. brucei*, intracellular *T. cruzi* amastigotes and extracellular *L. donovani* amastigotes, and mammalian cell lines. Growth inhibition measurements were generated with two or more independent biological replicates; with two technical replicates. Values shown are geometric mean ± standard deviation. Physicochemical properties such as polar surface area, hydrogen bond donors were calculated by using Medchem Focus software. In vivo pharmacokinetic properties for CT compounds were determined using mice (n =3). Oral bioavailability was determined using dose normalized exposures following oral and intravenous dosing of compounds and brain-to-plasma ratio was measured one hour after intravenous dosing in mice.

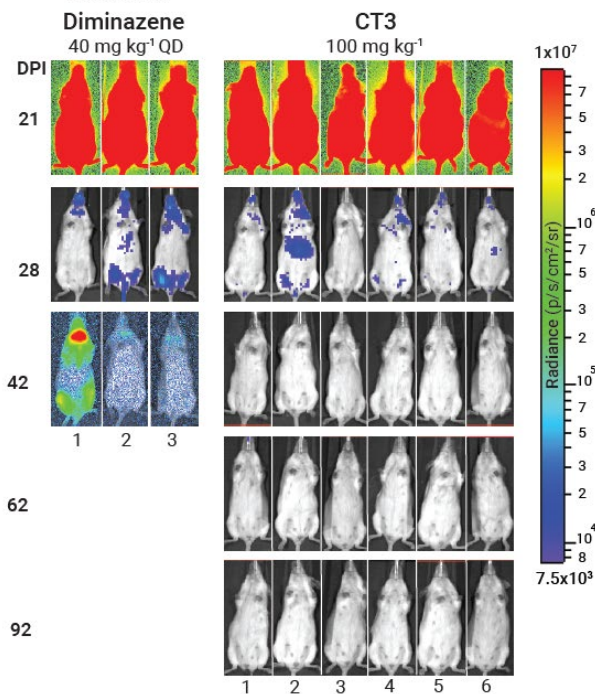
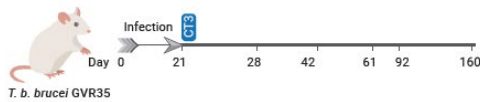
A



Ex-vivo Imaging



B



Ex-vivo Imaging

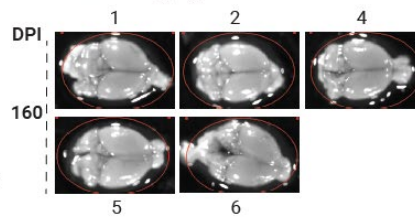


Figure 1 Cyanotriazoles efficacious against trypanosomatid parasites in vivo. (A)

In vivo assessment of non-treated, benznidazole (BZ) and CT3 treated mice during chronic stage *T. cruzi* infections as seen in the outline of experiment (top left). BALB/c mice were given vehicle (n=3), BZ (100 mg.kg⁻¹) (n=3), and CT3 (30 mg.kg⁻¹) (n=6) starting on day 102 (orally, 5 days, once daily). Ventral images of each mouse are shown at different time points after infection. All BZ and CT3 treated mice were immunosuppressed on days 116, 120 and 124 using cyclophosphamide (200 mg.kg⁻¹ intraperitoneally). All treated mice were bioluminescence negative at the experimental endpoint (day 141) and assessed further by ex vivo imaging (lower left panel and central ex vivo organs and tissue display). At this point, as an example, organs from non-treated mouse #3 were removed and assessed for bioluminescence. Note the infection in the lungs, mesentery, and cecum (black arrows). All treated mice were cured. Heat-maps are on log₁₀ scales and indicate intensity of bioluminescence from low (blue) to high (red). (B)

In vivo efficacy of CT3 in meningoencephalitis mouse model of HAT. After 21 days of infection with a bioluminescent *T. b. brucei* GVR35 strain, three mice were treated intraperitoneally with a single dose of 40 mg.kg⁻¹ of diminazene (negative control), and six mice were treated orally with one dose of 100 mg.kg⁻¹ of CT3. Parasitemia levels were monitored by imaging mice after administration of D-luciferin (150 mg.kg⁻¹, subcutaneously). Diminazene-treated mice relapsed by day 42 and were humanely euthanized, whilst CT3 treated mice remained parasitemia free for over 92 days; no brain signal was observed during ex vivo imaging on day 160 (mice 3 died due to natural causes in day 144, no parasitemia was detected). In both animal models, the presence of parasites is represented by bioluminescence radiance as indicated by the color scales.

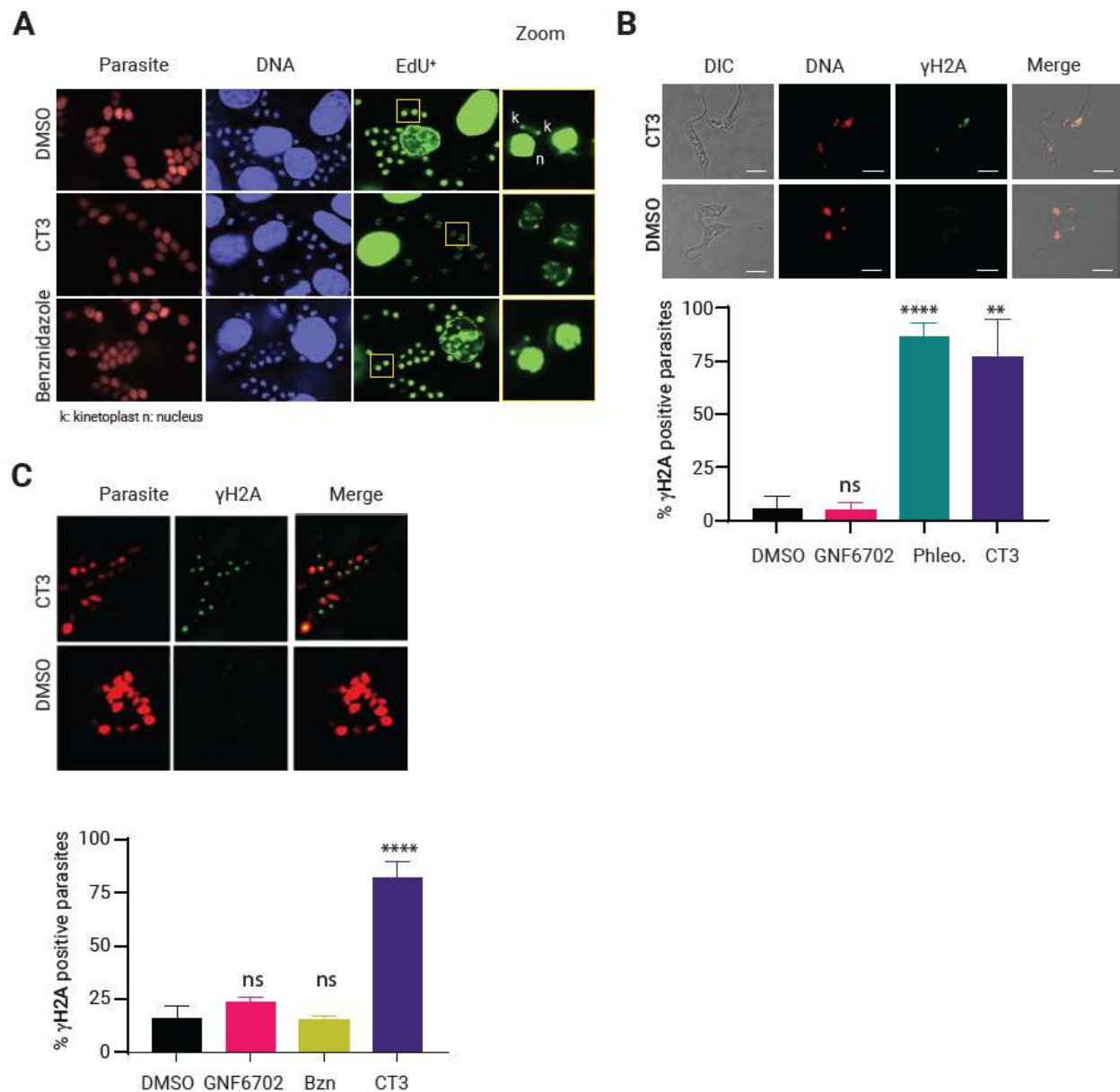


Figure 2 CTs induce a DNA damage response in trypanosomatid parasites. (A)

5 Evaluation of active DNA replication using EdU incorporation in *T. cruzi* parasites. Vero cells were infected with *T. cruzi* CL Brener tdTomato strain for 48 hours followed by two hours of treatment with DMSO (no drug), 50×EC₅₀ (4 μM) CT3 or benznidazole (BZN, 40 μM). Representative images of intracellular *T. cruzi* expressing tdTomato (red),

Hoechst stained nuclei (blue), EdU-labeling (green) are shown. Note reduction in EdU incorporation into *T. cruzi* parasites incubated with CT3 compared to the no drug control and BZN treated cultures. Images are representative of at least three independent experiments. Scale bar = 5 μ m. **(B)** Quantification of γ H2A induction in *T. b. brucei* treated with CT3 and other compounds. Representative microscopic images of *T. b. brucei*, DAPI stained DNA (red), *T. b. brucei* γ H2A antibody staining (green) and merged image suggesting localization of γ H2A induction with nuclear DNA (yellow) are shown. Parasites were treated with DMSO (no drug control), 11 \times EC₅₀ (2 μ M) of CT3, 20 μ M phleomycin (DNA damaging agent), or 285 \times EC₅₀ (20 μ M) of GNF6702 (kinetoplastid proteasome inhibitor) for 4 hours. Data show mean and SD of at least four independent biological replicates. Scale bar = 5 μ m. **(C)** Quantification of γ H2A induction in *T. cruzi* treated with CT3 and other compounds. Representative images of γ H2A induction (green) in *T. cruzi* intracellular amastigotes expressing tdTomato (red) are shown. Vero cells were infected with *T. cruzi* for 48 hours followed by 24 hours of DMSO (no drug control), 10 \times EC₅₀ (740 nM) of CT3, 25 \times EC₅₀ (20 μ M) of BZN or 200 \times EC₅₀ (20 μ M) of GNF6702. Data show mean and SD of at least four independent experiments. Scale bar = 5 μ m. Statistical analysis was carried out using student t-test (ns: non significant; ** p<0.01; **** p<0.0001)



25

in the presence of increasing concentrations of CTs. Mutants showed a significant EC₅₀ shift (represented in fold-over WT, left panel) when treated with CT compounds, compared to proteasome inhibitor (GNF6702), CLK1 inhibitor (AB1) and suramin, a known anti-trypanosomal agent. Representative EC₅₀ curves are shown for CT1, CT3 and CT5 (right panel). EC₅₀ values of two biological replicates were calculated from concentration-response curves performed in duplicate after nonlinear fitting with GraphPad Prism. Statistical analysis was carried out using student t-test (ns: nonsignificant; *p<0.05; **p<0.01; ***p<0.001; ****p<0.0001) (B) Schematic representation of the topoisomerase II domain structure. Triangles highlight positions of homozygous mutations. These mutations were mapped onto the yeast full-length topoisomerase II structure (PDB: 4GFH) in magenta and labeled with their type and residue number from the *T. b. brucei* sequence. One monomer of topoisomerase II is colored in cyan, and the second monomer is colored in green. (C) Anti-parasitic activity of CT compounds against parental and CRISPR *T. b. brucei* strains. Data presented were generated with a minimum of four independent biological replicates. Statistical analysis was carried out using student t-test (***p<0.001). Sanger sequencing of parental and CRISPR strain of *T. b. brucei*. Sequencing of the *topoIIα* and *topoIIβ* gene fragments around the mutated residue showed that both the alpha and beta variants had introduced the mutation, with the alpha variant appearing to have also converted to the beta sequence upstream. This suggests a probable recombination event with an initial introduction of the mutation into the beta variant followed by recombination to introduce the mutation plus surrounding residues to the alpha locus under drug selection. Triangles are homozygous mutations and circles are heterozygous mutations seen with CT resistant mutants.

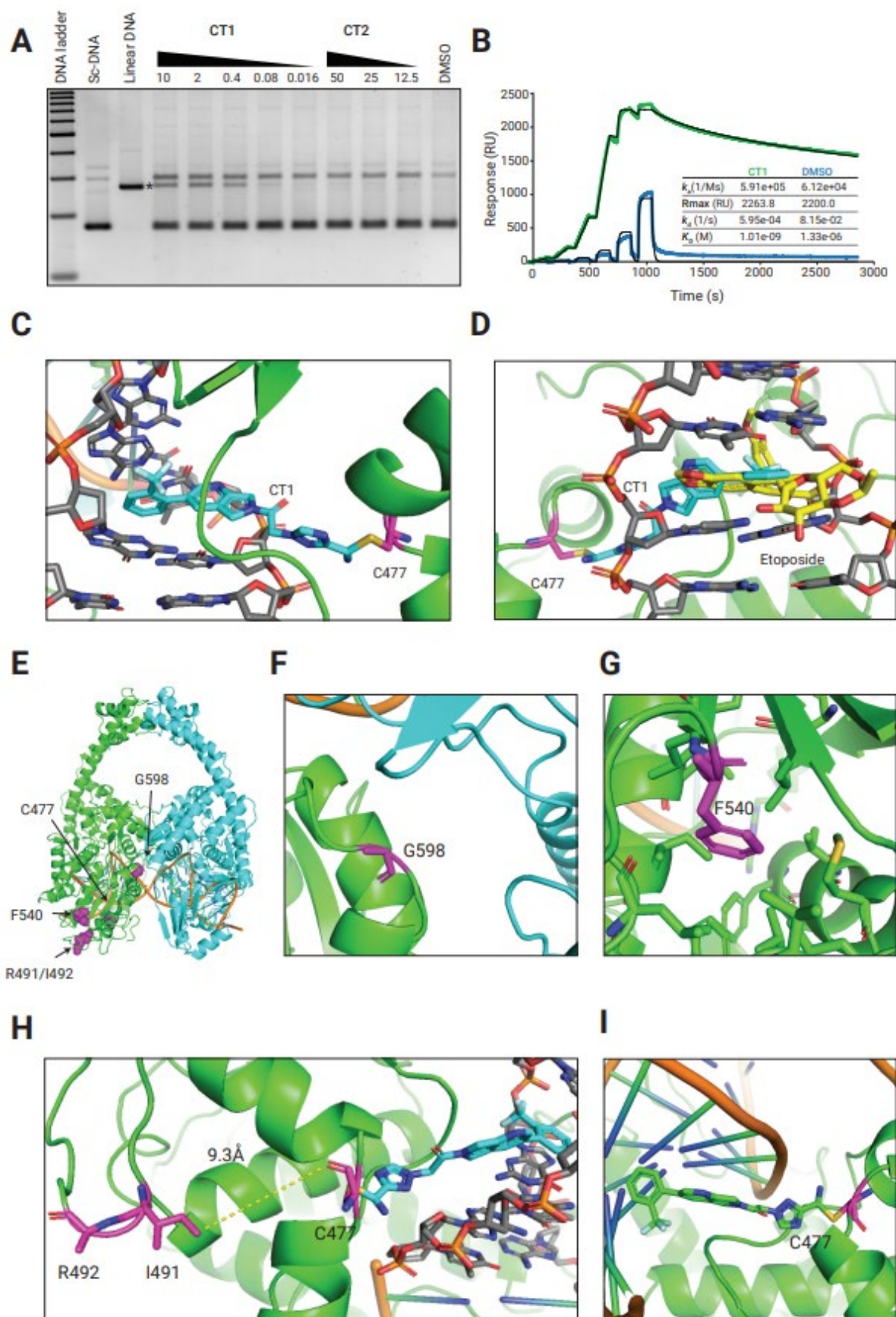


Figure 4 Biochemical and structural validation of Topoll as target of CTs (A)

Biochemical characterization using Topoll DNA cleavage assay in the absence of ATP.

Full-length *T. cruzi* Topoll was incubated with supercoiled DNA (ScDNA) in the

presence of varying concentrations (μM) of CT compounds, and the ability to induce

dsDNA breaks was measured by running products on a 1.2% agarose gel. The

experiment was conducted with two biological replicates; one of the representative

images is shown. Note that CT1 caused increasing levels of linear double-strand DNA

(asterix) to appear as the concentration increased (B) Representative surface plasmon

resonance (SPR) sensorgram of SPR experiment showing the association of truncated

T. cruzi topoll Δ C 2-1182 with immobilized dsDNA in the presence of CT1 (green),

DMSO control (blue). The 1:1 model of the response is shown (black). (C) CTs bind to

the DNA cleavage site as revealed by cryo-EM. View of the binding site of the TcTopoll-

DNA complex bound to CT1 (shown in cyan). CT1 intercalates between the DNA base

pairs at the DNA cleavage site and forms a covalent bond with the reactive cysteine

C477 (shown in magenta), which is conserved in trypanosomatid Topoll. (D) Etoposide

(from PDB 5GWK, shown in yellow) superimposed on the CT1 cyro-EM structure

reveals that CT1 binds to the same binding site as etoposide, which is a known human

TOP2A inhibitor. (E) Mutations found in *T. b. brucei* resistant mutants (CT1.1, CT1.2,

CT4.1, CT5.1 and CT5.2) are highlighted as magenta spheres on the cryo-EM structure

of the Tc Topoll DNA binding domain (amino acids 401-1178) bound to DNA and CT1.

TcTopoll monomers are colored in cyan and green and the DNA backbone is colored in

orange. (F-I) Close up view of the different resistant mutation sites with the mutated

amino acids shown in magenta in stick representation.

Supplementary Materials for

Topoisomerase II inhibitors rapidly cure trypanosome infections

Srinivasa P. S. Rao^{1*}, Matthew K. Gould², Jonas Noeske³, Manuel Saldivia¹, Rajiv S. Jumani¹, Pearly S. Ng⁴, Olivier René¹, Yen-Liang Chen¹, Marcel Kaiser^{5,6}, Ryan Ritchie², Amanda F. Francisco⁷, Nila Johnson¹, Debjani Patra¹, Harry Cheung¹, Colin Deniston⁸, Andreas D. Schenk⁹, Wilian A. Cortopassi³, Remo S. Schmidt^{5,6}, Natalie Wiedemar^{5,6}, Bryanna Thomas¹, Rima Palkar¹, Nahdiyah A. Ghafar⁴, Vanessa Manoharan⁴, Catherine Luu³, Jonathan E. Gable¹, Wan K. Fei⁴, Elmarie Myburgh¹⁰, Jeremy C. Mottram¹⁰, Whitney Barnes⁸, John Walker⁸, Charles Wartchow³, Natasha Aziz¹, Colin Osborne¹, Juergen Wagner⁴, Christopher Sarko¹, John M. Kelly⁷, Ujjini H. Manjunatha¹, Pascal Mäser^{5,6}, Jan Jiricek¹, Suresh B. Lakshminarayana¹, Michael P. Barrett^{2*}, Thierry T. Diagana^{1*}

Correspondence to: srinivasa.rao@novartis.com; michael.barrett@glasgow.ac.uk; thierry.diagana@novartis.com

This PDF file includes:

Materials and Methods

Figs. S1 to S16.

Tables S1 to S7

Data S1 (.xls)

References (37-50)

Materials and Methods

Cellular assays. Culture of kinetoplastid parasites and growth inhibition assays:

Kinetoplastid parasites, bloodstream forms of *Trypanosoma brucei brucei* Lister427, *T. b. gambiense* STIB930, *T. b. rhodesiense* STIB900, *T. cruzi* Tulahuen amastigotes and *Leishmania donovani* MHOM/SD/62/1 S-CL2D axenic amastigotes, were grown in appropriate media as described previously (8). Growth inhibition studies using these parasites were carried out using methods described earlier (8, 17, 37). EC₅₀ refers to the 50% growth inhibition potential of compounds as determined by the sigmoidal dose response values analyzed by HELIOS software.

Cytotoxicity measurement using 3T3 and HepG2 cell lines: The NIH 3T3 fibroblast and HepG2 human hepatoma cell lines were obtained from ATCC and grown in RPMI medium. Cytotoxicity of compounds against these cells were determined using standard protocols (8, 37)

Kill kinetics and washout assay against *T. b. brucei* Lister 427 strain were performed as described earlier (17). Briefly, for the kill kinetics assay, compound-containing plates were incubated with 1×10^5 parasites per mL and at each time point, CellTiter Glo (CTG) reagent (Promega) was added to lyse the parasites and the ATP content was measured by determining the luminescence units using a CLARIOstar plate reader (BMG Labtech). Wash-out experiments were carried out to determine the absolute concentration required to achieve sterile cure under in vitro conditions. For this, compound was incubated with 1×10^6 parasites per mL for 6 and 24 hours, removed by washing three times and the parasites then allowed to grow for another 48 hours. At the end of 48 hours, CTG reagent was added to lyse the parasites and ATP content, as a surrogate for viability, was measured by determining the luminescence units using a CLARIOstar plate reader.

Kill kinetics and washout experiments were performed using *T. cruzi* Tulahuen strain constitutively expressing *E. coli* β -galactosidase. For time to kill experiments, NIH 3T3 fibroblast cells were infected with *T. cruzi* Tulahuen trypomastigotes at a multiplicity of infection (MOI) of 5 and incubated at 37°C in 5% CO₂ for 48 hours. NIH 3T3 cells infected with *T. cruzi* intracellular amastigotes were harvested and adjusted to a density of 3×10^4 cells/mL. Approximately 1.2×10^3 NIH 3T3 infected cells (50 μ L) were seeded in 384-well white bottom plates (Greiner) containing 100 nL of test compounds at various concentrations ranging from 25 μ M to 1 nM. Each assay comprises a set of 6 plates, one plate per time point, incubated at 37°C in 5% CO₂. The time of cell addition was considered time 0. At time points of 0, 24, 48, 72, 96 and 120 hours, luminescence was measured using the Beta-Glo® Luciferase Assay System kit (Promega) as per the manufacturer's instructions and readings taken using a CLARIOstar microplate reader (BMG Labtech). The assay quantifies β -galactosidase activity, which is directly proportional to the number of metabolically active *T. cruzi* parasites. The parasitocidal activity was calculated after normalizing the relative luminescence units (RLU) of each

dose to the viability of the drug-free control (corresponding to 100%). As a reference, the parasitocidal activity of benznidazole (active control) at a concentration of 20 μM and a read-out time of 72 hours was used. This value also correlates with the background luminescence signal of the assay, calculated based on the residual counts obtained for monolayers of uninfected fibroblasts at various confluences. The data are represented as the mean and standard error of at least four replicates. For each time point, luminescence from each well was normalized to the average luminescence of the drug-free control wells to calculate percent (%) RLU relative to drug-free control. The drug-free control normalized %RLU for each time point and each concentration of compound were plotted using GraphPad Prism version 8.1.2 (GraphPad Software).

For washout assays, *T. cruzi* intracellular amastigotes were adjusted to a density of 1×10^4 cells.mL⁻¹. Infected cells (2.5×10^3 in a volume of 250 μL) were seeded in 48-well tissue culture plates (Thermo Fisher). Plates were incubated at 37°C in 5% CO₂ for 4 hours to allow cell attachment. Test compounds were added at various concentrations equivalent to multiples of the EC₅₀ values. Infected cells were incubated in the presence of compounds at 37°C in 5% CO₂ for either 4 or 8 days. Every 4 days, the media were replaced with fresh culture media with the adequate concentration of test compound. Once the treatment period was completed, monolayers were washed extensively with culture media devoid of test compound. Cells were then maintained by replacing culture media twice weekly. The observation of the compound-treated plates for the presence of intracellular amastigotes and motile trypomastigotes were conducted thrice weekly for up to 25 days by microscopy with a standard Zeiss microscope at 40x magnification. A volume of 100 μL of Gibco™ Trypsin-EDTA (0.05%) was added to wells in which motile parasites were not detected on day 12 of the observation period. The cells were mixed and 20 μL of the cell suspension was transferred into the well of a new 48-well plate containing 600 μL of fresh culture media. Plates were incubated up to day 25 at 37°C in 5% CO₂. On day 25, culture media was removed from the wells in which *T. cruzi* trypomastigotes were not detected and β -galactosidase activity was measured by addition of 100 μL of Beta-Glo® Assay System (Promega). Cell lysate was transferred to a 96-well white opaque plate (Thermo Fisher) for luminescence measurement using a CLARIOstar luminometer (BMG Labtech).

Growth inhibition against apicomplexan parasites. Activity against *Plasmodium falciparum* 3D7 and *Cryptosporidium parvum* strains were evaluated by following protocols published earlier (38, 39).

In vitro and in vivo pharmacokinetic (PK) parameters. In vitro PK parameters such as solubility, microsomal clearance, permeability and mouse plasma protein binding were measured using methods described elsewhere (17).

In vivo studies were conducted using non-randomized female BALB/c mice (n= 3, 8-10 weeks old). All procedures involving animals were reviewed and approved by the institutional animal care and use committees. Sample size was determined based on the minimum number of animals required for good data distribution and statistics.

Blinding was not possible in these experiments, but animals were randomly selected for each group. Cyanotriazoles were formulated in a suspension formulation for per oral dosing (Methylcellulose: Tween80: Water :: 0.5: 0.1: 99.4 w/w/v); and solution formulation for intravenous dosing (NMP:4%BSA in PBS 10/90, v/v).

5 The blood samples for pharmacokinetic studies were collected between 0 and 24h post dose. The concentrations of compounds at various time points were determined by high-performance liquid chromatography coupled with tandem mass spectrometry (LC-MS/MS). The samples were extracted with acetonitrile: methanol (50:50) containing CHIR073911 as internal standard, using a 4 to 1 extractant to plasma ratio. Analyte
10 quantitation was performed by LC/MS/MS. Liquid chromatography was performed using a waters ultra-performance liquid chromatography (UPLC) system with the Waters HSS column (2.1 x 50 mm) at an oven temperature of 50°C, coupled with a API5500 triple quadruple mass spectrometer (Sciex Applied Biosystems, Foster City, CA). Instrument control and data acquisition were performed using the Applied Biosystems software
15 Analyst, version 1.6.2. Pharmacokinetic parameters were determined by noncompartmental analysis using Phoenix WinNonLin™ (Certara, Princeton, NJ).

For measurement of brain-to-plasma ratio mice were dosed 1 mg.kg⁻¹ intravenously using solution formulation. Animals were euthanized at 60 min post dosing, blood and brain tissue were collected. Compound concentration in these matrices were measured
20 as described above.

Mouse efficacy models. *Mouse infection models for human African trypanosomiasis (HAT).* CT3 was evaluated in hemolympathic (stage 1 HAT efficacy) and meningoencephalitis (stage 2 HAT efficacy) mouse models using established protocols as described earlier (17, 21).

25 Briefly, for evaluation in hemolympathic HAT model, 6-8 week old female NMRI mice were randomly selected from the cage and color tagged (head, back, and hump) on the day of infection. Mice were infected with bioluminescent strain of *T. b. brucei* STIB900. In order to confirm infection, mice were imaged on day 3 post infection, non-infected mice (mice that did not show parasitemia as measured by bioluminescence) were
30 excluded from the study. On day 3 post-infection, infected mice (sample sizes noted in legend to fig. S4B) were treated with varying doses of CT3 by oral gavage. These experiments were conducted at the Swiss Tropical and Public Health Institute (Basel) (License number 2813) according to the rules and regulations for the protection of animal rights ("Tierschutzverordnung") of the Swiss "Bundesamt für Veterinärwesen".
35 They were approved by the veterinary office of Canton Basel-Stadt, Switzerland.

The meningoencephalic mouse model was carried out at University of Glasgow animal facility, using 8 week old female CD1 mice. Mice were infected with bioluminescent *T. b. brucei* GVR35 strain and all mice were randomly allocated into experimental groups. Sample size (see legend to Fig 1B & fig. S4C) was determined using power calculation

with knowledge from previous experiments (8, 21). On day 21 post-infection, mice were treated with varying doses of CT3 by oral gavage. All animal protocols and procedures were reviewed and approved by the UK Home Office (Project License PCF371688 entitled “Biochemistry, genetics, virulence and drug action against trypanosomes and Leishmania”) and University of Glasgow Ethics Committees, in accordance with the Animals (Scientific Procedures) Act 1986 (ASPA). For both HAT efficacy studies, no data was excluded from the analysis.

Chagas efficacy models. CT3 was also tested in acute and chronic Chagas mouse infection models by following protocols described earlier (18, 20). Briefly, 6-8 week old female BALB/c mice were infected with bioluminescent *T. cruzi* CL Brener strain. Once infection is established by imaging, mice were randomly assigned to experimental groups. Sample size (see legend to Fig 1A & fig. S4A) was determined by following 3R principles and priori knowledge of similar experiments carried out (18, 20). For acute efficacy, mice were treated with varying dose of CT3 post 14 day infection, whilst for chronic efficacy ~100 day post infection mice were treated with CT3 by oral gavage. Acute and chronic Chagas mouse efficacy studies were carried out at Novartis and LSHTM facilities, respectively. No data was excluded from the analysis for all mouse experiments.

All mouse studies conducted at Novartis were approved by institutional animal care and use committee as well as institutional biosafety committee. For chronic Chagas mouse model, animal infections were performed under UK Home Office project licences PPL 70/8207 and PPL P9AEE04E4 and approved by the LSHTM Animal Welfare and Ethical Review Board (AWERB). All protocols and procedures were conducted in accordance with the UK Animals (Scientific Procedures) Act 1986.

Phenotypic characterization. *T. b. brucei* and *T. cruzi* γ H2A microscopy: *T. b. brucei* experiments were performed as described in Glover and co-workers (25). 1×10^6 *T. b. brucei* parasites per well were seeded in 24-well plates and incubated in the presence of DMSO or compounds at the indicated concentrations for 4 hours. *T. brucei* parasites were then collected, pelleted (3,000g, 5 minutes, room temperature), supernatant removed and re-suspended in 4% paraformaldehyde (PFA) in PBS. Fixed parasites were adhered to glass coverslips pre-coated with poly-L-lysine. For investigation of *T. cruzi* γ H2A response, tdTomato expressing *T. cruzi* trypomastigotes were allowed to infect 5×10^3 Vero host cells (Greiner 384-well plate #353962) for 48 hours prior to compound addition. *T. cruzi* parasites were then incubated for 24 hours in the presence of compound and fixed in 4% PFA (final). Both parasite species were permeabilized with 0.5% Triton X-100 (Sigma) in PBS and blocked in bovine serum albumin (BSA; Sigma) in PBS. γ H2A was detected by sequentially incubating with affinity purified polyclonal rabbit antibody (*T. brucei* : KHAKA[pT]PSV; *T. cruzi*: KKARA[pT]PSA;

Thermo Fisher), diluted 1:250 in blocking buffer and a goat anti-rabbit AlexaFluor488 antibody (1:1000 in blocking buffer, Abcam 150081). *T. brucei* coverslips were mounted on microscope slides with hard-set vectashield mounting medium containing DAPI (Vector Laboratories H-1800). *T. cruzi* parasites were incubated for 15 minutes in Hoechst 33258 (AnaSpec) in 1% BSA (Sigma) in PBS before leaving in PBS and sealing the plates. Coverslips for *T. b. brucei* were imaged using 40x 0.95 NA air objective on Nikon Ti-2E. Plates for *T. cruzi* were imaged 20x water-immersion objective on Molecular Devices ImageXpress Confocal.

EdU incorporation assay: *T. cruzi* CL trypomastigotes expressing tdTomato were allowed to infect 5×10^3 Vero host cells per well in 384-well glass bottom plates (Cellvis) pre-coated with 50-100 $\mu\text{g/mL}$ of fibronectin (Corning, catalog# 354008) as per the manufacturer's protocol. After 48 hours of infection, compounds and EdU (final concentration, 10 μM) were added. After incubation of cells with EdU for 2 hours, cells were fixed by adding PFA (4% final concentration in well). PFA was removed, cells washed, permeabilized with 0.5% Triton X100, washed again and stained for EdU using the Click-iT® assay kit (Thermo Fisher Scientific, catalog# C10340) as per the manufacturer's instructions. Plates were imaged using 60x water-immersion objective on Molecular Devices ImageXpress Confocal.

γH2A Phosphorylation western blots: Whole cell protein extracts were harvested from $\sim 2.5 \times 10^6$ cells per sample that had been treated, or not, with CT1 (at 5x wildtype EC_{50} = 800 nM) for 4 hours, or else the mutagen MMS. Extraction involved boiling in 10 μL loading buffer (1X NuPAGE® LDS Sample Buffer (Life Technologies), 0.1% β -mecaptoethanol, 1X PBS) for 10 min. Proteins were separated using NuPAGE Novex® 10-12% Bis-Tris protein gels (Life Technologies) and transferred to PVDF membranes. Proteins were detected with anti- γH2A (1:1000) and mouse anti-Ef1 α clone CBP-KK1 (1:25,000; Millipore) primary antibodies, and goat anti-mouse/rabbit IgG (H+L) fluorescently tagged conjugates.

Metabolomics. 100 mL cultures were seeded with 1×10^5 bloodstream form trypanosomes/mL (*T. brucei* strain 427) in HMI-11 (HMI-9 supplemented with 10% Fetal Calf Serum) for 24 hours at 37 °C and 5% CO_2 . 1275 nM CT1 in 100 μL DMSO was added to the test culture, with 100 μL DMSO only added to the no-drug control culture and incubated for a further 4 hours at 37°C, 5% CO_2 . The cell density of each culture was then measured by hemocytometer and the volume of medium containing 1.5×10^8 cells was transferred to 50 mL Falcon tubes. The metabolism of the cells was immediately quenched by rapidly cooling the cultures to 4°C by submerging the Falcon tubes in a dry ice and ethanol bath and agitating vigorously. The cells were pelleted by centrifugation for 10 minutes at 1,250 rcf and 4°C and the majority of the supernatant was carefully removed. The cell pellet was gently resuspended in the remaining supernatant and transferred to 1.5 mL microfuge tubes, re-pelleted by centrifugation for 5 minutes at 1,900 rcf and 4°C, before all remaining medium was removed by pipette.

The cell pellet was washed once by resuspension in 1 ml PBS at 4 °C, followed by centrifugation at 1,900 rcf and 4 °C for 5 minutes. The PBS supernatant was removed by pipette and 300 µl of 4 °C extraction solvent (Chloroform:Methanol:Water, 1:3:1) was added to the cell pellet and thoroughly mixed by vortex. The microfuge tubes were then left shaking vigorously for 1 hour at 4 °C before a final centrifugation at maximum rcf for 10 minutes and 4 °C. 180 µl of the supernatant was transferred to pre-chilled glass mass spectrometry vials and the air replaced by Argon gas before sealing and storing at -80 °C. 4 biological replicates for each condition were generated over separate days. LCMS analysis was carried out by Glasgow Polyomics using pHILIC columns and an Orbitrap Fusion mass spectrometer according to standardized protocols (22). Relative abundance comparisons for each metabolite was carried out using IDEOM software package (40) Heatmaps and volcano plots were generated using MetaboAnalyst 5.0.

Mutant generation and whole genome sequencing. CT resistant mutants were generated using *T. b. brucei* Lister 427 strain. Parasites were incubated with sub-lethal concentration (0.1X EC₅₀) of various CT compounds and continually passaged until the growth rate matched *T. b. brucei* strain growing in the presence of 0.25% DMSO. Once the growth rate matched that of DMSO treated parasites, the concentration of CTs were increased by 2 fold (e.g. 0.1x EC₅₀ to 0.2x EC₅₀). Every time, before increasing the concentration of the CT compounds, parasites were tested for their ability to show drug resistance, by testing growth inhibition against respective CT compound. DMSO treated parasites were used as a control, and did not show shift in EC₅₀ against CTs. This process was repeated until parasites showed a significant shift in EC₅₀. It took 3-6 months to generate mutants that were resistant to CT compounds. Resistant clones were isolated using limiting dilution. Each clone was tested for its resistance to several CT and other compounds using methods described earlier (17).

Genomic DNA from resistant clones was isolated using Qiagen DNeasy kit (Qiagen). Whole genome sequencing was performed using Illumina Hiseq1000 next generation sequencing platform as described earlier (41).

Growth inhibition studies using RNAi constructs of *topoIIα*. Test compounds were doubly diluted in 96-well plates (Greiner) with HMI-11 medium for testing efficacy using a derivative of the alamar blue assay (42). For the Pulse RNAi experiments to determine impacts of transient *topoIIα* knockdown, RNAi lines were induced with the stated concentration of doxycycline (Sigma) for 24 hours before being diluted 100-fold in fresh HMI-11 medium without doxycycline. An equal volume (100 µL) of bloodstream form trypanosomes in medium was added to each well to give a final cell density of 1 × 10⁵ trypanosomes/ml. The plates were incubated for 72 hours at 37°C, 5% CO₂, after which 20 µL of 0.5 mM resazurin sodium salt (Sigma) in phosphate-buffered saline (PBS) was added to each well, followed by a further 4-hour incubation under the same conditions. Fluorescence was measured using a FLUOstar Optima fluorimeter (BMG Labtech) with excitation and emission filters of 544 nm and 590 nm, respectively. Data were analyzed using GraphPad Prism software, and EC_{50s} were derived from sigmoidal dose-response curves with variable slopes. The EC₅₀ values reported here are the

averages of at least three independent experiments. Efficacy of compounds was also tested against a range of strains engineered to lack particular genes involved in DNA repair including RAD51 (43) and BRCA2 (44).

CRISPR-directed mutagenesis. The *T. b. brucei* cell line with doxycycline-inducible Cas9 endonuclease expression, and constitutive transcription of guide-RNA that targets cleavage of *topoII α* , six bases downstream of the F540 codon was generated in the manner as described (45). The oligonucleotide pair 5'-AGGGTGGGAGTTATGAACTGCTGG-3' and 5'-AAACCCAGCAGTTCATAACTCCCA-3' were annealed to give BbsI-compatible overhangs by heating to 70 °C for 3 minutes followed by slow cooling and ligated to the BbsI digested pT7sgRNA construct. After sequencing to confirm its correct generation, the pT7sgRNA construct containing the gRNA was linearized with NotI before electroporation into the Tb427-2T1T7-Cas9 cell line (that inducibly expresses the Cas9 endonuclease) and selected for genomic integration with 2.5 $\mu\text{g.mL}^{-1}$ phleomycin. The resultant cell line was transfected with 40 μg of the repair template (with modification from original sequence in bold): 5'-GCCTGACCTGCTGAAAGTGCCTGGCTT**G**CTCCAGCAGTTCATAACTCCCATTGTGAAGGC-3' introducing the F540L mutation (the change underlined in bold text above).

Cas9 expression was induced with 1 $\mu\text{g.mL}^{-1}$ doxycycline or left uninduced and the transfected cultures were left to recover for 24 hours under standard culturing conditions. Acquisition of resistance to CT compounds was assessed in the induced and uninduced cultures by continuous growth in the presence or absence of 5x EC₅₀ value of CT1. CT-resistant cultures were cloned by limiting dilution and genomic DNA extracted using NucleoSpin Tissue gDNA extraction kits (Macherey-Nagel). The *Tb topoII α* and β loci were amplified separately by PCR for Sanger sequencing.

Protein expression. *T. cruzi* topoisomerase II (TcCLB.508699.10; UniProt#Q4DE53) was expressed using a baculovirus expression vector system (BEVS). Sf21 insect cells were infected with 3% virus at a cell density of 1.5×10^6 cells.mL⁻¹. Cells were harvested 48 hours post infection by centrifugation. Cell pellets were resuspended in Buffer A (20 mM Bis-Tris pH6.0, 250 mM KCl, 5% glycerol, 10 mM imidazole, 1mM TCEP) with 25 μM N-p-Tosyl-L-phenylalanine chloromethyl ketone, 2mM Phenylmethanesulfonyl fluoride solution, 1x Protease Inhibitor Tablet EDTA-free (Thermo) and Universal Nuclease (1:10K dilution, Thermo), at a 1:5 (pellet : lysate volume) ratio. The cell suspension was lysed in a microfluidizer (Microfluidics) with 2 passes at 19K psi. The lysate was cleared by centrifugation at 60 000 x g for 30 minutes at 4°C. The first step of purification involved immobilized metal ion affinity column chromatography (IMAC: nickel sepharose FF, Cytiva) with Buffer B (equivalent to Buffer A + 250 mM imidazole). The IMAC eluted fractions were pooled and incubated with recombinant Tev protease (rTev) and dialyzed against Buffer A without imidazole. The second step used a reverse IMAC, utilizing Buffer C (20 mM Bis-Tris

pH 6.8, 200 mM KCl, 5% glycerol, 10 mM Imidazole, 1 mM TCEP) and Buffer D (Buffer C with 250 mM imidazole), pooling the flowthrough and a 50 mM imidazole wash. The reverse IMAC pool was diluted four-fold with Buffer E (50 mM HEPES pH 6.8, 5% glycerol, 1 mM TCEP) and purified over an Ion Exchange Column (IEX), MonoQ (Cytiva), with a gradient from 350 mM KCl to 600 mM KCl (25 column volumes) using Buffer F (Buffer E + 50 mM KCl) and Buffer G (Buffer E + 1M KCl).

The pooled IEX fractions for TcTopoII (2-1182) were concentrated using a 100KDa MW cut off concentrator (Merck Millipore). This was followed by purification over a gel filtration column (SEC: Superdex 200, Cytiva) with Buffer H (50 mM Hepes pH 6.8, 200 mM KCl, 5% glycerol, 1 mM TCEP). The final sample of TcTopo (2-1182) was concentrated to 5.5mg/mL. For the purification of TcTopo-Tev-8xHis (2-1476) Full-length and TcTopoII (401-1178) DNA Binding Domain (DBD) the lysis step was the same as used in the purification of the C-terminal truncated domain, except all the buffers are in 50mM HEPES, pH 8.0. The first step of purification was by IMAC using step elution with Buffer C. The IMAC pooled fractions were incubated with rTev and dialyzed against buffer C without Imidazole. The second step was a reverse IMAC, pooling the flowthrough and 50 mM imidazole wash. The second IMAC pool was diluted with Buffer E (4-fold) and purified over an Ion Exchange Column (IEX), MonoQ (for TcTopo Full-length) HiTrapQ HP (Cytiva) (for TcTopo DBD), with Buffer F and G, using a gradient from 50 mM to 500 mM (20 column volumes) and 500 mM to 1M (5 column volumes). The TcTopo Full-length protein was dialyzed in final Buffer H and concentrated to 0.3mg.mL⁻¹. The final column purification of the TcTopo DBD was over a Gel Filtration Column (SEC: Superdex 200, Cytiva) using Buffer H. The pooled eluate was concentrated with a 50 KDa molecular weight cut off concentrator (MilliporeSigma). TcTopoII DBD was concentrated to 11.5mg/mL.

Biochemical assays. The TcTopo II cleavage assay was performed by first incubating 80 nM of recombinant *T. cruzi* Topo II in the presence of various concentrations of compounds in the reaction buffer containing 50 mM Tris-HCl (pH 8.0), 150 mM NaCl, MgCl₂, 500 μM DTT, 0.03 mg/ml bovine serum albumin (BSA) in 10 μL solution at room temperature for 30 minutes. The supercoiled pHOT-1 DNA (Topogen) was then added to start the reaction and the final volume of the reaction was 20 μL with 2.5 ng/ml of pHOT-1. The mixture was incubated at 37°C for 90 minutes. To stop the reaction, 4 μL SDS (10%) and 4 μL Proteinase K (2 mg/mL) were added and the reaction further incubated at 37°C for 15 minutes. To visualize the product, 6 μL of 6x loading dye (Promega) was added and the mixture loaded onto the 1.2% agarose gel and run at 17V for 20 hours. The gel was then stained with SYBR Gold at 1:10K dilution before being scanned and quantified.

Human topoisomerase IIα (hTOP2A) cleavage assay was performed with 500 ng of supercoiled pBR322 incubated with 1U of hTOP2A in the buffer containing 50 mM Tris

HCl (pH 7.5), 125 mM NaCl, 10 mM MgCl₂, 5 mM DTT, 0.5 mM EDTA, 0.1mg/ml bovine serum albumin (BSA) and 1mM ATP in 30 μ l reaction mixture at 37°C for 30 minutes. The reaction mixture was further incubated with 1% SDS and 0.5 μ g/ μ l of protease K for another 30 minutes and stopped with by addition of 30 μ l of chloroform/iso-amyl alcohol (24:1) and 30 μ l of Stop Dye. The 1% TAE gel for the assay contained 0.5 μ g/ml ethidium bromide was run at 85V for 2 hours. The gels were destained for 10 minutes in water before being scanned and quantified. Assays were performed at Inspiralis.

Surface plasmon resonance (SPR) and cryogenic electron microscopy (cryo-EM)

studies. DNA preparation. For SPR studies the following two custom made DNA oligonucleotides were ordered from IDT: forward: 5' Biotin-CAC GGT GCC GAG GAT AAC AAT GAG CTC ATT GTT ATC CTC GG 3'; reverse: 5' CC GAG GAT AAC AAT GAG CTC ATT GTT ATC CTC GGC ACC 3'. Each oligonucleotide was dissolved in IDT duplex buffer (30 mM HEPES, pH 7.5, 100 mM potassium acetate) to a final concentration of 4 mM. Equal volumes of forward and reverse oligonucleotide were mixed and annealed by heating the mixture to 90 °C for 5 minutes then slowly cooling the mixture to room temperature over a period of 2 hours. This yielded 2 mM annealed dsDNA. For EM studies a DNA oligonucleotide with the sequence 5' GG GAT AAC AAT GAG CTC ATT GTT ATC CC 3' was ordered from IDT and dissolved in IDT duplex buffer to a final concentration of 6 mM. The DNA oligonucleotide was self-annealed using the annealing protocol as described above for the SPR DNA yielding 3 mM annealed dsDNA.

Analysis of TcTopoll:dsDNA interaction by SPR. SPR analysis for the determination of K_D , k_a and k_d , were performed with a Biacore 8K instrument in 20 mM Hepes pH 7.3, 100 mM KCl, 10 mM MgCl₂, 5% glycerol, 0.05% Tween-20, and 0.5 mM TCEP at 20°C and 100 mL/min flow rate. dsDNA for this experiment is as follows: forward: 5' Biotin-CACGGTGCCGAGGATAACAATGAGCTCATTGTTATCCTCGG 3'; reverse: 5' CCGAGGATAACAATGAGCTCATTGTTATCCTCGGCACC 3') covalently modified with biotin at the 5' end of the forward oligo. dsDNA was loaded onto a streptavidin-coated Biacore Sensor Chip SA (GE Healthcare) to 100 RU. TcTopoll (residues 2-1182) binding to dsDNA in the presence or absence of 350 μ M compound CT1 was measured using a 6 point, 3X dilution series starting at 1 μ M Topoll with the single cycle kinetics method according to instrument control software instructions. Data were analyzed using the Biacore Evaluation application to generate affinity constants (K_D), association rate constant (k_a), dissociation rate constant (k_d), and maximum response unit (R_{max}).

Cryo-electron microscopy for structure determination.

Complex formation for cryo-EM. For cryo-EM studies, the complex of *T. cruzi* Topoll DNA-binding domain (*T. cruzi* Topoll DBD, amino acids 401-1178) bound to dsDNA (5'

GG GAT AAC AAT GAG CTC ATT GTT ATC CC 3') and CT1 was formed using the following protocol. 21.4 μM (or 1.91 mg/mL) *T. cruzi* Topoll DBD was incubated in the presence of 75 μM dsDNA and 300 μM CT1 in 20 mM HEPES, pH 7.3, 100 mM KCl, 3 mM MgCl_2 , 1 mM TCEP for 1 hour on ice. Prior to applying the complex sample to the grid, the complex was diluted to 0.5 mg/mL in the above-mentioned buffer keeping the CT1 concentration constant at 300 μM .

Vitrified sample preparation and data collection. 300-mesh Quantifoil UltrAu 1.2/1.3 grids (Quantifoil, Micro Tools GmbH, Grossl bichau, Germany) were glow discharged for 90 s at 15 mA in a PELCO EasyGlowTM glow discharger (Ted Pella, Redding, CA, USA) directly before use.

4 μl of complex was applied to each grid and the grids were blotted for 5 s using standard Vitrobot filter paper, $\varnothing 55/20\text{mm}$, Grade 595 (Ted Pella) with a blot force of 25 and plunged into liquid ethane using a Vitrobot MK4 (Thermo Fisher Scientific, Waltham, MA, USA) operated at 4 $^\circ\text{C}$ and 100 % chamber humidity.

All cryo-EM data were acquired at nominal magnification of 75,000x using a Cs-corrected Titan Krios transmission electron microscope (Thermo Fisher Scientific) operated at 300 kV acceleration voltage.

Tilted and untilted data were collected to counter the effect of preferred particle orientation visible in the untilted data.

Movies for a 30 $^\circ$ tilted dataset were collected in EPU 3.0 (Thermo Fisher Scientific) using a bottom mounted Falcon 4i direct electron detector (Thermo Fisher Scientific) in Electron Event Representation (EER) mode with an exposure time of 3.8 s and an exposure rate of 9.23 e/pixel/s at a calibrated pixel size of 0.845 \AA /pixel. EPU was configured to record groups of 3x3 foil holes by image shift to speed up data collection. The defocus range for the central foil hole of the group was set from -1.4 μm to -1.8 μm in 0.2 μm increments.

Movies for an untilted dataset were collected in EPU 3.0 (Thermo Fisher Scientific) in EER mode using a bottom mounted Falcon 4 direct electron detector (Thermo Fisher Scientific) with an exposure time of 3.98 s and an exposure rate of 8.74 e/pixel/s at a calibrated pixel size of 0.845 \AA /pixel. EPU was configured to record groups of 3x3 foil holes by image shift. The defocus range was set from -0.6 μm to -2.0 μm in 0.2 μm increments.

Data Analysis. Recorded movies for tilted and untilted datasets were processed in parallel to data acquisition by using CryoFLARE(46). Motion correction was performed using the Relion 3.1.2 EER motion correction implementation. EER movies were fractionated into 50 frames. CTF parameters were determined using GCTF in a two-stage refinement.

The best 3,014 micrographs in the tilted dataset in terms of drift and CTF fit were exported from CryoFLARE for further processing in CryoSPARC. The CTF for the

micrographs was estimated using patch CTF to account for the defocus gradient from tilting, and particles were picked using blob picker with a circular and elliptic blob of diameter 120 Å – 150 Å, yielding 955,991 particles. Particles were extracted using an initial box size of 384x384 pixels, which was down sampled to 192x192 pixels. Poorly picked particles were filtered out by two subsequent rounds of 2D classification into 50 classes using CryoSPARC default parameters. All subsequent model generation, classification and refinement steps were performed in C2 symmetry using CryoSPARC default parameters unless otherwise noted. The resulting particle stack of 343,936 particles was used to generate 10 initial models. The highest resolution initial model was used as a model to run homogenous refinement for the whole particle stack followed by non-uniform refinement. Particles were re-extracted with a box size of 384x384 pixels and classified into 3 classes by hetero refinement with a refinement box-size of 384, using the volume from the previous non-uniform refinement as reference. The highest resolution class from hetero refinement containing 139,502 particles was further refined by one round of homo refinement followed by non-uniform refinement, local CTF refinement and another round of non-uniform refinement.

The best 2,220 micrographs in the untilted dataset in terms of drift and CTF fit were exported from CryoFLARE for further processing in CryoSPARC 4. The CTF for the micrographs was estimated using patch CTF, and particles were picked using blob picker with a circular and elliptic blob of diameter 120Å – 150Å, yielding 703,407 particles. Particles were extracted using an initial box size of 384x384 pixels, which was down sampled to 192x192 pixels. Poorly picked particles were filtered out by two subsequent rounds of 2D classification into 50 classes using the CryoSPARC default parameter. The resulting particle stack of 280,556 particles was re-extracted with a box size of 384x384 pixels.

The resulting particles from tilted and untilted datasets were merged and hetero refined into 3 classes using the non-uniform refined volume from the tilted dataset as reference. All resulting classes were homo refined. The highest resolution refined class containing 179,787 particles was further refined using one round of non-uniform refinement, yielding a map at 2.94 Å resolution.

The local resolution for the final refined map was calculated using ResMap (47). The sphericity and directional FSC was evaluated using 3DFSC (48).

Model refinement: The Alphafold structure of *T. cruzi* DNA Topoisomerase II (Uniprot accession code Q4DE53) was used as a starting model for the refinement process. In Phenix dock_in_map was used to initially place the Alphafold model into the EM map (49). The model was then refined using phenix.real_space_refine with standard settings including secondary structure and NCS restraints. In the first refinement run rigid body refinement was enabled. Grade from Global Phasing was used to generate a restraint file for the ligand and the ligand was manually placed into the EM density (50). In order to improve the geometry around the covalent bond, the sulfur of C477 was included in

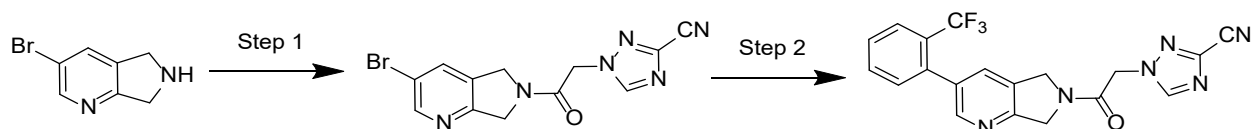
the restraint file of the ligand. In phenix.real_space_refine a parameter file was included to define the link between the C477 CB and the sulfur.

Chemistry. Synthesis of cyanotriazoles

5 All reactions were performed under an atmosphere of argon. HPLC grade solvents were purchased and used as is. All compounds are >95% pure by HPLC analysis.

Preparation of 1-(2-Oxo-2-(3-(2-(trifluoromethyl)phenyl)-5,7-dihydro-6H-pyrrolo[3,4-b]pyridin-6-yl)ethyl)-1H-1,2,4-triazole-3-carbonitrile (CT1)

10



15

20

Step 1. 1-(2-(3-Bromo-5,7-dihydro-6H-pyrrolo[3,4-b]pyridin-6-yl)-2-oxoethyl)-1H-1,2,4-triazole-3-carbonitrile : To a mixture of 3-bromo-6,7-dihydro-5H-pyrrolo[3,4-b]pyridine (300 mg, 1.51 mmol), 2-(3-cyano-1H-1,2,4-triazol-1-yl)acetic acid (344 mg, 2.26 mmol) and triethylamine (305 mg, 3.0 mmol) in dichloromethane (5 mL) was added 2,4,6-tripropyl-1,3,5,2,4,6-trioxatriphosphinane 2,4,6-trioxide (50% in DMF, 2.8 g, 4.5 mmol) in the presence of argon gas. The resulting reaction mixture was stirred at room temperature for 12 hours. The solvent was removed under reduced pressure and the product was purified by silica gel column chromatography (0-100% ethyl acetate in cyclohexane) to give the title compound (450 mg, 90% yield) as a white solid. LCMS ES⁺ *m/z* = 333.1 [M+1]⁺.

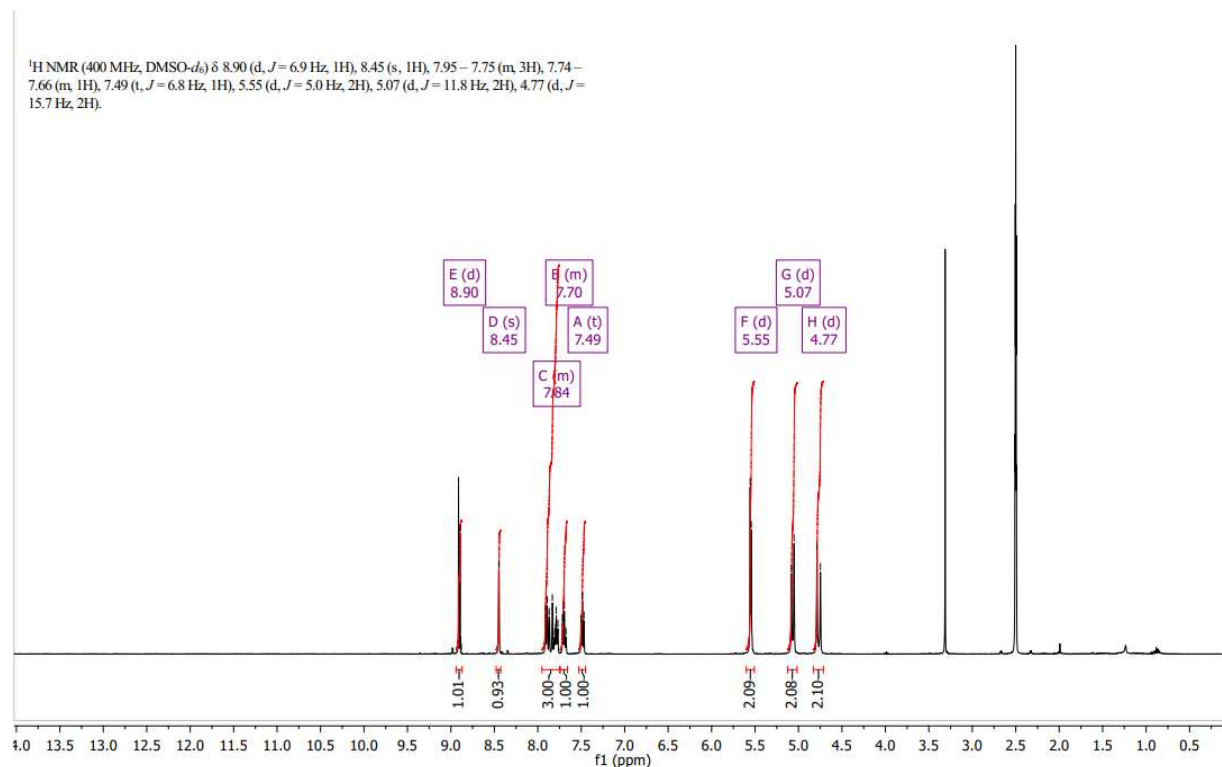
25

30

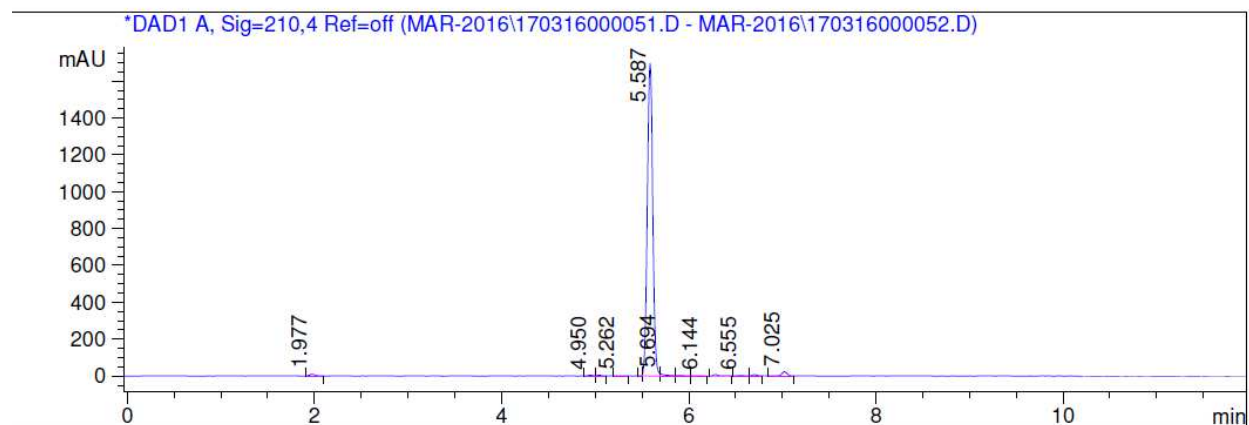
35

Step 2. 1-(2-Oxo-2-(3-(2-(trifluoromethyl)phenyl)-5,7-dihydro-6H-pyrrolo[3,4-b]pyridin-6-yl)ethyl)-1H-1,2,4-triazole-3-carbonitrile: A vial was charged with 1-(2-(3-Bromo-5,7-dihydro-6H-pyrrolo[3,4-b]pyridin-6-yl)-2-oxoethyl)-1H-1,2,4-triazole-3-carbonitrile (300 mg, 0.90 mmol), (2-(trifluoromethyl)phenyl)boronic acid (171 mg, 0.90 mmol), palladium diacetate (10 mg, 0.045 mmol), (9,9-dimethyl-9H-xanthene-4,5-diyl)bis(diphenylphosphine) (78 mg, 0.14 mmol), 1M sodium carbonate solution (1.80 mmol) and *N,N*-dimethylformamide (1 mL) in presence of argon gas. The resulting reaction was heated under microwave irradiation for 15 minutes at 120 °C. The reaction mixture was then adsorbed on silica gel and purified by silica gel column chromatography (0-100% ethyl acetate in cyclohexane) to give the title compound (63 mg, 17% yield) as a white solid. ¹H NMR (400MHz, DMSO-*d*₆) δ 8.90 (d, *J* = 6.9 Hz, 1H), 8.45 (s, 1H), 7.95 – 7.75 (m, 3H), 7.74 – 7.66 (m, 1H), 7.49 (t, *J* = 6.8 Hz, 1H), 5.55

(d, $J = 5.0$ Hz, 2H), 5.07 (d, $J = 11.8$ Hz, 2H), 4.77 (d, $J = 15.7$ Hz, 2H); LCMS ES⁺ m/z = 399.2 [M+1]⁺.



Column : Zorbax xdb C 18 5 μ 150x4.6MM
 Mobile Phase : A= 0.01% TFA inWater, B= ACETONITRILE
 GRADIENT : Time/%B:: 0/30, 2/40, 5/90, 7/100, 9/100, 10/30, 12/30
 Flow : 1.0 mL/min
 Temperature : 40°C

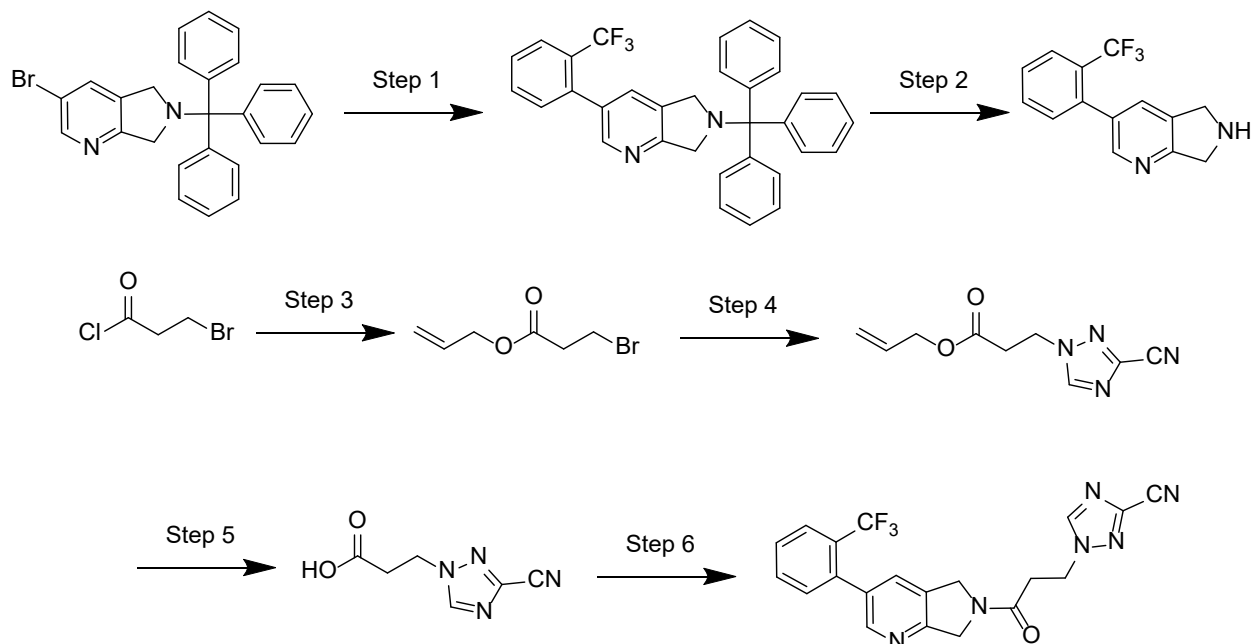


Signal 1: DAD1 A, Sig=210,4 Ref=off

Peak #	RT [min]	Width [min]	Area	Area %
1	1.977	0.076	43.578	0.607
2	4.950	0.065	15.567	0.217
3	5.044	0.058	13.776	0.192
4	5.262	0.080	5.350	0.075
5	5.500	0.023	7.000	0.097
6	5.587	0.067	6.859e3	95.524
7	5.694	0.049	48.121	0.670
8	5.913	0.121	19.576	0.273
9	6.144	0.110	10.128	0.141
10	6.286	0.067	31.352	0.437
11	6.555	0.097	12.125	0.169
12	6.704	0.061	25.493	0.355
13	7.025	0.064	89.295	1.244

Preparation of 1-(3-Oxo-3-(3-(2-(trifluoromethyl)phenyl)-5,7-dihydro-6H-pyrrolo[3,4-b]pyridin-6-yl)propyl)-1H-1,2,4-triazole-3-carbonitrile (CT2).

5



Step 1. 3-(2-(Trifluoromethyl)phenyl)-6-trityl-6,7-dihydro-5H-pyrrolo[3,4-b]pyridine:

A flask was charged with 3-bromo-6-trityl-6,7-dihydro-5H-pyrrolo[3,4-b]pyridine (5.0 g, 11 mmol), (2-(trifluoromethyl)phenyl)boronic acid (3.2 g, 17 mmol), Pd(dppf)Cl₂ (0.52 g, 0.057 mmol), potassium phosphate tribasic (3.6 g, 17 mmol), followed by 1,4-dioxane (50 mL) and water (15 mL), and the mixture was purged with argon. The reaction was

10

then stirred at 100 °C for 2 hours, then poured over ice water, extracted with ethyl acetate and concentrated. The product was purified by silica gel column chromatography (0-10% ethyl acetate in hexane) to give the title compound (3.9 g, 68% yield). LCMS ES⁺ m/z = 507.2 [M+1]⁺.

5

Step 2. 3-(2-(Trifluoromethyl)phenyl)-6,7-dihydro-5*H*-pyrrolo[3,4-*b*]pyridine: To a solution of 3-(2-(trifluoromethyl)phenyl)-6-trityl-6,7-dihydro-5*H*-pyrrolo[3,4-*b*]pyridine (7.8 g, 15 mmol) in dichloromethane (80 mL) and methanol (40 mL) at 0 °C was added trifluoroacetic acid (20 mL) and the reaction was stirred at room temperature for 2 hours. The reaction mixture was concentrated under reduced pressure and the residue was triturated with diethylether, decanted and dried to get the crude compound (13 g), which was used without further purification. LCMS ES⁺ m/z = 379.1 [M+1]⁺.

10

Step 3. Allyl 3-bromopropanoate: To a solution of bromopropionyl chloride (5.0 g, 29 mmol) in dichloromethane (50 mL) was added allylic alcohol (2.6 g, 44 mmol) and potassium phosphate tribasic (9.4 g, 44 mmol), and the reaction was stirred at room temperature for 12 hours. The reaction mixture was quenched with water, extracted with ethyl acetate, dried over sodium sulfate, concentrated and purified by silica gel column chromatography (5% ethyl acetate in hexane) to give the title compound (5.0 g, 89% yield), which was carried forward to the next step without characterization.

15

20

Step 4. Allyl 3-(3-cyano-1*H*-1,2,4-triazol-1-yl)propanoate: To a solution of allyl 3-bromopropanoate (5.0 g, 26 mmol) in acetonitrile (10 mL) was added 1*H*-1,2,4-triazole-3-carbonitrile (3.7g, 39 mmol) and potassium carbonate (5.4 g, 39 mmol), and the mixture was stirred at 80 °C for 12 hours. The reaction mixture was quenched with water, extracted with ethyl acetate, dried over sodium sulfate, concentrated and purified by silica gel column chromatography (50% ethyl acetate in hexane) to give the title compound (3.0 g, 56% yield). LCMS ES⁺ m/z = 206.1 [M+1]⁺.

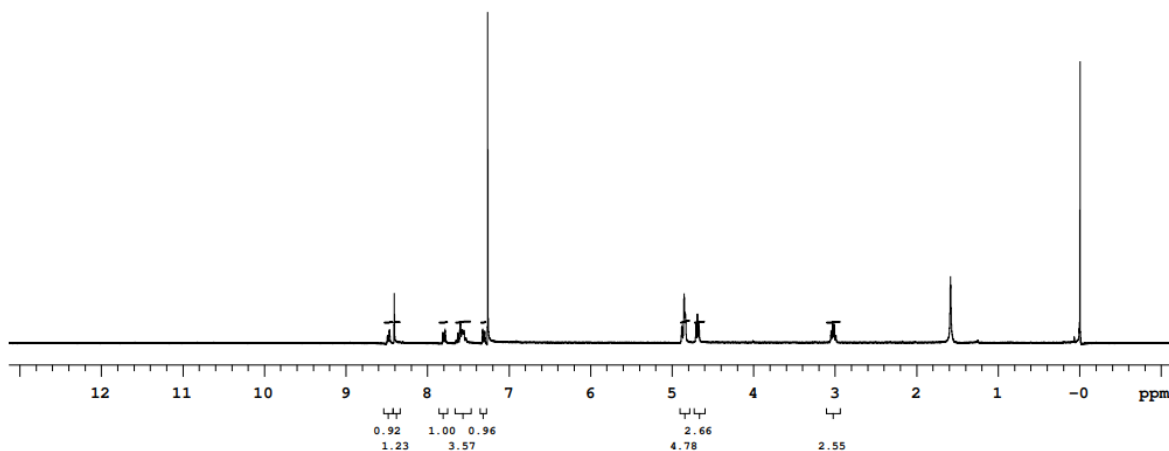
25

Step 5. 3-(3-Cyano-1*H*-1,2,4-triazol-1-yl)propanoic acid: To a stirred solution of allyl 3-(3-cyano-1*H*-1,2,4-triazol-1-yl)propanoate (3.0 g, 15 mmol) in dichloromethane (50 mL) was added tetrakis(triphenylphosphine)palladium(0) (1.7 g, 1.5 mmol), morpholine (2.0g, 15 mmol) and triphenylphosphine (3.8 g, 15 mmol), and the reaction was stirred at room temperature for 12 hours. The reaction mixture was filtered through celite filtered and concentrated to give crude compound. The crude compound was dissolved in 20 ml of water and washed with ethyl acetate to remove non polar impurities, then acidified the water layer to pH-6 with solid citric acid, then extracted with 10% MeOH in dichloromethane. The organic layer was concentrated to give the title compound (2.2 g) which was used without further purification. LCMS ES⁺ m/z = 167.1 [M+1]⁺.

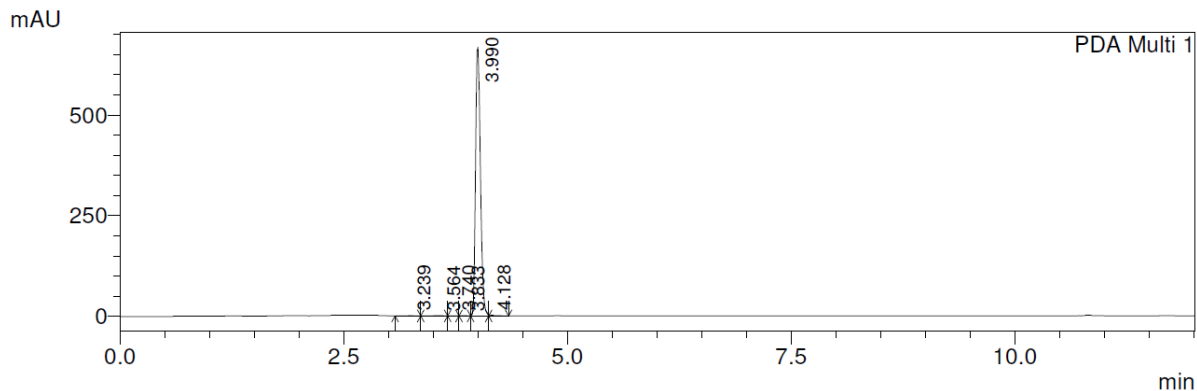
30

35

Step 6. 1-(3-Oxo-3-(3-(2-(trifluoromethyl)phenyl)-5,7-dihydro-6*H*-pyrrolo[3,4-*b*]pyridin-6-yl)propyl)-1*H*-1,2,4-triazole-3-carbonitrile: To a solution of 3-(3-cyano-1*H*-1,2,4-triazol-1-yl)propanoic acid (80 mg, 0.49 mmol) in *N,N*-dimethylformamide (10 mL) was added *N,N*-diisopropylethylamine (150 mg, 1.2 mmol), 1-[bis(dimethylamino)methylene]-1*H*-1,2,3-triazolo[4,5-*b*]pyridinium 3-oxide hexafluorophosphate (110 mg, 0.61 mmol) and 3-(2-(trifluoromethyl)phenyl)-6,7-dihydro-5*H*-pyrrolo[3,4-*b*]pyridine (100 mg, 0.40 mmol), and the reaction was stirred at room temperature for 12 hours. The reaction mixture was quenched with water, extracted with ethyl acetate, dried over sodium sulfate, concentrated and purified by silica gel column chromatography (0-20% methanol in dichloromethane), followed by reverse-phase HPLC purification (Waters X Bridge Prep C18 (19X150 mm, 5 μ) mobile phase: 0.02% NH_4OH in acetonitrile) to give the title compound (50 mg, 25% yield) as a white solid. ^1H NMR (300MHz, CDCl_3) δ 8.49 – 8.47 (m, 1H), 8.41 (s, 1H), 7.81 – 7.78 (m, 1H), 7.63 – 7.55 (m, 3H), 7.32 – 7.30 (m, 1H), 4.88 – 4.84 (m, 4H), 4.71 – 4.67 (m, 2H), 3.05 – 2.99 (m, 2H); LCMS ES^+ m/z = 413.0 $[\text{M}+1]^+$.



Column : ZORBAX XDB C18 5 μ 150X4.6mm
 Mobile phase : 0.01%TFA in water(A) , ACN(B)
 Gradient : Time / % B 0/30, 1/70, 6/100, 8/100, 10/30, 12/30
 Flow : 1.0 ml/min
 Temp : 40°C



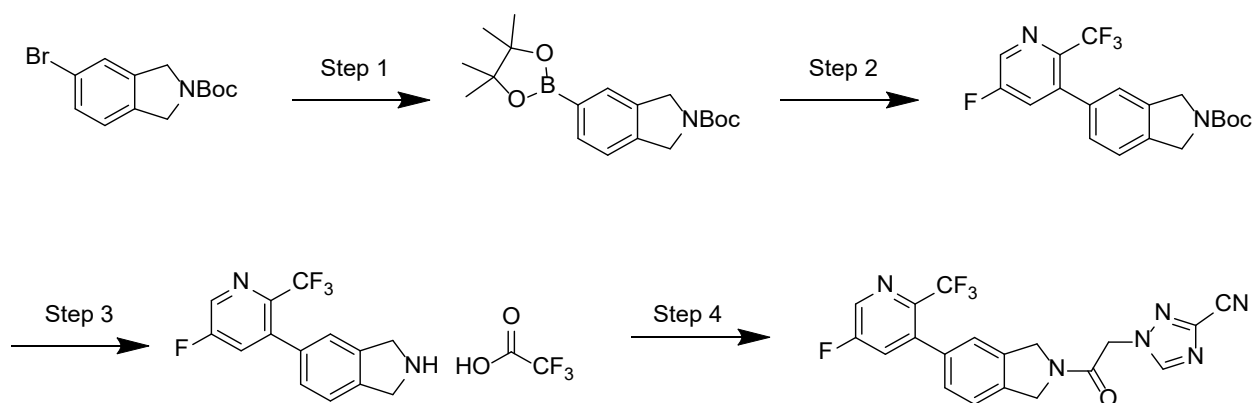
1 PDA Multi 1/210nm 4nm

PeakTable

PDA Ch1 210nm 4nm

Peak#	Ret. Time	Area	Height	Area %
1	3.239	2163	372	0.086
2	3.564	3094	512	0.123
3	3.740	743	191	0.029
4	3.833	2459	638	0.098
5	3.990	2504426	666825	99.359
6	4.128	7694	2505	0.305
Total		2520580	671044	100.000

- 5 *Preparation of 1-(2-(5-(5-Fluoro-2-(trifluoromethyl)pyridin-3-yl)isoindolin-2-yl)-2-oxoethyl)-1H-1,2,4-triazole-3-carbonitrile (CT3).*



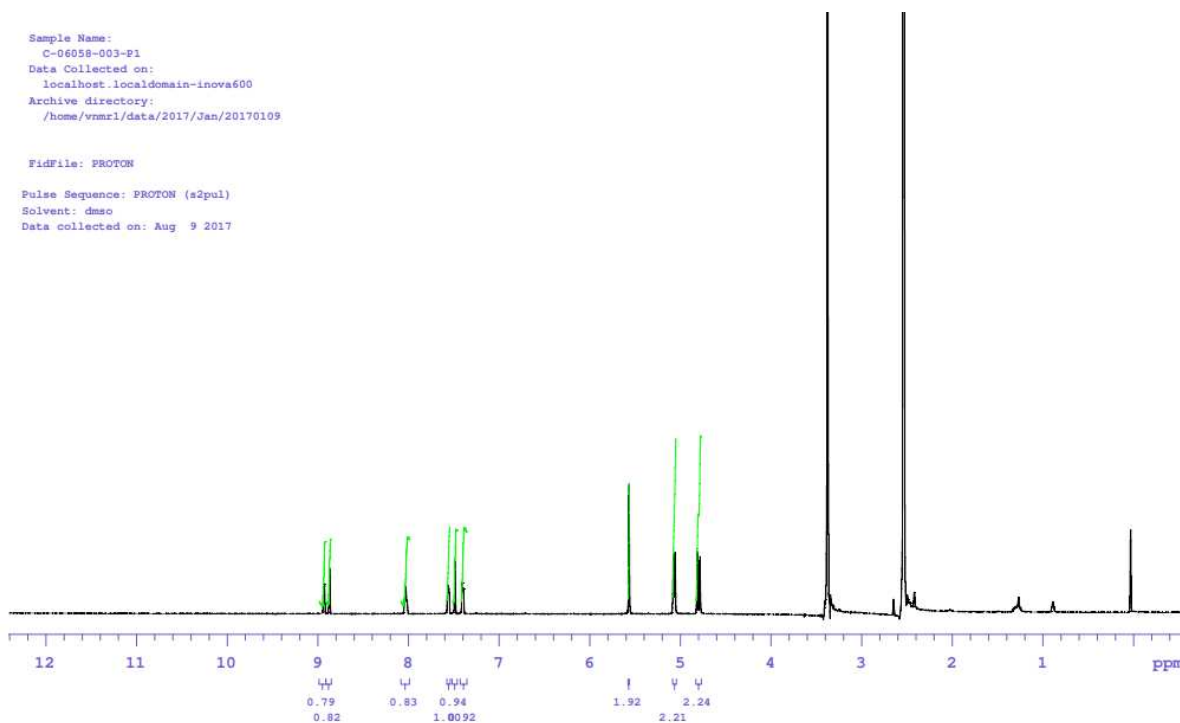
Step 1. *tert*-Butyl 5-(4,4,5,5-tetramethyl-1,3,2-dioxaborolan-2-yl)isindoline-2-carboxylate: *tert*-Butyl-5-bromoisindoline-2-carboxylate (20 g, 67 mmol) was dissolved in 1,4-dioxane (200 mL) and the solution was purged with argon gas for 10 minutes. Bispinacolato diborane (34 g, 134 mmol), KOAc (26 g, 268 mmol) and Pd(PPh₃)₄ (7.8 g, 6.7 mmol) were added and the reaction mixture was stirred at 80 °C for 12 hours. The reaction mixture was diluted with water, extracted with EtOAc. The combined organic layers were washed with water (500 mL), brine (300 mL), dried over sodium sulfate and concentrated under vacuo. The crude compound was purified by silica gel column chromatography (10% EtOAc in n-hexane) to give the title compound (23 g, 99% yield) as a white solid. ¹H NMR (300 MHz, CDCl₃) δ 7.72-7.65 (m, 2H), 7.31-7.20 (m, 1H), 4.70-4.60 (m, 4H), 1.40 (s, 9 H), 1.37 (s, 12H).

Step 2. *tert*-Butyl 5-(5-fluoro-2-(trifluoromethyl)pyridin-3-yl)isindoline-2-carboxylate: *tert*-Butyl 5-(4,4,5,5-tetramethyl-1,3,2-dioxaborolan-2-yl)isindoline-2-carboxylate (5.6 g, 16 mmol) was dissolved in 1,4-dioxane:H₂O (8:2) (100 mL), purged with argon gas for 10 minutes, K₃PO₄ (8.7 g, 41 mmol), 3-bromo-5-fluoro-2-(trifluoromethyl)pyridine (4.0 g, 16 mmol) and Pd(dppf)Cl₂.DCM (1.3 g, 1.6 mmol) were added and the reaction mixture was stirred at 100 °C for 3 hours. The reaction mixture was diluted with water, extracted with EtOAc twice. The combined organic layers were washed with water (300 mL), brine (300 mL), dried over sodium sulfate and concentrated in vacuo. The crude compound was purified by silica gel column chromatography (25% EtOAc in n-hexane) to afford title compound (3.0 g, 48% yield) as a brownish solid. ¹H NMR (300 MHz, CDCl₃) δ 8.56 (d, *J* = 2.4 Hz, 1H), 7.50-7.32 (m, 2H), 7.32-7.15 (m, 2H), 4.75 (s, 2H), 4.71 (s, 2H), 1.52 (s, 9H); LCMS ES⁺ *m/z* = 282.8 [M-Boc+1]⁺.

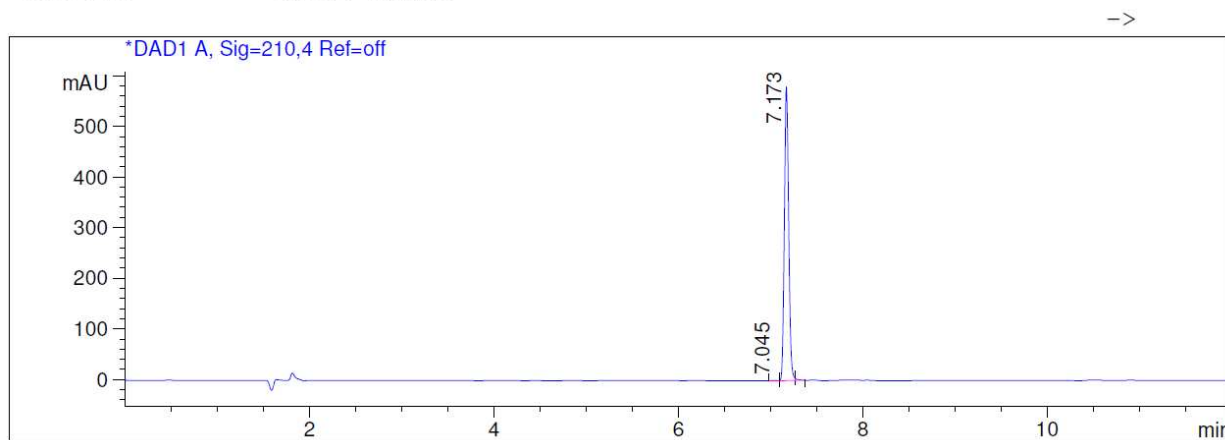
Step 3. 5-(5-Fluoro-2-(trifluoromethyl)pyridin-3-yl)isindoline, trifluoroacetic acid salt: *tert*-Butyl 5-(5-fluoro-2-(trifluoromethyl)pyridin-3-yl)isindoline-2-carboxylate (3 g, 7.7 mmol) was dissolved in dichloromethane (15 mL) and trifluoroacetic acid (15 mL) was added at 0 °C. The reaction mixture was stirred for 1 hour and concentrated under vacuo. The crude compound was purified by 10% diethyl ether in n-pentane washings

to afford title compound (3.0 g) which was used without further purification. LCMS ES⁺ m/z = 282.9 [M-TFA+1]⁺.

Step 4. 1-(2-(5-(5-Fluoro-2-(trifluoromethyl)pyridin-3-yl)isoindolin-2-yl)-2-oxoethyl)-1*H*-1,2,4-triazole-3-carbonitrile: To a stirred solution of 5-(5-fluoro-2-(trifluoromethyl)pyridin-3-yl)isoindoline trifluoroacetic acid salt (3.0 g, 7.6 mmol) and 2-(3-cyano-1*H*-1,2,4-triazol-1-yl)acetic acid (7.3 g, 48 mmol) in dichloromethane (45 mL) were added *N,N*-diisopropylethylamine (4.9 g, 39 mmol), propyl phosphonic anhydride (T3P) (50% EtOAc solution) (6.3 mL, 9.8 mmol) at 0 °C and stirred at room temperature for 3 hours. The reaction mixture was diluted with water, extracted with dichloromethane twice. The combined organic layers were washed with water (200 mL), brine (150 mL), dried over sodium sulfate and concentrated in vacuo. The crude compound was purified by silica gel column chromatography using (70% EtOAc in n-hexane) to afford the title compound (2.5 g, 79% yield) as a white solid. ¹H NMR (600 MHz, DMSO-*d*₆) δ 8.89 (dd, *J* = 6.0 Hz and 1.8 Hz, 1H), 8.84-8.82 (m, 1H), 7.99 (t, *J* = 8.6 Hz, 1H), 7.54-7.51 (m, 1H), 7.45 (s, 1H), 7.36 (d, *J* = 7.8 Hz, 1H), 5.53 (s, 2H), 5.04 and 5.02 (s, 2H), 4.77 and 4.75 (s, 2H); LCMS ES⁺ m/z = 416.7 [M+1]⁺.



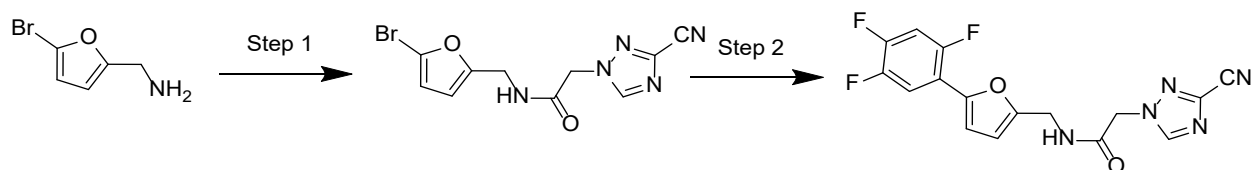
COLUMN : ZORBAX C18 150X4.6mm 5.0µ
 FLOW RATE : 1.0 ml/min
 MOBILE PHASE : 0.01% TFA in water (A) / ACN:MEOH (1:1) (B)
 TEMP : 40°C
 GRADIENT : 0/5, 1/5, 6/100, 8/100, 10/5, 12/5
 DILUENT : ACN: WATER



Signal 1: DAD1 A, Sig=210,4 Ref=off

Peak #	RT [min]	Width [min]	Area	Area %
1	7.045	0.081	4.112	0.210
2	7.173	0.056	1.951e3	99.437
3	7.267	0.026	6.929	0.353

5 **Preparation of 2-(3-Cyano-1H-1,2,4-triazol-1-yl)-N-((5-(2,4,5-trifluorophenyl)furan-2-yl)methyl)acetamide (CT4).**



10 Step 1. *N*-((5-Bromofuran-2-yl)methyl)-2-(3-cyano-1H-1,2,4-triazol-1-yl)acetamide: 2-(3-Cyano-1H-1,2,4-triazol-1-yl)acetic acid (310 mg, 2.0 mmol) and 2-(3H-[1,2,3]triazolo[4,5-*b*]pyridin-3-yl)-1,1,3,3-tetramethylisouronium hexafluorophosphate (1550 mg, 4.1 mmol) were dissolved in *N,N*-dimethylformamide (6 mL) and the reaction was stirred at 25 °C for 20 minutes before adding a solution of (5-bromofuran-2-yl)methanamine (476 mg, 2.24 mmol) and *N,N*-diisopropylethylamine (1.1 mL, 6.1 mmol) in *N,N*-dimethylformamide (1 mL). The reaction was quenched with water,

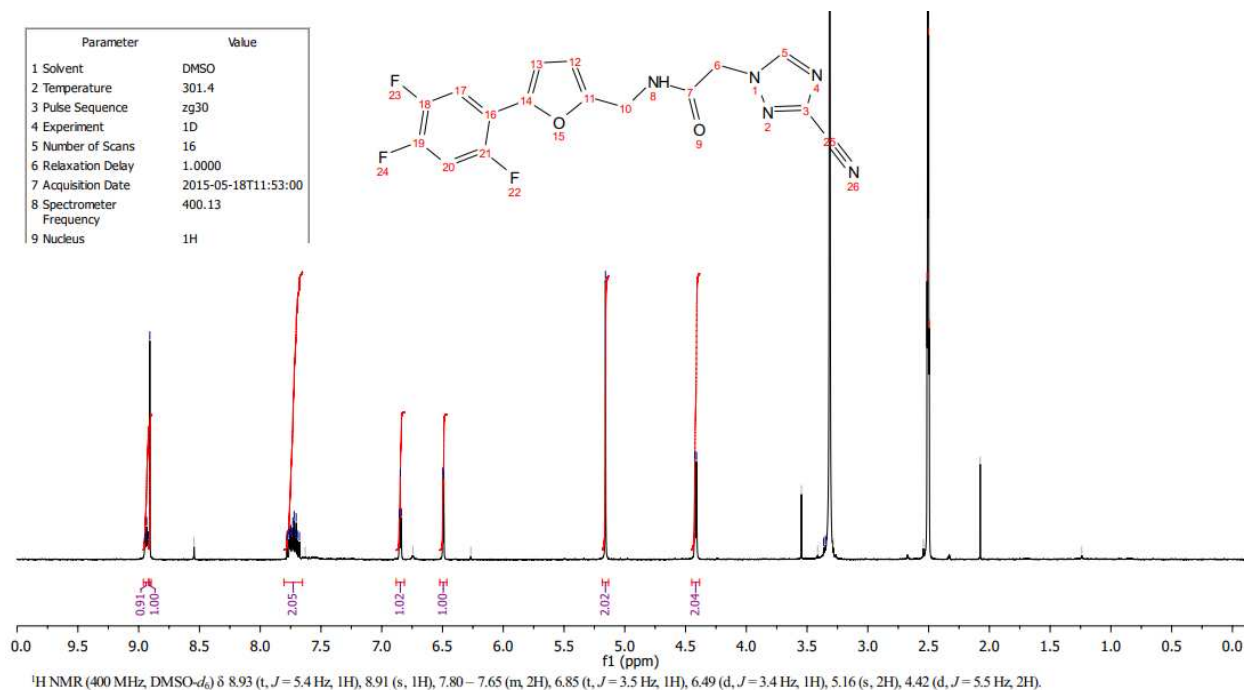
extracted with EtOAc, dried over Na₂SO₄, filtered, concentrated and purified by reverse-phase HPLC purification (Waters X Bridge Prep C18 (19x150 mm, 5 μm) mobile phase: 0.02% NH₄OH in acetonitrile) to give the title compound (80 mg, 13% yield). LCMS ES⁺ *m/z* = 311.9 [M+1]⁺.

5

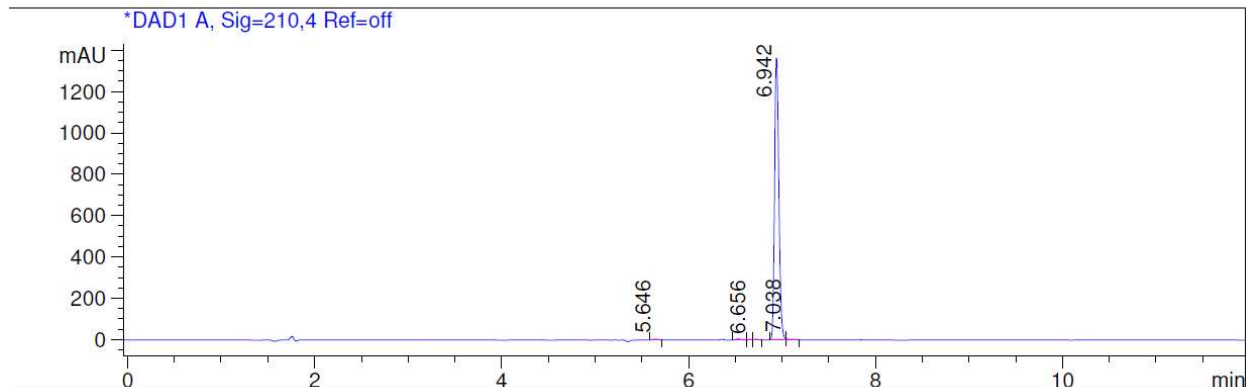
Step 2. 2-(3-Cyano-1H-1,2,4-triazol-1-yl)-*N*-((5-(2,4,5-trifluorophenyl)furan-2-yl)methyl)acetamide: *N*-((5-Bromofuran-2-yl)methyl)-2-(3-cyano-1H-1,2,4-triazol-1-yl)acetamide (40 mg, 0.13 mmol), (2,4,5-trifluorophenyl)boronic acid (45 mg, 0.26 mmol), and cesium fluoride (32 mg, 0.26 mmol) were dissolved in 1,4-dioxane (3 mL) and water (0.75 mL). Reaction mixture was degassed with argon for 5 minutes before adding Pd(PPh₃)₄ (15 mg, 0.013 mmol). The reaction mixture was heated at 80 °C for 4 hours, and then quenched with water, extracted with EtOAc, dried over Na₂SO₄, filtered and concentrated. The crude mixture was purified by reverse-phase HPLC (Sunfire, mobile phase 0.01% HCOOH in acetonitrile) to give the title compound (24 mg, 51% yield) as a white solid. ¹H NMR(400MHz, DMSO-*d*₆) δ 8.93 (t, *J* = 5.4Hz, 1H), 8.91 (s, 1H), 7.80 – 7.65 (m, 2H), 6.85 (t, *J* = 3.5Hz, 1H), 6.49 (d, *J* = 3.4Hz, 1H), 5.16 (s, 2H), 4.42 (d, *J* = 5.5Hz, 2H); LCMS ES⁺ *m/z* = 361.9 [M+1]⁺.

10

15



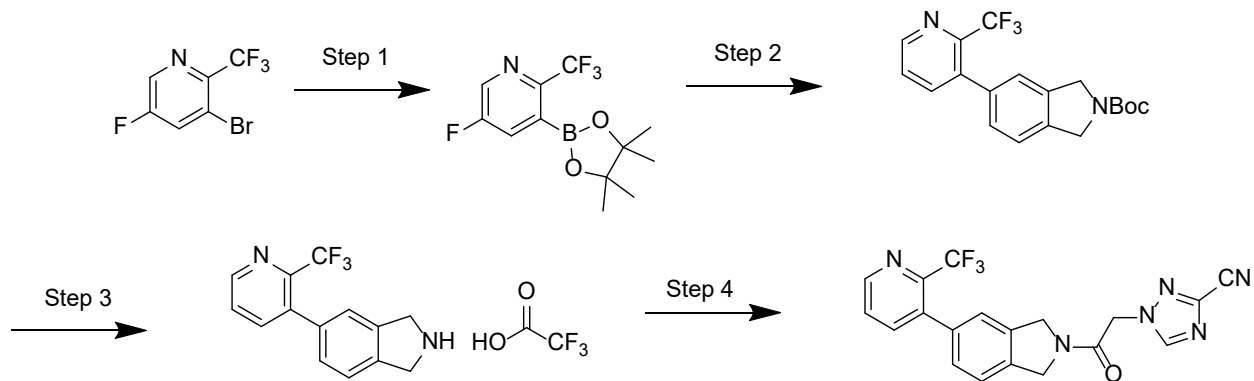
Column : Zorbax , C18 , (150*4.6mm), 5 micron
 Mobile Phase : 0.01% TFA IN WATER & ACETONITRILE
 GRADIENT : Time/%B : : 0/5, 1/5, 6/100, 8/100, 10/5, 12/5
 Flow : 1.0 mL/min
 Temperature : 40°C



Signal 1: DAD1 A, Sig=210,4 Ref=off

Peak #	RT [min]	Width [min]	Area	Area %
1	5.646	0.057	14.698	0.330
2	6.531	0.054	14.083	0.316
3	6.656	0.054	3.335	0.075
4	6.720	0.057	9.030	0.203
5	6.942	0.053	4.397e3	98.779
6	7.038	0.032	13.197	0.296

5 **Preparation of 1-(2-Oxo-2-(5-(2-(trifluoromethyl)pyridin-3-yl)isoindolin-2-yl)ethyl)-1H-1,2,4-triazole-3-carbonitrile (CT5).**



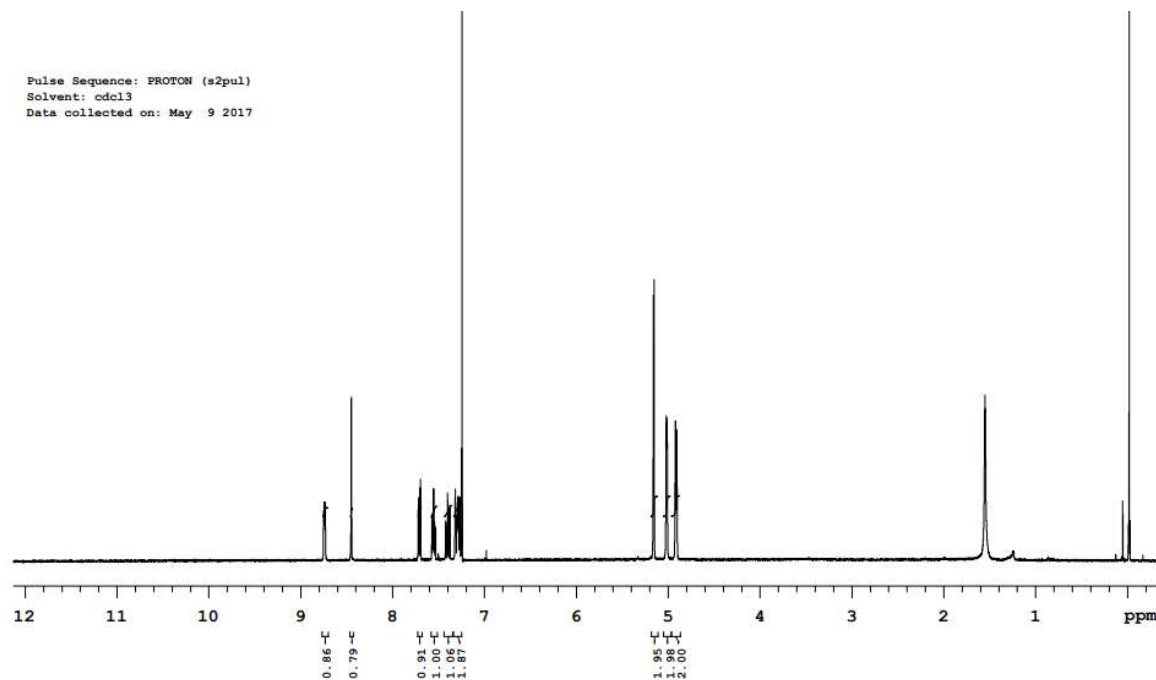
Step 1. 3-(4,4,5,5-Tetramethyl-1,3,2-dioxaborolan-2-yl)-2-(trifluoromethyl)pyridine: A 250 ml sealed tube of 3-bromo-2-(trifluoromethyl)pyridine (7.0 g, 31 mmol) in 1,4-dioxane (70 mL) was purged with argon gas for 10 minutes and bispinacalato diborane (8.6 g, 34 mmol), KOAc (6.1 g, 62 mmol) and Pd(dppf)Cl₂.DCM (1.3 g, 1.5 mmol) were added and the reaction mixture was stirred for 16 h at 100 °C. The reaction mixture was diluted with water, extracted with EtOAc twice. The combined organic layers were washed with water (300 mL), brine (300 mL), dried over sodium sulfate and concentrated under vacuo. The crude compound was purified by silica gel column chromatography (10% EtOAc in n-hexane) to afford title compound (7.0 g, 83% yield) as a brownish solid. ¹H NMR (300 MHz, CDCl₃) δ 6 8.72-8.70 (m, 1H), 8.10-8.00 (m, 1H), 7.50-7.42 (m, 1H), 1.37 (s, 12H); LCMS ES⁺ *m/z* = 274.0 [M+1]⁺.

Step 2. *tert*-Butyl 5-(2-(trifluoromethyl) pyridin-3-yl) isoindoline-2-carboxylate: A 250 ml sealed tube with *tert*-butyl 5-bromoisindoline-2-carboxylate (7.0 g, 23 mmol) in 1,4-dioxane:H₂O (8:2) (100 mL) was purged with argon gas for 10 minutes. K₃PO₄ (12 g, 59 mmol), 3-(4,4,5,5-tetramethyl-1,3,2-dioxaborolan-2-yl)-2-(trifluoromethyl)pyridine (7.0 g, 26 mmol) and Pd(dppf)Cl₂.DCM (1.9 g, 2.3 mmol) were added and the reaction mixture was stirred for 5 hours at 100 °C. The reaction mixture was diluted with water, extracted with EtOAc twice. The combined organic layers were washed with water (300 mL), brine (300 mL), dried over sodium sulfate and concentrated under vacuo. The crude compound was purified by silica gel column chromatography (25% EtOAc in n-hexane) to afford title compound (6.0 g, 70% yield). ¹H NMR (300 MHz, CDCl₃) δ 5 8.73 (d, *J* = 3.6 Hz, 1H), 7.72 (d, *J* = 7.8 Hz, 1H), 7.56-7.51 (m, 1H), 7.38-7.28 (m, 1H), 7.25-7.17 (m, 2H), 4.75 (s, 2H), 4.71 (s, 2H), 1.52 (s, 9H).

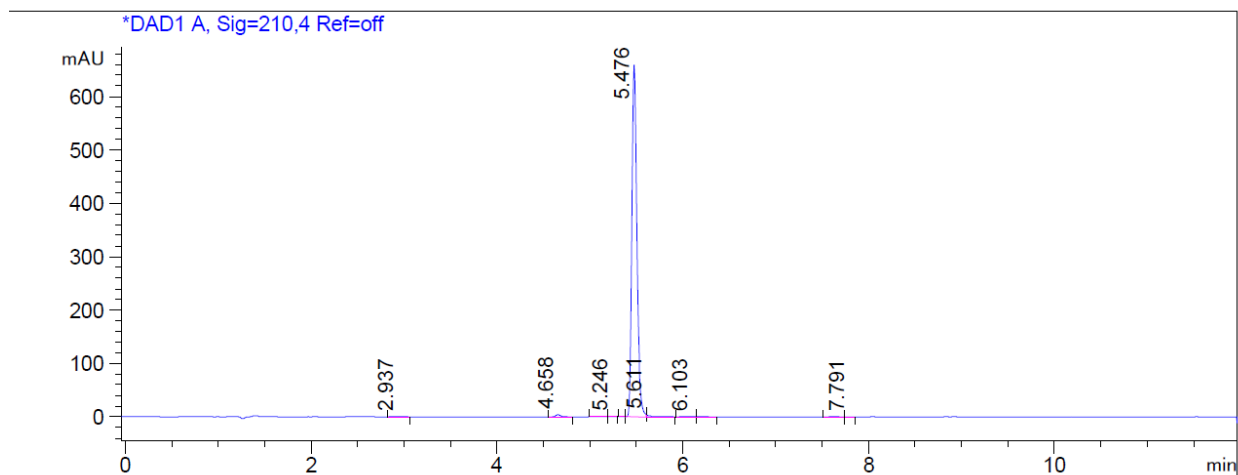
Step 3. 5-(2-(Trifluoromethyl) pyridin-3-yl) isoindoline, trifluoroacetic acid salt: *tert*-Butyl 5-(2-(trifluoromethyl)pyridin-3-yl)isoindoline-2-carboxylate (6.0 g, 16 mmol) was dissolved in dichloromethane (20 mL) and trifluoroacetic acid (15 mL) was added at 0°C. The reaction mixture was stirred for 2 hours and concentrated under vacuo. The crude compound was purified by 10% diethyl ether in n-pentane washings to afford title compound (7.0 g) which was used without further purification. LCMS ES⁺ *m/z* = 264.9 [M-TFA+1]⁺.

Step 4. 1-(2-Oxo-2-(5-(2-(trifluoromethyl)pyridin-3-yl)isoindolin-2-yl)ethyl)-1*H*-1,2,4-triazole-3-carbonitrile: To a stirred solution of the 5-(2-(trifluoromethyl) pyridin-3-yl) isoindoline, trifluoroacetic acid salt (7.0 g, 19 mmol) and 2-(3-cyano-1*H*-1,2,4-triazol-1-yl)acetic acid (7.3 g, 48 mmol) in dichloromethane (100 mL), *N,N*-diisopropylethylamine (12 g, 97 mmol) and propyl phosphonic anhydride (T3P) (50% EtOAc solution) (14.5 mL, 23 mmol) were added at 0°C and stirred at room temperature for 1 hour. The reaction mixture was diluted with water, extracted with dichloromethane twice. The

combined organic layers were washed with water (200 mL), brine (150 mL), dried over sodium sulfate and concentrated under vacuo. The crude compound was purified by silica gel column chromatography (50% EtOAc in n-Hexane) to afford the title compound (3.1 g, 40% yield) as a grey solid. ^1H NMR (400 MHz, DMSO- d_6) δ 8.90 (d, J = 4.3 Hz, 1H), 8.80 (d, J = 4.6 Hz, 1H), 7.99-7.91 (m, 1H), 7.86-7.77 (m, 1H), 7.52 (d, J = 7.8 Hz, 1H), 7.42 (s, 1H), 7.33 (d, J = 7.8 Hz, 1H), 5.53 (d, J = 1.8 Hz, 2H), 5.04 (d, J = 6.4 Hz, 2H), 4.77 (d, J = 10.3 Hz, 2H); LCMS ES $^+$ m/z = 399.0 $[\text{M}+1]^+$.



Column : Zorbax, C 18 5 μ 150x4.6MM
 Mobile Phase : A= 0.01% TFA inWater, B= ACETONITRILE
 GRADIENT : Time/%B:: 0/30,2/40,5/90,7/100,9/100,10/30,12/30
 Flow : 1.0 mL/min
 Temperature : 40°C



Signal 1: DAD1 A, Sig=210,4 Ref=off

Peak	RT	Width	Area	Area %
#	[min]	[min]		
1	2.937	0.110	5.791	0.232
2	4.658	0.068	16.339	0.653
3	5.058	0.092	1.044	0.042
4	5.246	0.064	0.135	0.005
5	5.402	0.017	0.377	0.015
6	5.476	0.062	2.452e3	98.064
7	5.611	0.054	12.012	0.480
8	6.103	0.103	3.141	0.126
9	6.209	0.070	5.358	0.214
10	7.626	0.092	3.616	0.145
11	7.791	0.070	0.609	0.024

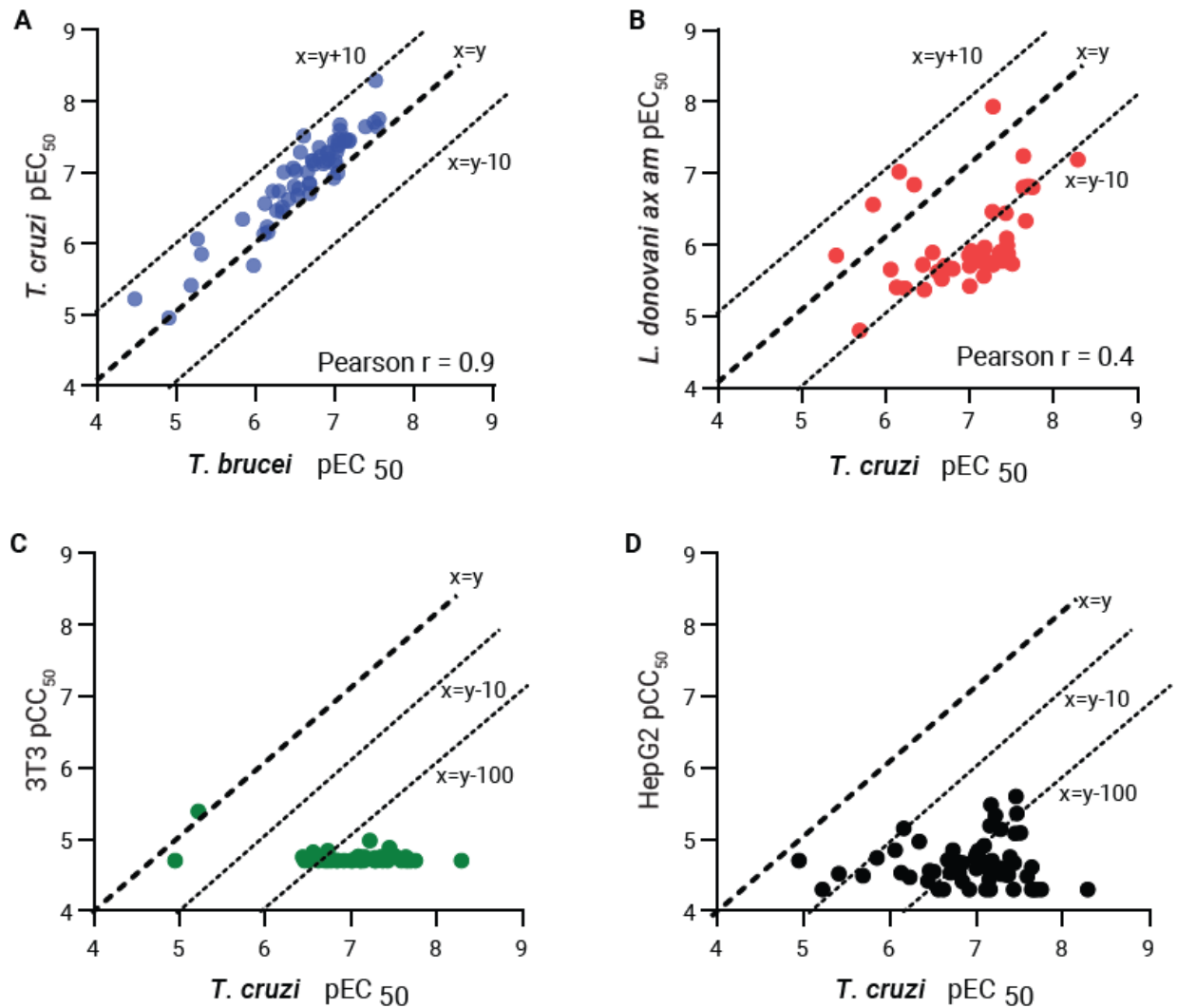


Figure S1. Pan kinetoplastid activity of CT compounds. (A) Positive correlation between growth inhibition (pEC₅₀) of *T. b. brucei* bloodstream form parasites and intracellular *T. cruzi* parasites (n=59; Pearson correlation coefficient, $r = 0.9$). The dashed black line represents equimolar potency and the dashed grey lines represent 10-fold lower and higher potency. (B) Positive correlation between growth inhibition (pEC₅₀) of intracellular *T. cruzi* and *L. donovani* axenic amastigote parasites (n=47; Pearson correlation coefficient, $r = 0.4$). No correlation was observed between parasite growth inhibition and cytotoxicity (pCC₅₀) of 3T3 fibroblast (C) or HepG2 hepatic cells (D).

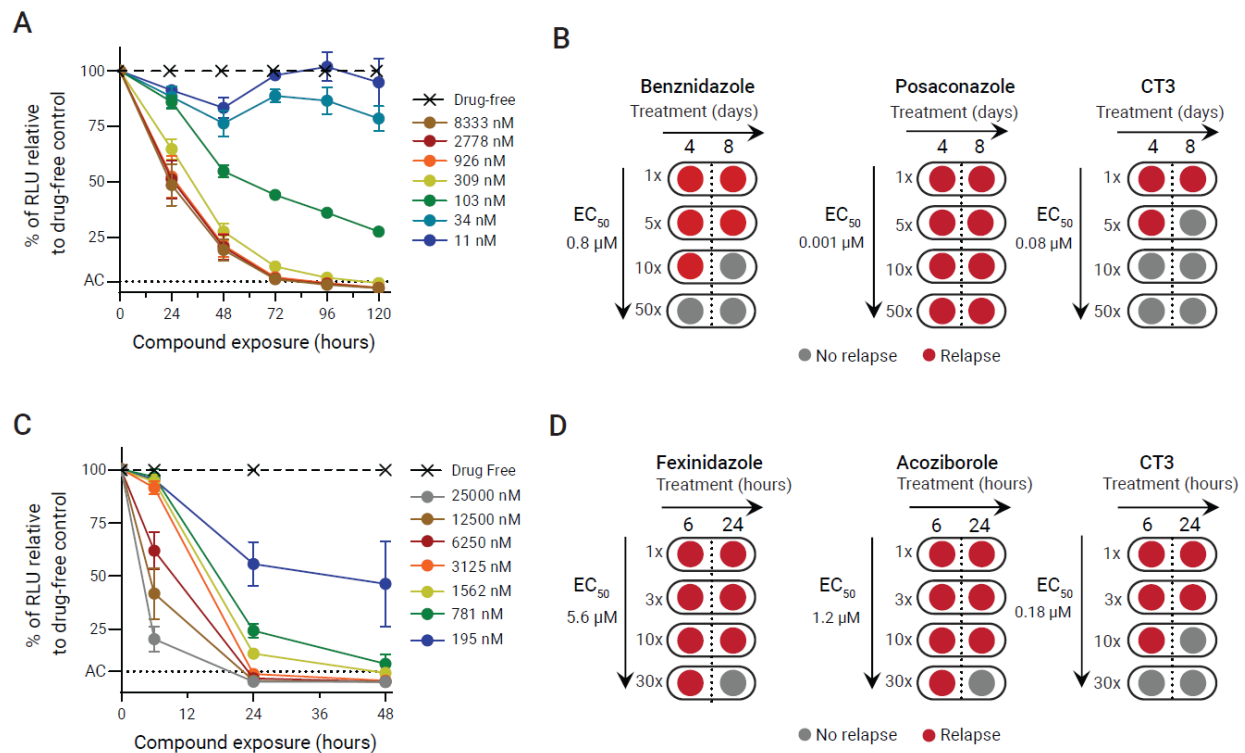
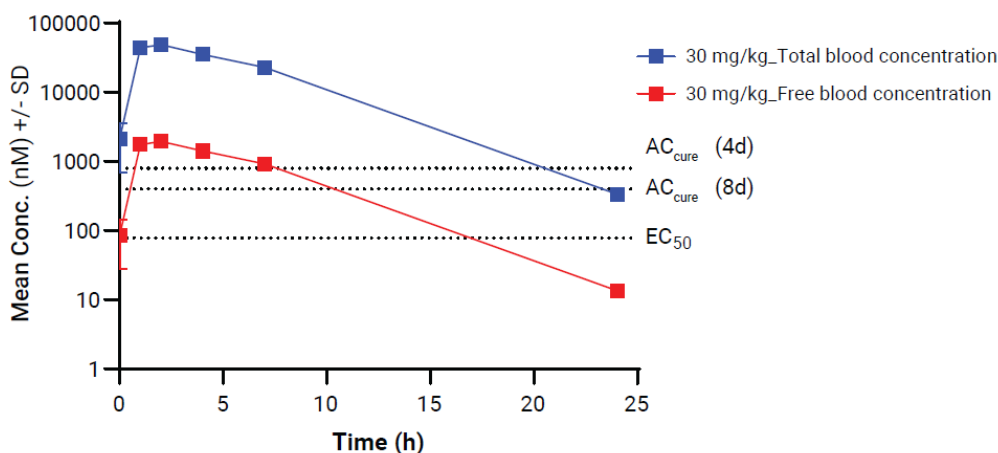


Figure S2. Experimental anti-parasitic properties of CT3. (A) Time to kill of CT3 of intracellular *T. cruzi* parasites. Data represent the mean \pm SEM of three independent biological replicates, where the rate of kill was calculated after comparing each treatment point to a drug-free control over 120 hours. An experimental curative benznidazole dose was used as an active control (AC). (B) Required absolute concentration (AC_{cure}) of CT3, benznidazole and posaconazole to achieve sterile cure of intracellular *T. cruzi* parasites after four and eight days of incubation. Data correspond to three independent in vitro experiments, the absence of motile parasites by live microscopy after 25 days of monitoring was considered no relapse. (C) Time to kill analysis of CT3 against of bloodstream form of *T. b. brucei* parasites. The data represent the mean \pm SEM (n=3 independent biological replicates). With both parasites, note the concentration and time-dependent killing by CT3. (D) The absolute concentrations (AC_{cure}) required to achieve sterile cure under in vitro conditions of bloodstream form of *T. b. brucei* parasites with six and 24-hour incubation of CT3, acoziborole and fexinidazole. Luminescence relative units (RLU) of a curative concentration of melarsoprol were used as a threshold for determining the “no relapse” point in treated samples. Data correspond to 3 independent experiments.

A



B

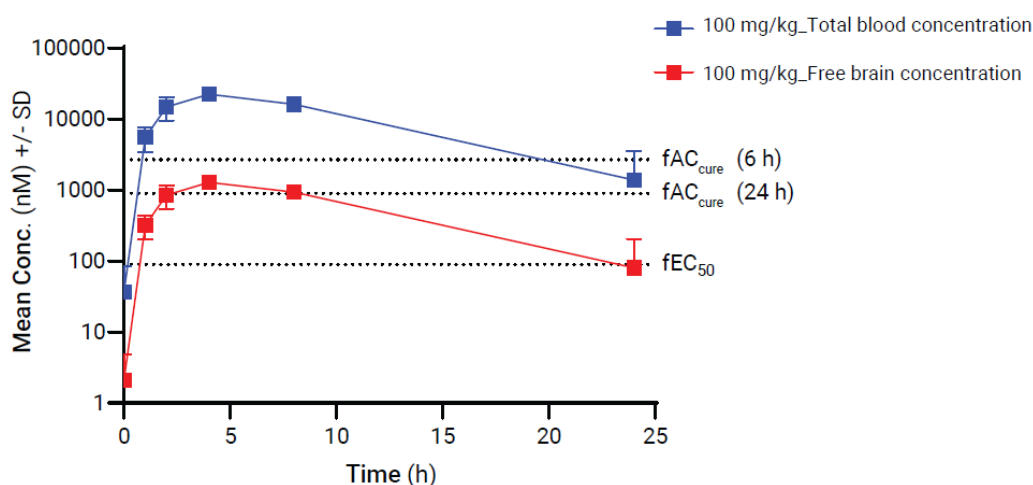
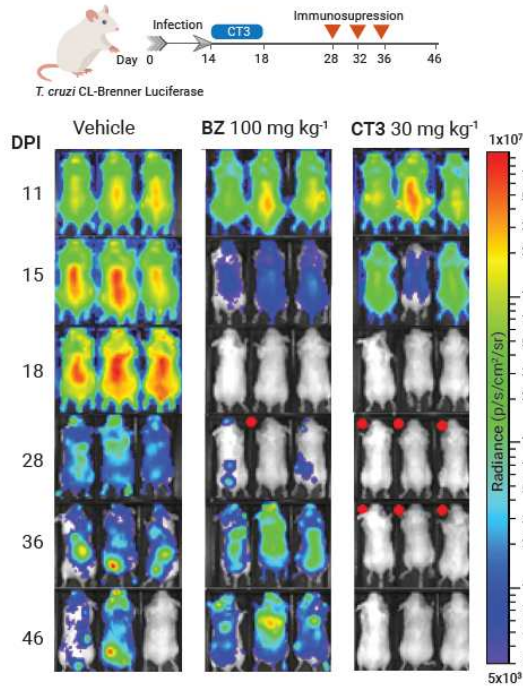


Figure S3. Pharmacokinetic analysis of CT3. (A) PK analysis of CT3 in a chronic Chagas mouse model. Total and free blood concentration of CT3 at various timepoints, after the last dose are presented. Three mice were bled at each time point and the data represents mean \pm standard deviation. Free blood concentration was calculated using mouse plasma protein binding (96%). Note the free blood concentration of CT3 was above EC_{50} for ~17 hours, above AC_{cure} (absolute concentration required to achieve relapse-free cure in vitro)-4 days for ~7 hours and AC_{cure} -8 days for ~10 hours. The potency values were highlighted using horizontal dotted black lines. AC_{cure} for 4 days ($10 \times EC_{50} = 800$ nM) and 8 days ($5 \times EC_{50} = 400$ nM) were derived from Fig S2B. **(B)** PK analysis of CT3 from a stage II HAT mouse model. Total blood and free brain concentration of CT3 at various time points, after dosing are presented. At each time point 3 mice were bled and the data represents mean \pm standard deviation. Free brain concentration was calculated taking into consideration the brain to plasma ratio (0.7),

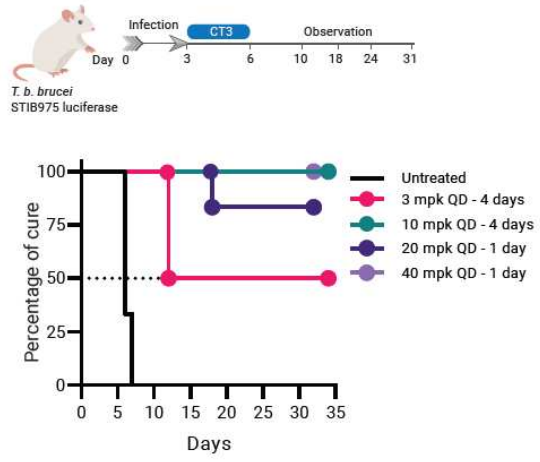
5

mice plasma protein binding (96%) and rat brain tissue binding (91.8%). Note the free brain concentration of CT3 was above fEC_{50} for ~24 hours, above fAC_{cure} (24h) for ~6 hours. The AC_{cure} values for 6 hours ($30 \times EC_{50} = 5400$ nM) and 24 hours ($10 \times EC_{50} = 1800$ nM) were derived from Fig S2B. The fEC_{50} and fAC_{cure} for *T. b. brucei* were calculated using media protein binding (50%) as the culture media had 20% fetal bovine serum. The time above potency of free compound concentration were derived from the PK plots.

A



B



C

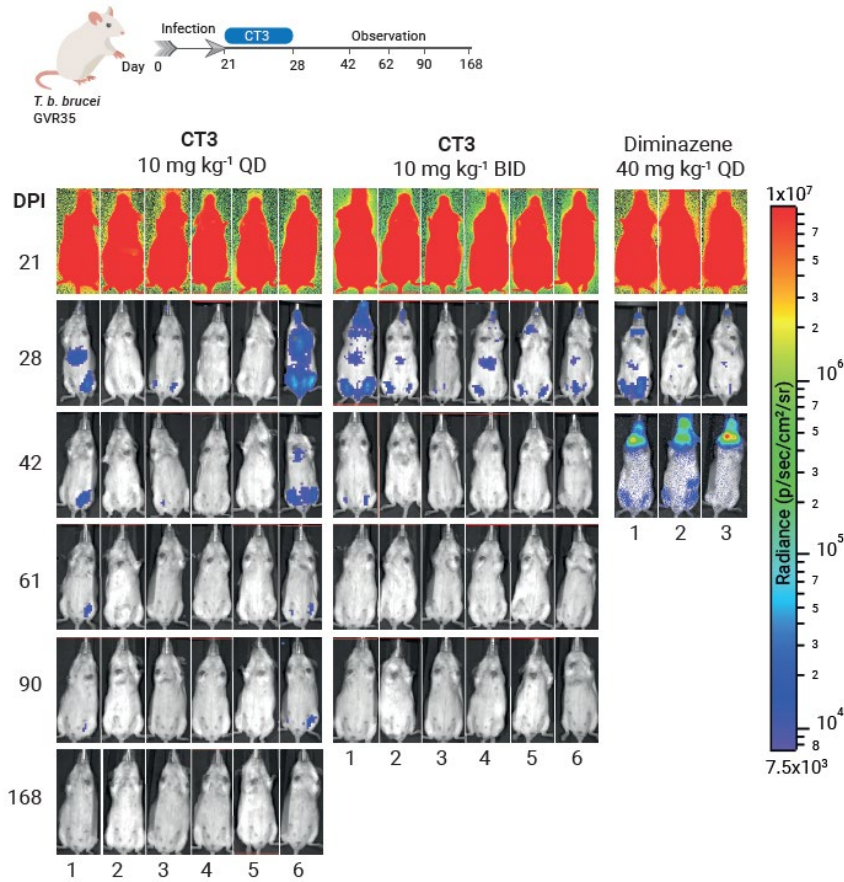


Figure S4. CT3 efficacy in mouse models of trypanosome infection. (A) In vivo efficacy of CT3 in a mouse model of acute Chagas disease. At 14 days post-infection (DPI) with the *T. cruzi* CL Brener luciferase strain, each experimental group (three mice) was dosed orally for five days with vehicle control, 100 mg.kg⁻¹ once daily (QD) benznidazole, or 30 mg.kg⁻¹ QD of CT3. At various time points, parasite load was measured by imaging the mice after administering 150 mg.kg⁻¹ D-luciferin. One mouse from the benznidazole group and the entire CT3 group were immunosuppressed on days 28, 32, and 36 using cyclophosphamide (200 mg.kg⁻¹ intraperitoneally). CT3 outperforms benznidazole as a treatment for experimental *T. cruzi* infections as all mice relapsed in the benznidazole-treated group, while all mice treated with CT3 remained parasite-free. (B) In vivo efficacy of CT3 in the hemolymphatic mouse model of HAT. Three days post-infection with the *T. b. brucei* STIB975 strain, three mice received a vehicle control, and six mice each were treated with 3 or 10 mg.kg⁻¹ CT3 once daily for four days, or with single doses of 20 or 40 mg.kg⁻¹. Mice were monitored using in vivo imaging and direct parasitemia counting by microscopy until 32 DPI. A cure plot (Kaplan-Meier plot) showing the percentage of mice cured over time is shown. Mice treated with 10 mg.kg⁻¹ QD for 4 days or a single dose of 40 mg.kg⁻¹ showed relapse free cure. (C) In vivo efficacy of CT3 in a meningoencephalitis mouse model of HAT. At 21 DPI with bioluminescent *T. b. brucei* GVR35, three mice were treated intraperitoneally with one dose of 40 mg.kg⁻¹ diminazene (negative control) and six mice each were treated orally with CT3 at 10 mg.kg⁻¹ QD or twice daily (BID) for seven days. Parasitemia levels were monitored by imaging mice injected with D-luciferin (150 mg.kg⁻¹, intraperitoneally). Diminazene treated mice relapsed on day 42 and were humanely sacrificed. Mice treated with 10 mg.kg⁻¹ CT3 BID showed complete parasite clearance (day 61 and 90), whilst two out of six mice treated with in the 10 mg.kg⁻¹ QD treated group showed a slight bioluminescent signal on day 61 and 90. However, this signal was undetectable in subsequent imaging and no parasitemia relapse occurred by the end point at day 168.

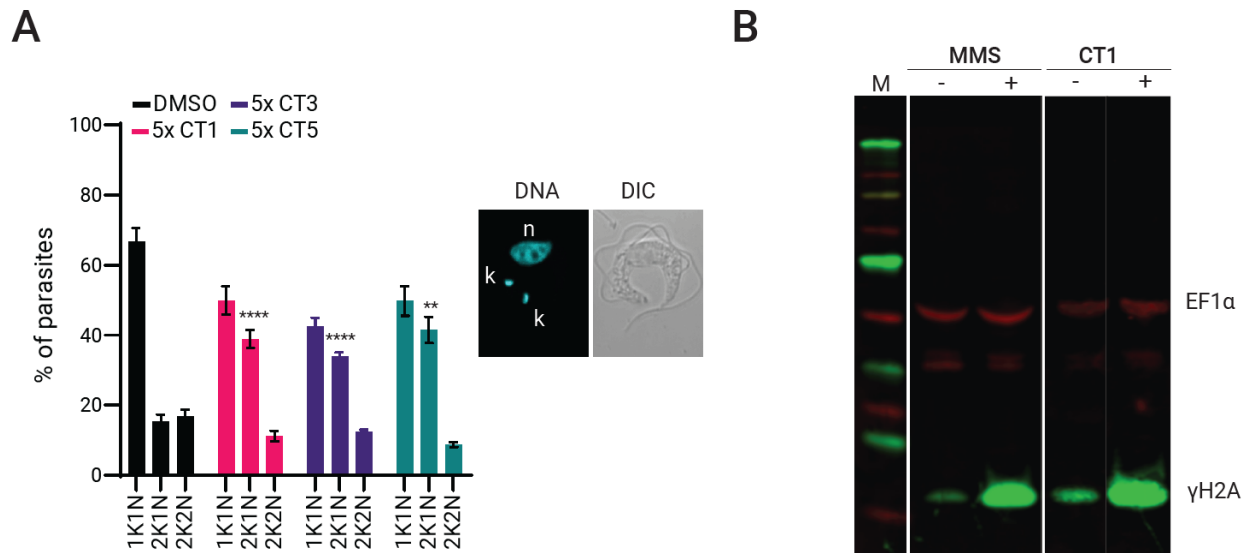


Figure S5. Phenotypic impact of CTs (A) CTs perturb nuclear DNA replication of trypanosomatid parasites. Microscopic images of *T. b. brucei* incubated with 5x EC₅₀ of CT1 (800nM), CT3 (900nM) and CT5 (650nM) for six hours. Note that nuclear staining using DAPI showed an increased presence of 2K1N parasites compared to no drug control. The increase in 2K1N was statistically significant as analysed by 2 way ANOVA with Dunnett's multiple comparison test (** p<0.0011; **** p<0.0001). (B) CTs induce a DNA damage response in trypanosomatid parasites. Immunoblotting using γH2A antibodies using whole-cell protein extracts of *T. b. brucei* incubated with MMS (0.0003% v/v), a known DNA damaging agent and CT1. Note the increased γH2A protein in cells treated with CT1 and MMS, whilst the loading control EF1α remains unchanged.

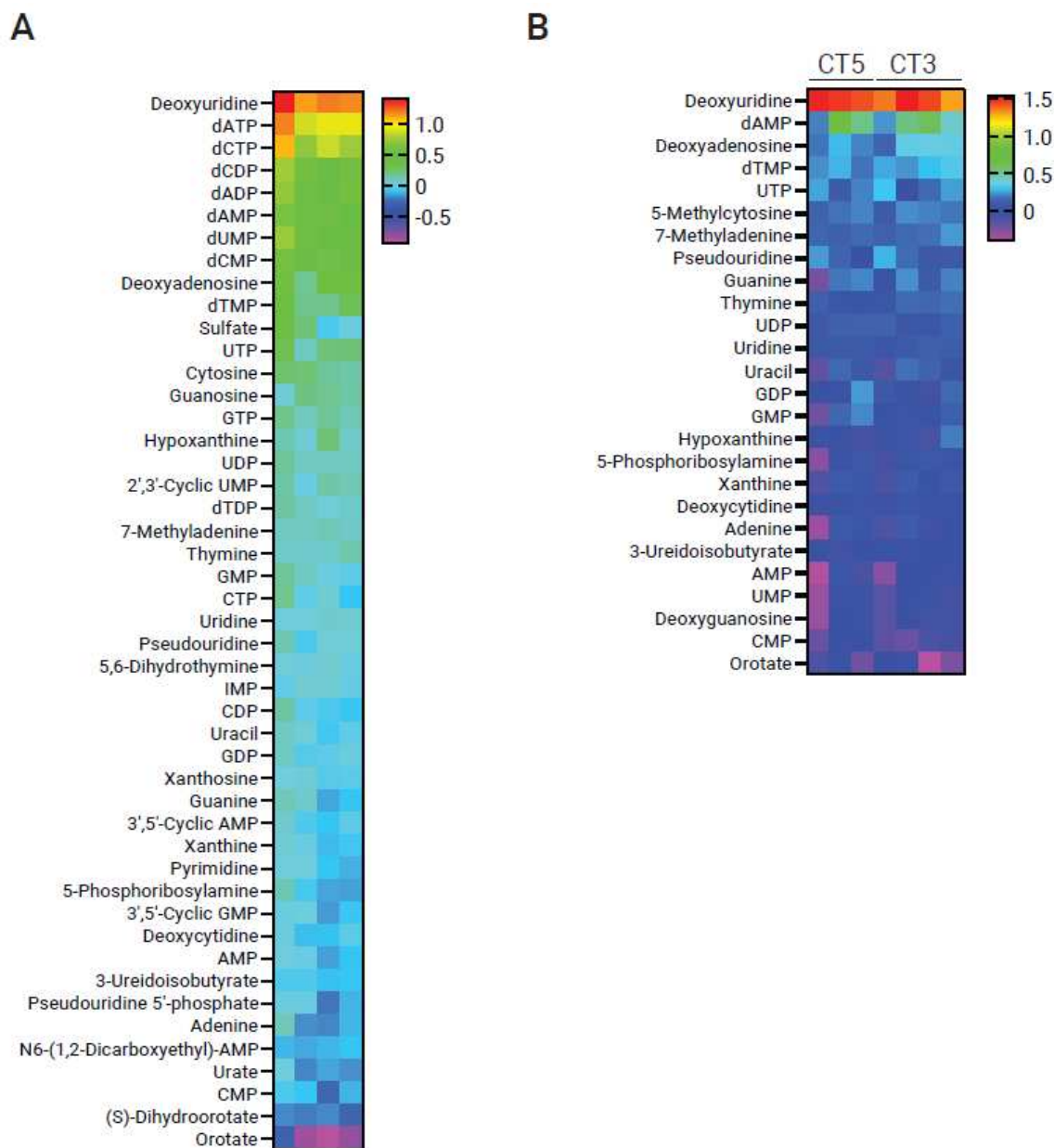


Figure S6. Untargeted metabolomics profile showing increased deoxynucleotides in *T. b. brucei* incubated with CT1. Heatmap of the fold-change in relative abundance of each nucleotide metabolite identified by untargeted metabolomics of *T. b. brucei* treated with 5x EC₅₀ of CT1 (800 nM) (**A**), CT3 (850 nM) and CT5 (1000 nM) (**B**) compared to the respective mean abundance in the control group [no drug control (DMSO only); n=4]. Shown are 4 independent biological replicates, with the color gradient scale depicting the log₁₀ of the fold-change and plotted as a heatmap using GraphPad Prism.

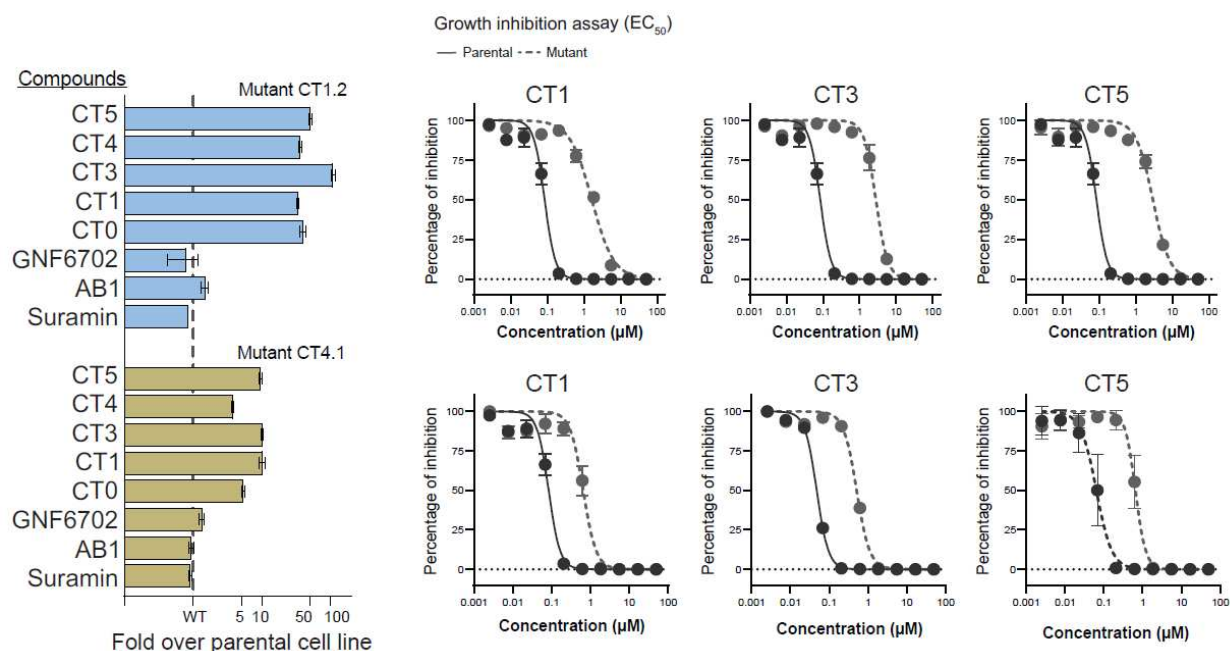
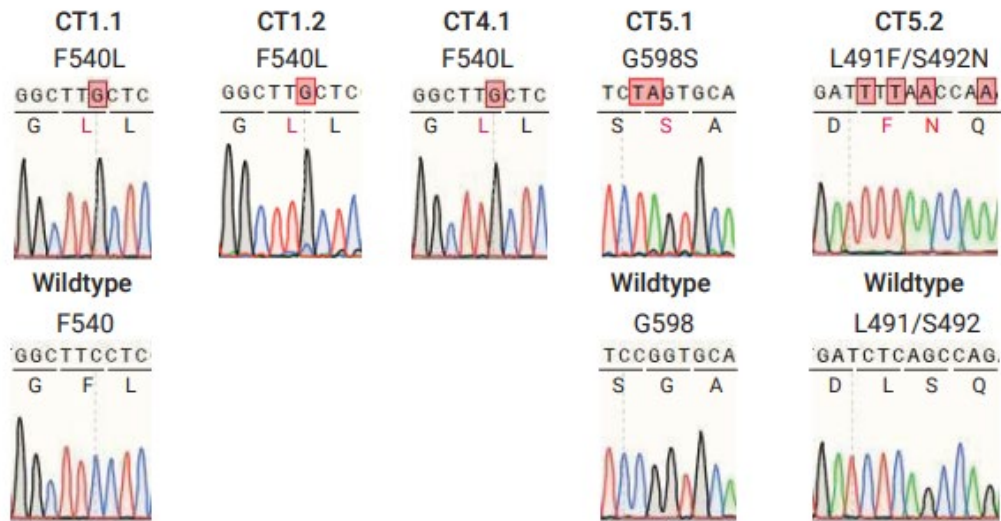


Figure S7. CT mutants are resistant to CT compounds. Concentration-response curves for *T. b. brucei* wild type (WT) and CT-resistant bloodstream forms in the presence of increasing concentrations of CTs. Mutants showed a significant EC_{50} shift (represented in fold-over WT, left panel) when treated with CT compounds, compared to an unrelated proteasome inhibitor (GNF6702), CLK1 inhibitor (AB1) and suramin, a known anti-trypanosomal agent. Representative EC_{50} curves are shown for CT1, CT3 and CT5 (right panel). EC_{50} values of two biological replicates were calculated from concentration-response curves performed in duplicate after nonlinear fitting with GraphPad Prism.

A



B

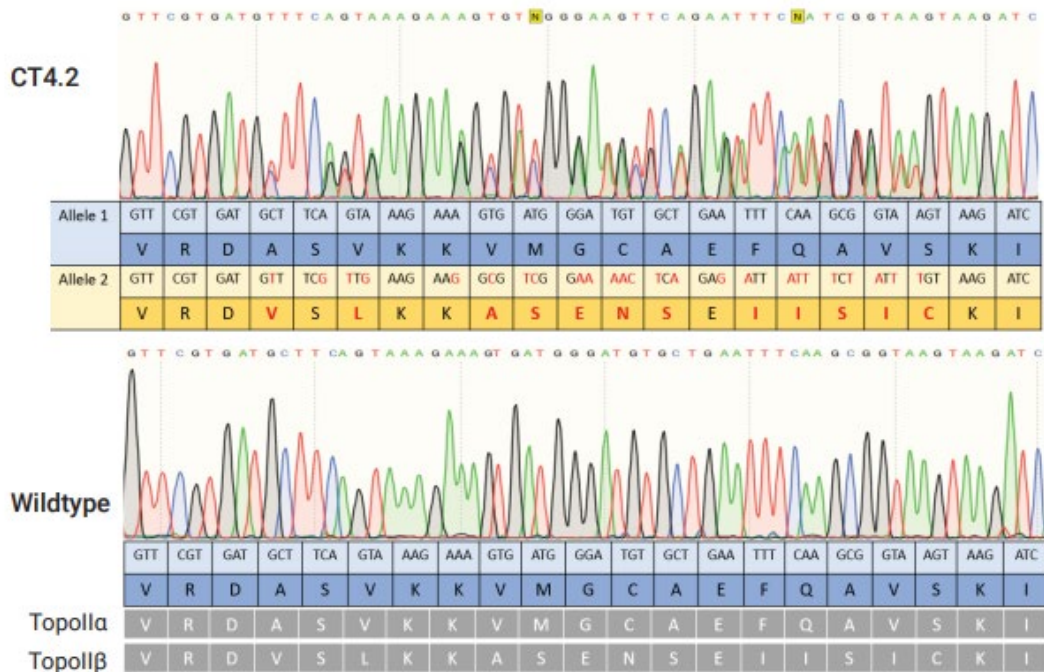


Figure S8. Sanger sequencing of *T. b. brucei topollα* from wild-type and CT mutant strains. (A) Sanger sequencing of mutants CT1.1, CT1.2 and CT4.1 showing homozygous mutation F540L in *T. b. brucei topollα*. CT5.1 shows homozygous mutation G598S, whilst CT5.2 shows homozygous mutations L491F and S492N in *topollα*. **(B)** Multiple heterozygous mutations in *topollα* were seen in mutant CT4.2. These mutations resembled *topollβ* sequence.

TbbTopoll α MSGRTVEEIIYQKKTQHEHILARPDYIGTIEPVTEDEVVYDEADNVMLRKCTWTPGLYKIFDEILVNAADNKVRDPHGO 80
TbbTopoll β MSGRTVEEIIYQKKTQHEHILARPDYIGTIEPVTEDEVVYDEADNVMLRKCTWTPGLYKIFDEILVNAADNKVRDPHGO 80

TbbTopoll α TTIKVWVDAARGLVRVYNNNEGIPVQRHREHDLWVPEMIFGHLLTSSNYDDTEAKVTGGRNGFGAKLTNVFSTRFEVE TV 160
TbbTopoll β TTIKVWVDAARGLVRVYNNNEGIPVQRHREHDLWVPEMIFGHLLTSSNYDDTEAKVTGGRNGFGAKLTNVFSTRFEVE TV 160

TbbTopoll α HSRSRKKFFMRWRNNMLENEEAVITPCDGPDYTVVTFYPDFEFKNLEGFTEDMVLIMQRRVYDIAGCTDKSLCCYLNDTR 240
TbbTopoll β HSRSRKKFFMRWRNNMLENEEAVITPCDGPDYTVVTFYPDFEFKNLEGFTEDMVLIMQRRVYDIAGCTDKSLCCYLNDTR 240

TbbTopoll α IACRSFPEYVDLYPTMGEEERKPSYSRVNDRWEVCVRVSNVGFQQVSFVNSIATTRGGTHVKYIVDQIIAKVTDQAMRKS 320
TbbTopoll β IACRSFPEYVDLYPTMGEEERKPSYSRVNDRWEVCVRVSNVGFQQVSFVNSIATTRGGTHVKYIVDQIIAKVTDQAMRKS 320

TbbTopoll α KTEVKPHMIRPHLFIIFVNSLIENPSFDSQTKETLNTPKARFGSTCDLPASLIDCVLKSSIIVERAVEMANSRLNREMAKMK 400
TbbTopoll β KTEVKPHMIRPHLFIIFVNSLIENPSFDSQTKETLNTPKARFGSTCDLPASLIDCVLKSSIIVERAVEMANSRLNREMAKMK 400

TbbTopoll α RNTNRKQILGIPKLDDANEAGGKYSQRCTLILTEGDSAKALCTAGLAVENRDYFGVFPLRGKPLNVRDASVKKVMGCAEF 480
TbbTopoll β RNTNRKQILGIPKLDDANEAGGKYSQRCTLILTEGDSAKALCTAGLVKNRDYFGVFPLAGKPLNVRDASVKKVMGCAEF 480

TbbTopoll α QAVSKIMGLDLSQKYTSTEGRLRYGHLIMSDQDHGSHIKGLIINMIHNYWPDLLKVPGLQQFITPIVKARKKGRGNND 560
TbbTopoll β ISICKIMGLDFNQKYTSTEGRLRYGHLIMSDQDHGSHIKGLIINMIHNYWPDLLKVPGLQQFITPIVKARKKGRGNND 560

TbbTopoll α EGTISFFSMPDYFEWKNAVGEGIKNVELRYKGLGTSSAKEGREYFENIDRHRLNFVYEDRKDDDDIVMAFAKDKVDERK 640
TbbTopoll β EGTISFFSMPDYFEWKNAVGEGISDVEVKYKGLGTSSAKEGREYFENIDRHRLNFVYSGKKDDDSIVLAFADKDKVDERK 640

TbbTopoll α RWITEFKANTNINESMNYNVRNVSYSFVHKELILFSVADCERSIPSVVDGLKPGQRKIMFSAFKRNLRSLKVAQLAGY 720
TbbTopoll β RWVMSMSARRFESLSYNARDVSYSFVHKELILFSVADCERSIPSVVDGLKPGQRKIMFSAFKRNLRSLKVARFAGY 720

TbbTopoll α VSEHAAYHHGEQSLVQTVGLAQDYVGANNVPLLVRDGGFGTRLQGGKDHAAGRYIFTRLTDIARRIYHPSDDFIVEYRD 800
TbbTopoll β VSEHAAYHHGEQSLVQTVGLAQDYVGANNVPLLVRDGGFGTRLQGGKDHAAGRYISTRLTDIARRIYHPSDDFIVEYRD 800

TbbTopoll α DDGLSVEPFYVVPVIMVNLVNGTAGIGTGAFATNIPNYSPLDVINDLNRLSGEELQPMKPWFYFGFTGTIEEREKGFVSS 880
TbbTopoll β DDGLSVEPFYVVPVIMVNLVNGTAGIGTGAFATNIPNYSPLDVINDLNRLSGEELQPMKPWFYFGFTGTIEEREKGFVSS 880

TbbTopoll α GCATVRPDGVVHITELPIGTWTQYKKFLEDLREREIVIQYREHNTDVTVD FEVF IHP EVL RQWVAQGCVEERLQLREYI 960
TbbTopoll β GCATVRPDGVVHITELPIGTWTQYKKFLEDLREREIVIQYREHNTDVTVD FEVF IHP EVL RQWVAQGCVEERLQLREYI 960

TbbTopoll α HATNIIAFDREGKITKYLDAESVLKEFYLVRLLEYARRREFLLEQLQRAALKLENMVRVFNVEIDGTFIIVTRRSMDVVK 1040
TbbTopoll β HATNIIAFDREGKITKYLDAESVLKEFYLVRLLEYARRREFLLEQLQRAALKLENMVRVFNVEIDGTFIIVTRRSMDVVK 1040

TbbTopoll α DLKQRGYTPFPPOQKKKMSSTTIVDEEEETERNTAATSADAE EAVLVQDELIGPGGGGAQE EPEV - - - KQNARDYDYI 1117
TbbTopoll β DLKQRGYTPFPPOQKKKMSSTTIVDEEDNDGAR KILPDVFEFESVPLCE - - - QVIGKILCTAEP E - EINMVKGVLEVDYI 1117

TbbTopoll α GLRLWNLTAEMSARLKAQLDAAREKYENIAKRTPKDLWREDLQLLRP DVEKLFDERREK EIASIQKKREK KRPFDASRL 1197
TbbTopoll β LSLRMVDLTVEAMMYFRTKREQMLNKHNFVLSASSKDLWREDLQLLRSDIEKLFDERREK EIALIQCKLEK RQFEDVSRL 1197

TbbTopoll α RVPLLSDAARKA - - - - - LLRET I KEEKKSVRGDT S - - - - - TRG DGP SAGD SKNPRGVKT ASSGKGRK - - - - - KDSDD 1264
TbbTopoll β RVPLLSDAARKADRSLALRQSNCKREMS SKCASES FALLVDAGVRVSGLTESSICDINEARR - KYGHSVAGG KRRLVHR 1276

TbbTopoll α DDFDDFTGFSDDGDDYRPDDSDNGGATAASGGSTAKVKRAPAKQAPAKQA AVKPRSGRAKTLKKEEETKL GASDDL DLDLC 1344
TbbTopoll β DEVSKRGK FSSCGDQRHVSLSDGSDTDCS I G - - - - - APSVS SDATPATQKS - - - - - RKISDSSYG - - - - - 1333

TbbTopoll α FGIEALTGSLQKTSSSKLPSPPSTGVFAEDEEEALLLGITSAQGKTPSRVASKGRVKQSSGKPS TQAKVPKKRRRGGG 1424
TbbTopoll β FGIEGEVDIFFEDTVGED - - - - - FSEPATQANIV - - - - - RSKSESPVLDFAEYATE - - - PKSKRPR 1389

TbbTopoll α SDVSASDENI - - - - - VDDDDDDDDDDDESSLDFSD - - - 1455
TbbTopoll β IEDN - - - - - DENTCFYVVDVVGEDVEYSDQCIGDACVF 1424

Figure S9. Multiple sequence alignment of *T. b. brucei* Topoll α and Topoll β . Black triangle symbol below amino acids highlight the homozygous mutations seen in CT mutants (CT1.1, CT1.2, CT4.1, CT5.1 & CT5.2). Blue filled circles below amino acids represent the heterozygous mutations seen in CT4.2 mutant. Sequences were aligned using CLC Genomics workbench.

		1	10	20	30	40	50	60							
T.brucei	MSGR	TVRE	LYOKKTQ	HEID	APDM	MYICTIE	FVTED	VVYD	ADNV	KIK	KC	TWT	PCLYK	
T.cruzi	MANR	TVRE	LYOKKTQ	HEID	APDM	MYICTIE	FVTED	VVYD	ADNV	KIK	KC	TWT	PCLYK	
L.donovani	MGK	TVRE	LYOKKTQ	HEID	APDM	MYICTIE	FVTED	VVYD	ADNV	KIK	KC	TWT	PCLYK	
S.cerevisiae	MSTEPV	SASDK	YOKIS	LEID	KRPD	TICSVET	QEQ	QV	YD	ETDCM	IKEN	TV	PCLYK	
H.sapiens	MEVSP	LQPVNEN	QVNI	KKNE	DAKKRI	SVHR	LYOKKTQ	LEID	KRPD	TICSVET	QEQ	QV	YD	ETDCM	
		70	80	90	100	110	120	130	140						
T.brucei	IFDEILVNAADNKVRDP	HGQT	IKVW	DAARGL	VRVYNN	CE	CIDV	QR	REHD	LWVPEM	IFC	LLTSSNYDD	TEA	VITCCRNCF	
T.cruzi	IFDEILVNAADNKVRDP	LGQT	IKVW	DAARGM	VRVYNN	CE	CIDV	QR	REHD	LWVPEM	IFC	LLTSSNYDD	TEA	VITCCRNCF	
L.donovani	IFDEILVNAADNKVRDP	IGQT	IKVW	DAARGM	VRVYNN	CE	CIDV	QR	REHD	LWVPEM	IFC	LLTSSNYDD	TEA	VITCCRNCF	
S.cerevisiae	IFDEILVNAADNKVRDP	SM	KR	IDVNI	HAEEHT	EVKNC	K	CIDV	QR	REHD	LWVPEM	IFC	LLTSSNYDD	TEA	
H.sapiens	IFDEILVNAADNKVRDP	KM	S	IRVTI	DPENNL	S	LNW	K	CIDV	QR	REHD	LWVPEM	IFC	LLTSSNYDD	
		150	160	170	180	190	200	210	220						
T.brucei	AKL	LVFS	RFEV	TVHSRS	KKKF	FM	QR	NLM	LENE	SAV	T	FC	D	CP	
T.cruzi	AKL	LVFS	RFEV	TVHSRS	KKKF	FM	QR	NLM	LENE	SAV	T	FC	D	CP	
L.donovani	AKL	LVFS	RFEV	TVHSRS	KKKF	FM	QR	NLM	LENE	SAV	T	FC	D	CP	
S.cerevisiae	AKL	LVFS	RFEV	TVHSRS	KKKF	FM	QR	NLM	LENE	SAV	T	FC	D	CP	
H.sapiens	AKL	LVFS	RFEV	TVHSRS	KKKF	FM	QR	NLM	LENE	SAV	T	FC	D	CP	
		230	240	250	260	270	280	290							
T.brucei	TDR	SC	YLN	DT	IA	CR	SP	FE	VVD	Y	PTM	CE	ER	
T.cruzi	TDR	SC	YLN	DT	IA	CR	SP	FE	VVD	Y	PTM	CE	ER	
L.donovani	TDR	SC	YLN	DT	IA	CR	SP	FE	VVD	Y	PTM	CE	ER	
S.cerevisiae	TDR	SC	YLN	DT	IA	CR	SP	FE	VVD	Y	PTM	CE	ER	
H.sapiens	TDR	SC	YLN	DT	IA	CR	SP	FE	VVD	Y	PTM	CE	ER	
		300	310	320	330	340	350	360	370						
T.brucei	CCT	RV	Y	Y	Y	Y	Y	Y	Y	Y	Y	Y	Y	Y	
T.cruzi	CCT	RV	Y	Y	Y	Y	Y	Y	Y	Y	Y	Y	Y	Y	
L.donovani	CCT	RV	Y	Y	Y	Y	Y	Y	Y	Y	Y	Y	Y	Y	
S.cerevisiae	CCT	RV	Y	Y	Y	Y	Y	Y	Y	Y	Y	Y	Y	Y	
H.sapiens	CCT	RV	Y	Y	Y	Y	Y	Y	Y	Y	Y	Y	Y	Y	
		380	390	400	410	420	430	440	450	460					
T.brucei	S	I	V	R	A	V	E	M	A	N	S	R	I	N	R
T.cruzi	S	I	V	R	A	V	E	M	A	N	S	R	I	N	R
L.donovani	S	I	V	R	A	V	E	M	A	N	S	R	I	N	R
S.cerevisiae	S	I	V	R	A	V	E	M	A	N	S	R	I	N	R
H.sapiens	S	I	V	R	A	V	E	M	A	N	S	R	I	N	R
		470	480	490	500	510	520	530	540						
T.brucei	F	I	N	V	R	E	A	S	V	K	V	M	C	A	F
T.cruzi	F	I	N	V	R	E	A	S	V	K	V	M	C	A	F
L.donovani	F	I	N	V	R	E	A	S	V	K	V	M	C	A	F
S.cerevisiae	F	I	N	V	R	E	A	S	V	K	V	M	C	A	F
H.sapiens	F	I	N	V	R	E	A	S	V	K	V	M	C	A	F
		550	560	570	580	590	600	610	620						
T.brucei	F	I	T	P	I	V	K	A	R	K	K	G	R	N	S
T.cruzi	F	I	T	P	I	V	K	A	R	K	K	G	R	N	S
L.donovani	F	I	T	P	I	V	K	A	R	K	K	G	R	N	S
S.cerevisiae	F	I	T	P	I	V	K	A	R	K	K	G	R	N	S
H.sapiens	F	I	T	P	I	V	K	A	R	K	K	G	R	N	S
		630	640	650	660	670	680	690	700						
T.brucei	V	M	A	P	A	D	K	V	D	E	R	R	E	M	I
T.cruzi	V	M	A	P	A	D	K	V	D	E	R	R	E	M	I
L.donovani	V	M	A	P	A	D	K	V	D	E	R	R	E	M	I
S.cerevisiae	V	M	A	P	A	D	K	V	D	E	R	R	E	M	I
H.sapiens	V	M	A	P	A	D	K	V	D	E	R	R	E	M	I
		710	720	730	740	750	760	770	780						
T.brucei	F	A	R	N	L	V	R	S	A	V	A	Q	A	C	Y
T.cruzi	F	A	R	N	L	V	R	S	A	V	A	Q	A	C	Y
L.donovani	F	A	R	N	L	V	R	S	A	V	A	Q	A	C	Y
S.cerevisiae	F	A	R	N	L	V	R	S	A	V	A	Q	A	C	Y
H.sapiens	F	A	R	N	L	V	R	S	A	V	A	Q	A	C	Y
		790	800	810	820	830	840	850	860	870					
T.brucei	Y	H	P	S	D	D	F	V	E	Y	R	D	D	G	L
T.cruzi	Y	H	P	S	D	D	F	V	E	Y	R	D	D	G	L
L.donovani	Y	H	P	S	D	D	F	V	E	Y	R	D	D	G	L
S.cerevisiae	Y	H	P	S	D	D	F	V	E	Y	R	D	D	G	L
H.sapiens	Y	H	P	S	D	D	F	V	E	Y	R	D	D	G	L
		880	890	900	910	920	930	940							
T.brucei	R	E	K	C	K	F	V	S	C	A	T	V	R	F	D
T.cruzi	R	E	K	C	K	F	V	S	C	A	T	V	R	F	D
L.donovani	R	E	K	C	K	F	V	S	C	A	T	V	R	F	D
S.cerevisiae	R	E	K	C	K	F	V	S	C	A	T	V	R	F	D
H.sapiens	R	E	K	C	K	F	V	S	C	A	T	V	R	F	D
		950	960	970	980	990	1000	1010	1020	1030					
T.brucei	V	E	R	L	Q	R	E	Y	H	A	T	N	I	A	D
T.cruzi	V	E	R	L	Q	R	E	Y	H	A	T	N	I	A	D
L.donovani	V	E	R	L	Q	R	E	Y	H	A	T	N	I	A	D
S.cerevisiae	V	E	R	L	Q	R	E	Y	H	A	T	N	I	A	D
H.sapiens	V	E	R	L	Q	R	E	Y	H	A	T	N	I	A	D

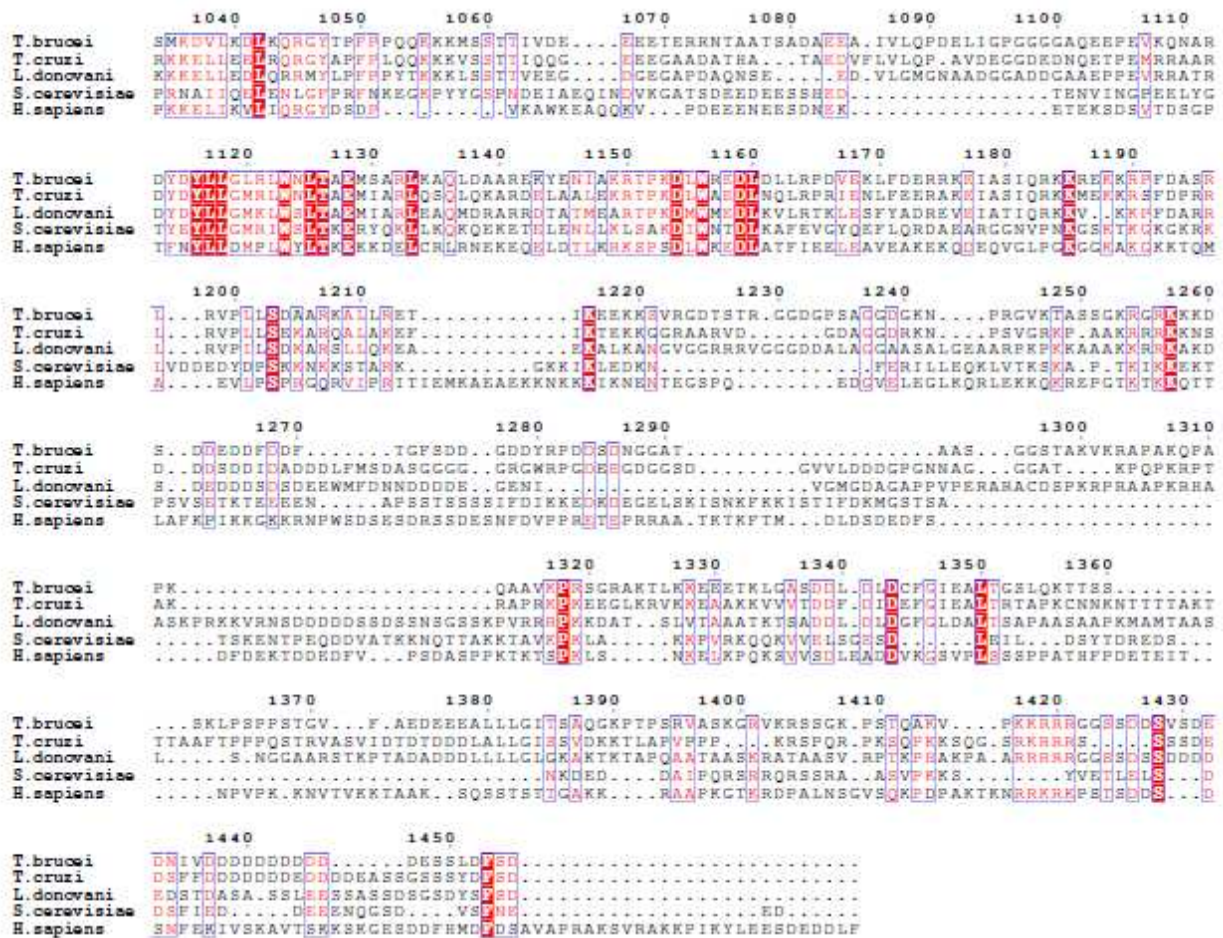


Figure S10. Multiple sequence alignment of topoisomerases II sequences. For the sequence alignment, sequences with the following Uniprot identifiers were used: *T. b. brucei* (Q2PQ59), *T. cruzi* (Q4DE53), *L. donovani* (E9BJW5), *S. cerevisiae* (P06786), *H. sapiens* (P11388). Sequences were aligned using Clustal Omega and visualized using ESPrnt.

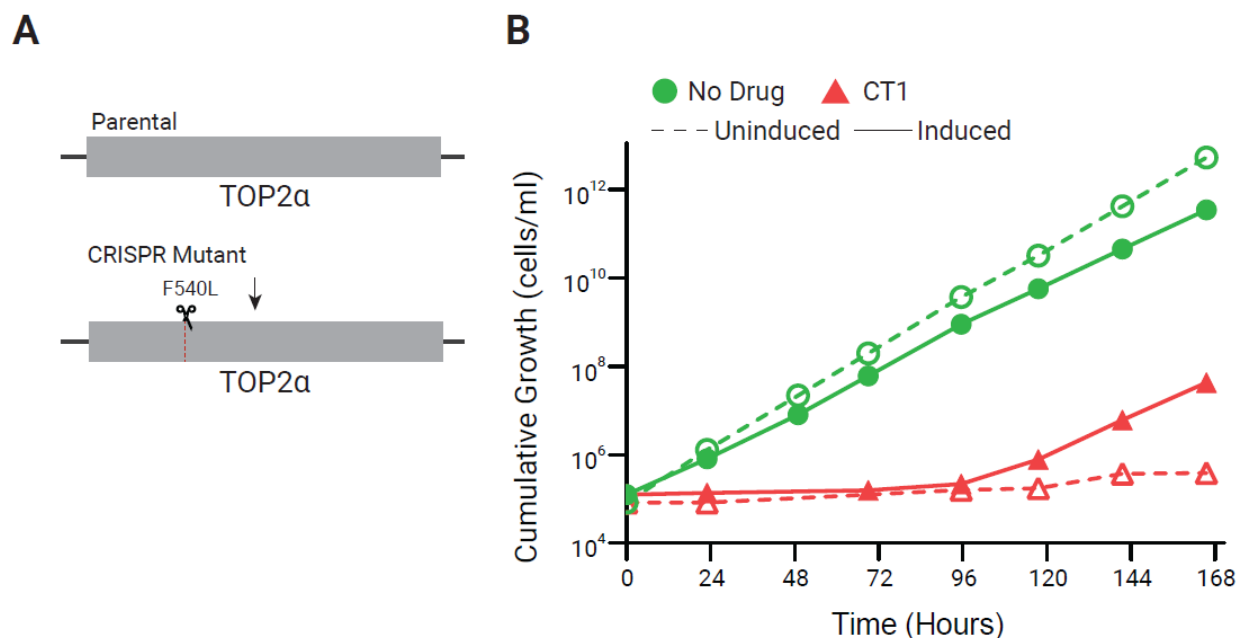


Figure S11. CRISPR Cas9 mutants of *topollα* in *T. b. brucei*. (A) Schematic representation of parental and CRISPR *topollα*. (B) *T. b. brucei* strain (427-2T1t7-cas9), with constitutive transcription of a pT7 sgRNA construct targeting the F540 locus of the *topollα* gene for cleavage on induction of Cas9 expression, was transfected with a repair template oligonucleotide introducing the F540L mutation. Transfectants were selected in a normally lethal concentration of CT1 and their growth profile over a period of 168 hours is shown. Note the growth of *T. b. brucei* cells in the presence of CT1 after 96 hours of incubation.

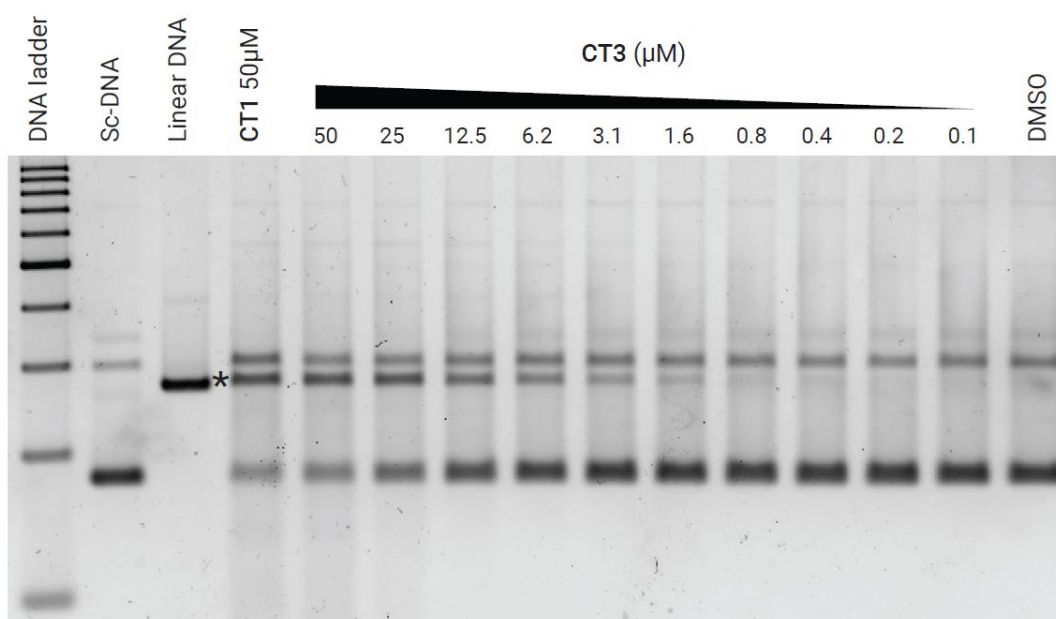


Figure S12. Biochemical characterization of CT3 in DNA cleavage assay. Full-length *T. cruzi* Topoll was incubated with supercoiled DNA (ScDNA) in the presence of varying concentrations (μM) of CT3, and the ability to induce dsDNA breaks (in the absence of ATP) was measured by running products on a 1.2% agarose gel. The experiment was conducted with two biological replicates; one of the representative images is shown. Note that CT3 caused concentration dependent increase in levels of linear double-strand DNA (asterix).

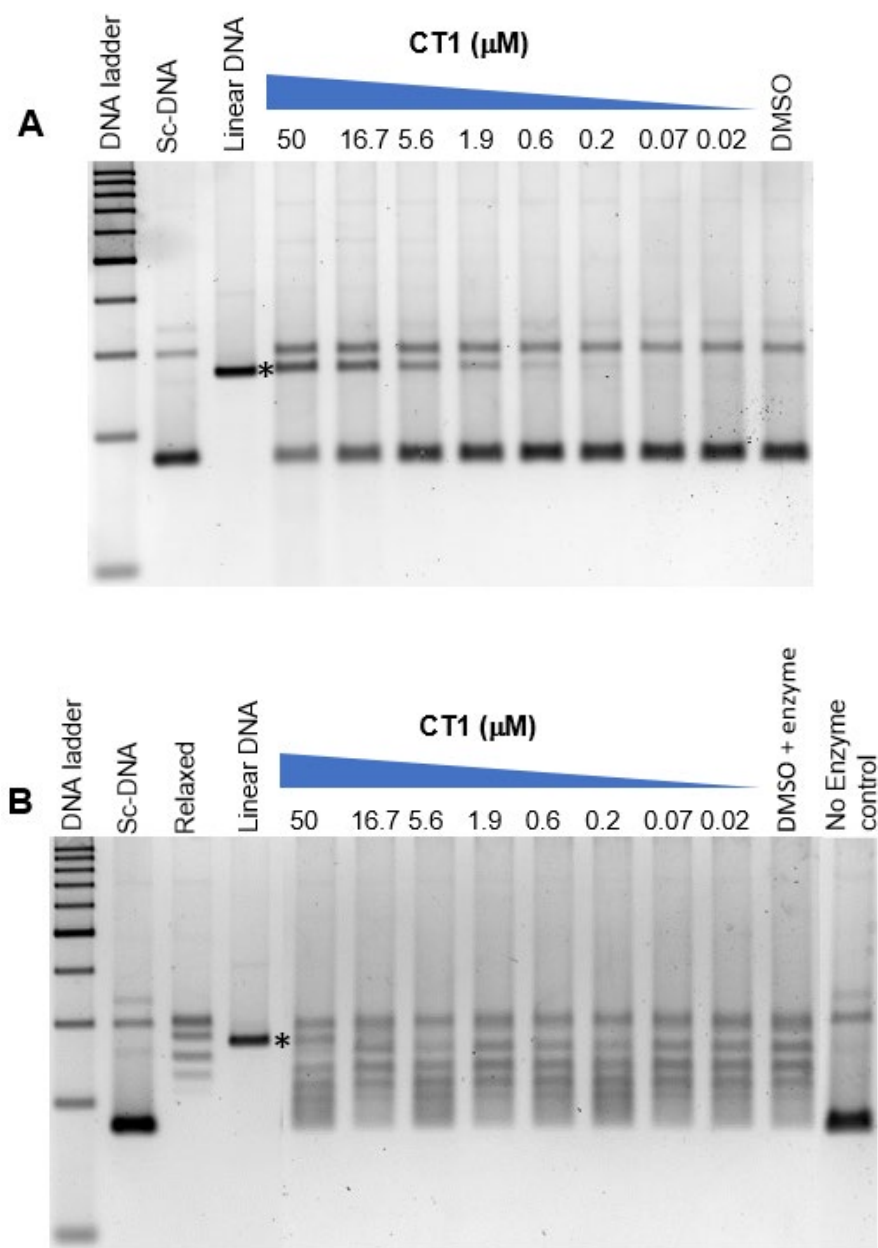


Fig. S13. Biochemical characterization of CT1 inhibition using *T. cruzi*

topoisomerase II. Full-length *T. cruzi* TopoII was incubated with supercoiled DNA (ScDNA) in the presence of varying concentrations (μM) of CT1, and the ability to induce dsDNA breaks in the absence (**A**) and presence (**B**) of ATP was measured by running products on a 1.2% agarose gel. *T. cruzi* topo II has shown a robust relaxation of supercoiled DNA in presence of ATP, one of the relaxed topoisomer band overlaps with linear double stranded DNA. The experiment was conducted with two biological replicates; one of the representative images is shown. Note that CT1 caused concentration dependent increase in levels of linear double-strand DNA (asterix).

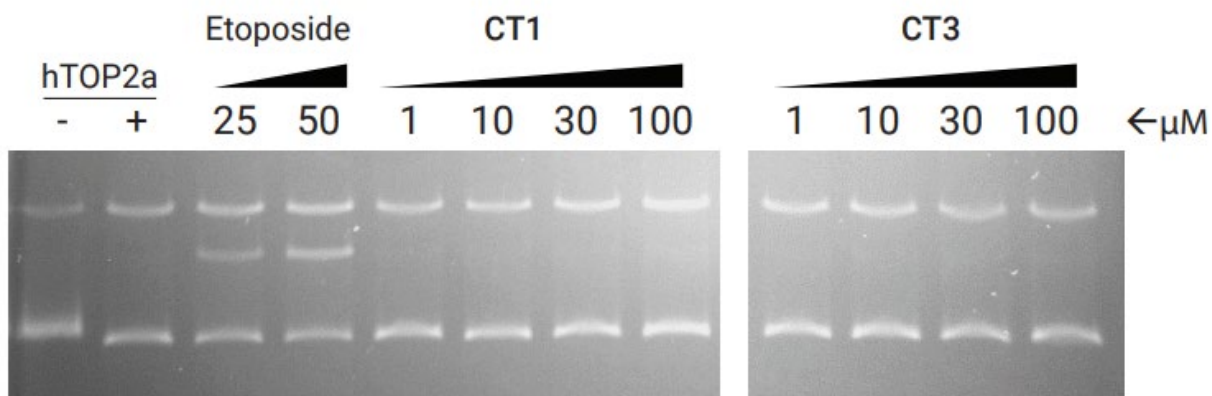


Figure S14. Human TOP2A relaxation activities were not affected by CT. Human TOP2A cleavage assay to specifically address whether there is formation of double stranded break upon addition of CTs. In the absence of TOP2A, there are two bands appearing on the gel. The upper band corresponds to the nicked open circular DNA whereas the bottom band represents the negatively supercoiled DNA. In the presence of TOP2A, the negatively supercoiled band was relaxed and in the presence of ethidium bromide, it was running slightly faster than the negatively supercoiled DNA. The presence of etoposide (25, 50 μM) acts as a poison and a linear DNA band was observed in the middle of the gel. In the presence of various concentration of CT1 and CT3 (1 μM , 10 μM , 30 μM and 100 μM), there is no presence of linear DNA. All the experiments were performed with biological duplicates and the representative gel image shown above.

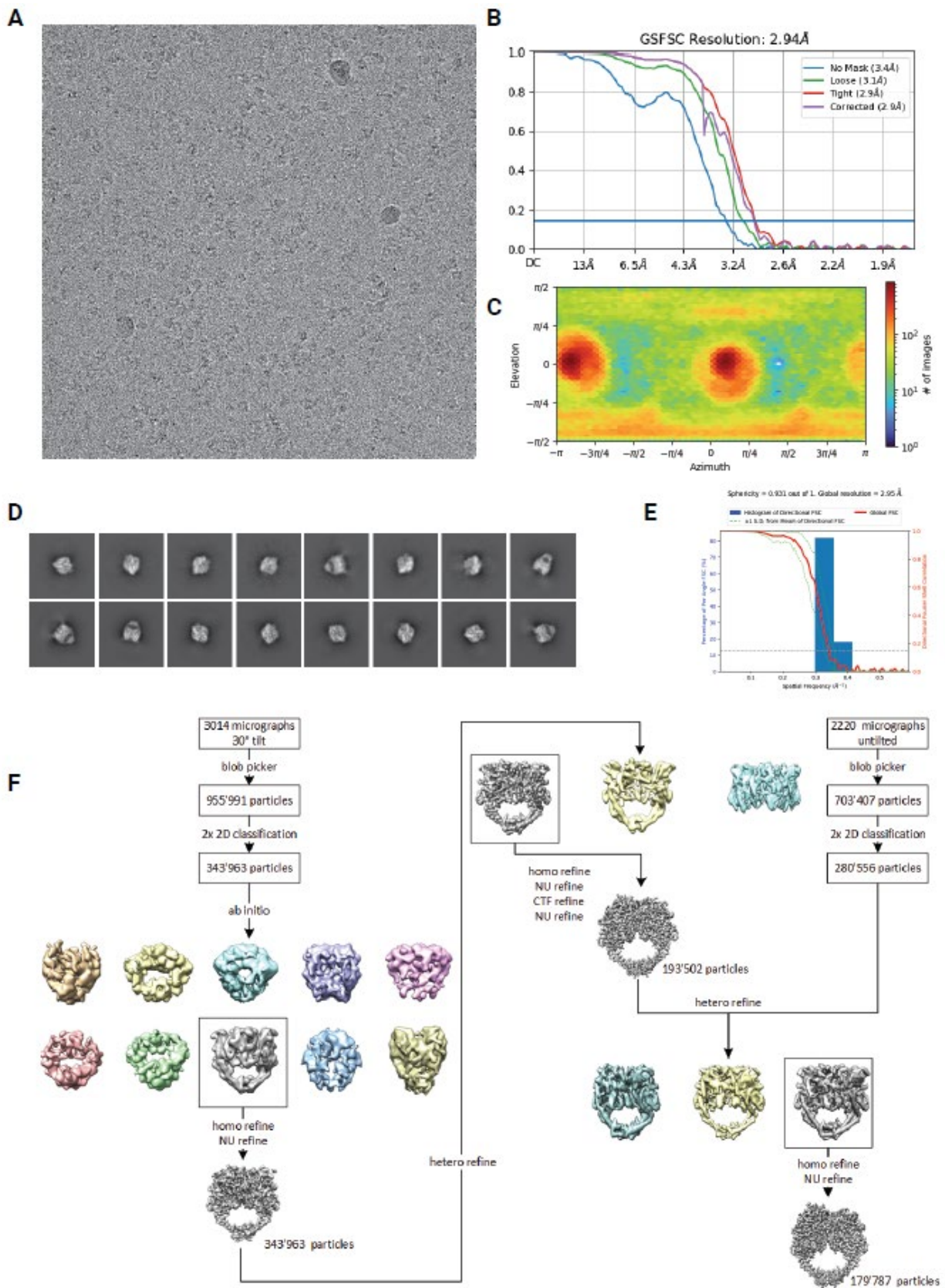


Figure S15. Structure determination using cryo electron microscopy. (A)

Representative electron micrograph (**B**) The final reconstruction shows an average resolution of 2.94 Å, determined by Gold Standard Fourier Shell Correlation with a cutoff of 0.143 (**C**) Euler distribution plot (**D**) Representative 2D classes of tilted (top row) and untilted (bottom row) data (**E**) .Histogram of directional FSC calculated by 3DFSC (**F**)

5 Flowchart of the single particle EM analysis

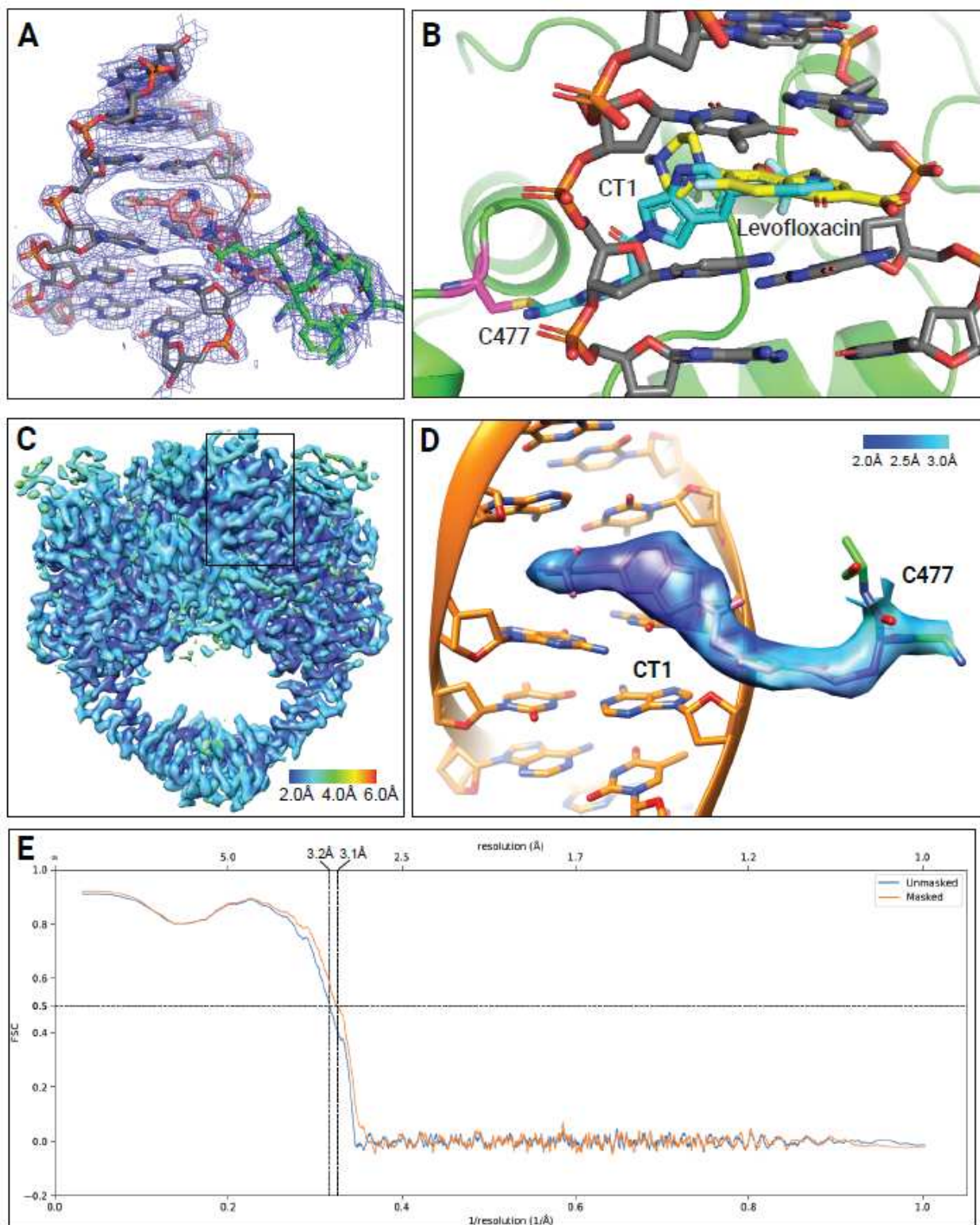


Figure S16. CT1 binds to the DNA cleavage site of *T. cruzi* Topoll. (A) Representative section around the CT1 binding site shows the experimental EM map. (B) CT1 (shown in cyan) binds to the same binding site as the bacterial gyrase inhibitor

5

fluoroquinolone levofloxacin (shown in yellow), here superimposed from 5EIX on the Tc TopoII DBD-DNA cryo-EM complex structure bound to CT1. **(C)** Local resolution of cryo-EM map as determined by ResMap. Box indicates approximate section depicted in panel D. **(D)** The EM density unambiguously reveals the binding mode of CT1 and shows continuous EM density with cysteine C477 colored by local resolution supporting a covalent binding mode. **(E)** Model-to-Map FSC, with resolution at 0.5 FSC cutoff denoted

Table S1. Growth inhibition activity of cyanotriazoles against apicomplexan parasites and bacterial pathogens.

Compounds	CT0	CT1	CT3	CT4	CT5
<i>Apicomplexan parasites</i> (EC ₅₀ in μ M)					
<i>Plasmodium falciparum</i> 3D7	>10	> 10	5.85	> 10	> 10
<i>Cryptosporidium parvum</i>	nt ^a	> 20	> 20	> 20	nt
<i>Bacterial pathogens</i> (MIC in μ M)					
<i>Pseudomonas aeruginosa</i> 20	> 200	nt	nt	> 200	> 200
<i>Escherichia coli</i> 72imp	> 200	nt	nt	> 200	> 200
<i>E. coli</i> 70	> 200	nt	nt	> 200	> 200
<i>Staphylococcus aureus</i> 80	> 200	nt	nt	> 200	> 200
<i>P. aeruginosa</i> 40	> 200	nt	nt	> 200	> 200
<i>P. aeruginosa</i> 19	> 200	nt	nt	> 200	> 200
<i>Klebsiella pneumonia</i> 01	> 200	nt	nt	> 200	> 200
<i>E. coli</i> 77	> 200	nt	nt	> 200	> 200

^ant: not tested; all values are in μ M

Table S2. In vitro and in vivo pharmacokinetic properties of cyanotriazoles.

	CT0	CT1	CT3
<i>Physicochemical properties</i>			
Molecular weight	332.3	398.3	416.3
cLogP	0.7	0.86	1.15
HBA	8	7	7
<i>In vitro pharmacokinetic properties</i>			
Permeability (MDR MDCK) A-B / ER	nt	13 / 0.7	14.3 / 0.81
Microsomal clearance Clint (M /R/H)	24.4 / 28.3 / 24.5	<25 / < 25 / <25	<25 / < 25 / <25
Mouse plasma protein binding (%)	82	90.9	96
Rat brain tissue binding (%)	91.2	93.5	91.8
<i>In vivo pharmacokinetic properties (mice)</i>			
Dose i.v. / p.o. (mg.kg ⁻¹)	1 / 50	1 / 25	1 / 2
Clearance (mL.min ⁻¹ .kg ⁻¹)	14.4	23.5	6.06
Volume of distribution (L.kg ⁻¹)	3.04	2.1	1.12
Exposure, AUC (POPK, nM*h)	723	33914	13300
Cmax (POPK, nM)	7863	5763	2500
Tmax (h)	2	0.75	0.5

cLogP: calculated lipophilicity; HBA: hydrogen bond acceptors; nt: not tested; The intravenous (i.v.) PK parameters were obtained by dosing animals with solution formulation (NMP:4%BSA in PBS (10:90 v/v)); per oral (p.o.) PK parameters were obtained by dosing with suspension formulation (Methylcellulose:Tween80:Water (0.5:0.1:99.4 w/w/v)); Cmax, maximum concentration achieved; Tmax, time of peak concentration, AUC, area under the curve.

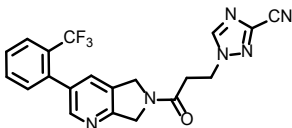
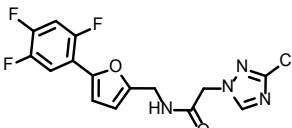
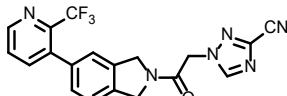
5

Table S3. Activity of CTs against DNA repair system knock out mutants of *T. b. brucei*.

Compounds	EC ₅₀ (nM)				
	2T1 WT	BRCA2		RAD51	
	Mean ± SE	Mean ± SE	KO/WT ratio	Mean ± SE	KO/WT ratio
CT1	169.5 ± 1.0	88.9 ± 5.8	0.52**	77.8 ± 2.7	0.46**
CT3	162.9 ± 1.2	93.2 ± 4.2	0.57**	80.4 ± 2.9	0.49**
CT4	30.9 ± 1.9	12.2 ± 0.6	0.39**	10.8 ± 0.7	0.35**
CT5	179 ± 4.4	105.9 ± 3.7	0.59**	93.2 ± 3.9	0.52**
Melarsen Oxide	26.5 ± 4.1	39.9 ± 4.6	1.51 ^{ns}	42.7 ± 6.4	1.61 ^{ns}
Pentamidine	3.1 ± 0.5	6.8 ± 1.2	2.23 ^{ns}	4.9 ± 0.3	1.59 ^{ns}

EC₅₀ concentrations are represented as mean ± standard error (SE); 2T1 WT: *T. b. brucei* 2T1 wild-type strain; BRCA2 KO: *T. b. brucei* BRCA2 knock out strain; RAD51 KO: *T. b. brucei* knock out strain. Melarsen oxide and pentamidine are anti-trypanosomal agents. Statistical analysis using student t-test comparing respective knock out strain vs 2T1 wild-type EC₅₀; **: p<0.01; ns: non-significant p>0.05.

Table S4. Chemical structures and profiles of other cyanotriazole molecules used for selection of mutants, metabolomics and biochemical studies.

<div style="display: flex; justify-content: space-around; align-items: flex-end;"> <div style="text-align: center;">  <p>CT2</p> </div> <div style="text-align: center;">  <p>CT4</p> </div> <div style="text-align: center;">  <p>CT5</p> </div> </div>			
	CT2	CT4	CT5
<i>In vitro anti-parasitic activity</i> EC₅₀ (nM)			
<i>T. brucei</i>	33,410 ± 2300	30 ± 17	130 ± 63
<i>T. brucei gambiense</i>	>50, 000	47 ± 1	25 ± 16
<i>T. brucei rhodesiense</i>	>50,000	45 ± 5	44 ± 5
<i>T. cruzi</i>	6,000 ± 395	11 ± 3	73 ± 19
<i>L. donovani</i>	nt	65 ± 31	247 ± 115
<i>Cytotoxicity</i> CC₅₀ (nM)			
HepG2	>50,000	>50,000	>50,000
NIH 3T3	4,100	>20,000	>20,000

nt: not tested; HepG2: human hepatocellular carcinoma cells; NIH 3T3: fibroblast cells

Table S5. Growth inhibition activity of CTs against *T. b. brucei* 2T1 cells expressing RNAi construct targeting *topoll* α

Compound	EC ₅₀ (nM)						
	RNAi uninduced	0.125 ng.mL ⁻¹ dox		0.25 ng.mL ⁻¹ dox		0.5 ng.mL ⁻¹ dox	
	Mean \pm SE	Mean \pm SE	Res. F	Mean \pm SE	Res. F	Mean \pm SE	Res. F
CT1	65.9 \pm 3.4	96.8 \pm 6.8	1.5*	160.2 \pm 27.2	2.4*	229.3 \pm 4.5	3.5**
CT3	67.3 \pm 3.3	101.9 \pm 2.9	1.5**	170 \pm 12.6	2.5**	216.1 \pm 7.8	3.2**
CT4	13.7 \pm 1.2	18.5 \pm 0.8	1.4**	22.1 \pm 2.2	1.6*	30.3 \pm 2.3	2.2**
CT5	77.7 \pm 3.4	108.5 \pm 3.9	1.4**	176 \pm 22	2.3*	214.6 \pm 10.1	2.8**
Suramin	63.5 \pm 2.5	67.2 \pm 2.6	1.1 ^{ns}	64.2 \pm 3.4	1.0 ^{ns}	67.8 \pm 3.2	1.1 ^{ns}

EC₅₀ concentrations are represented as mean \pm standard error (SE); Res. F: Resistance factor indicates shift in EC₅₀ with *Tb topoll* α RNAi induction by increasing concentrations of doxycycline. Statistical analysis using student t-test comparing uninduced vs induced EC₅₀; *: p<0.05; **: p<0.01; ns: non-significant p>0.05.

Table S6. Cryo-EM data collection, refinement and validation statistics

Topoll DNA domain bound to double stranded DNA and CT1		
Data collection and processing		
EMDB ID	EMD-29930	
Microscope	ThermoFisher Titan Krios G2	
Magnification (nominal)	75000	
Magnification (calibrated)	165680	
Voltage (kV)	300	
Total electron exposure (e-/Å2)	50	
EER fractionation	50	
Pixel size (Å)	0.845	
Automation software	EPU 3.0	
# of particles in final map	179787	
Resolution at 0.143 FSC (masked/unmasked)	2.94/3.36	
Resolution at 0.5 FSC (masked/unmasked)	3.29/3.9	
Resolution half-bit FSC (masked/unmasked)	2.96/3.45	
Local resolution range for voxels covered by atomic model	2.0-5.2	
3DFSC Sphericity value	0.931	
Map sharpening B factor (Å2)	115.4	
	30° tilted data	untilted data
Detector	ThermoFisher Falcon 4i	ThermoFisher Falcon 4
Defocus range (µm)	-1.4 to -1.8 *	-0.6 to -2.0
Exposure rate (e-/pixel/s)	9.23	8.74
# Micrographs used	3014	2220
Total # of extracted particles	955991	703407
Total # of refined particles	343936	280556
	6	
Refinement		
Initial Alphafold model used	AF-Q4DE53-F1	
PDB-ID	8GCC	

Model composition	
Non-hydrogen atom	11705
protein residues	1414
DNA	48
ligands	2
Atomic modeling refinement package(s)	Phenix 1.20
CCvolume/CCmask	0.83/0.85
B factors	
protein residues	45.86
DNA	52.27
Ligands	32.79
RMSD	
Length (Å)	0.004
Angles (°)	0.507
Molprobity score	1.79
All-atom clashscore	4.7
Rotamer outliers (%)	2.54
Ramachandran percentiles (%)	
Favored	96.43
Allowed	3.57
Outliers	0.00
CaBLAM outliers (%)	1.29
EMRinger score	3.46

* for central foil hole in 3x3 group

Table S7. In vitro pre-clinical safety profiling

hERG activity	IC₅₀ (μM)	Kinases	IC₅₀ (μM)
Binding	>30	CDK4	>30
Qpatch	14.2	DMPK	>30
Patch Clamp Nac1.5 Quattro (Sodium current)	>50	EGFR	>30
Patch Clamp Cac1.5 Quattro (Calcium current)	>50	EPHA4	>30
GPCRs*		ERBB2	>30
5HT1a (Serotonin 5-HT 1A receptor)	>30	FGFR2	>30
5HT2b_agonist (Serotonin 5-HT2b receptor)	>30	FGFR4	>30
Al1a_agonist (Adrenergic α1A receptor)	>30	Fit-1	>30
Al1a_antagonist (Adrenergic α1A receptor)	>30	GRK1	>30
Al2a (Adrenergic α2A receptor)	>30	GSK3b	>30
D1 (Dopamine D1 receptor)	>30	IGF1R	>30
D3 (Dopamine D3 receptor)	>30	INSR	>30
H3 (Histamine H3 receptor)	>30	JAK1	>30
M1_agonist (Muscarinic M1 receptor)	>30	JAK2	>30
M1_antagonist (Muscarinic M1 receptor)	14.4	JAK3	>30
TP_agonist (Prostanoid TP)	>30	KDR	>30
TP_antagonist (Prostanoid TP)	14.6	KIT	>30
Nuclear receptors*		LCK	>30
AR (agonist)	>30	MAP14	>30
Era (Estrogen receptor)	26.7	MAPK1	>30
PR-B (Progesterone receptor)	11.7	MAPKAPK2	>30
Transporters*		MAPKAPK5	>30
DAT (Dopamine transporter)	>30	MET	>30
5HTT (Serotonin transporter)	28.5	MKNK2	>30
NET (norepinephrine transporter) (antagonist)	>30	PDPK1	>30
Enzymes		PIM1	>30
ACES (acetylcholinesterase)	>30	PRK2	>30
MAO-A (Monoamine oxidase A)	>30	PRKAA2	>30

Thrombin	>30	PRKCA	>30
Kinases		PRKCQ	>30
ABL1	>30	RAF1	>30
AKT1	>30	RET	>30
ALK	>30	ROCK2	>30
ATM	>30	RPS6KB1	>30
AURKA	>30	SYK	>30
AXL	>30	TGFBR1	>30
CAMK1	>30	TYK2	>30
CAMK2D	>30	ZAP70	>30
CDK2	>30		

*Radioligand assays

Data S1 (separate file)

Metabolomics profile of *T. b. brucei* treated with cyanotriazoles.

5

Data S2. (separate file)

Single nucleotide polymorphism in CT mutants. Whole genome sequencing of CT1.1, CT1.2, CT4.1 and CT4.2 was carried out using Illumina sequencing system. Mutations mapping is shown.

10